A FINE-DETAILED ANALYSIS OF THE CHEMICAL ABUNDANCES FOR THE PECULIAR A-STAR BETA CORONAE BOREALIS

By

THOMAS MORRIS JORDAN

Bachelor of Arts
Indiana State University
Terre Haute, Indiana
1969

Master of Science
Oklahoma State University
Stillwater, Oklahoma
1974

Submitted to the Faculty of the Graduate College
of the Oklahoma State University
in partial fulfillment of the requirements
for the Degree of
DOCTOR OF PHILOSOPHY
July, 1977

A FINE-DETAILED ANALYSIS OF THE CHEMICAL ABUNDANCES FOR THE PECULIAR A-STAR BETA CORONAE BOREALIS

Thesis Approved:

Leon W. Schroeder
Thesis Adviser

Charles V. Butler

Delleen L. Puttedge

Franklin R. Leach

Norman N. Durham
Dean of the Graduate College

ACKNOWLEDGMENTS

The author would like to acknowledge Dr. Leon W. Schroeder, my adviser, for suggesting the topic, supplying the tracings used in this study, and providing guidance throughout the preparation of this dissertation.

I also wish to extend a special thanks to Dr. John C. Evans of the George Mason University for use of his unpublished computer programs used in this study and for his exceedingly helpful suggestions and comments.

In addition, the author acknowledges Mr. Ron M. Opitz for his permission to use certain data from his thesis; the contributions made by the other members of my graduate committee, Dr. D. L. Rutledge, Dr. C. T. Butler, Dr. H. L. Scott, and Dr. F. R. Leach for their counseling during the formulation of this study; and Oklahoma State University Research Foundation for financial support for the use of the computer.

I would also like to express sincere gratitude to my parents for their interest and encouragement at all times during my educational career. And I would like to express appreciation to my daughter, Cecilie, for her understanding and sacrifice during this study.

Finally, I would like to express deep appreciation to my wife, Teresa, for her constant understanding and encouragement as well as her unfailing assistance during the preparation of this investigation.

TABLE OF CONTENTS

LIST OF TABLES

LIST OF FIGURES

CHAPTER I

INTRODUCTION

Statement of the Problem

Abundance determinations have long fascinated investigators in the field of astrophysics. The value of these abundance determinations from stellar spectra give clues to the history of the stellar material. For a fixed set of abundances it is possible to make a one-to-one correspondence between the net emergent flux and the surface gravity and the coordinates on the Hertzsprung-Russell diagram, on which one may plot the evolutionary path of a star. In general, the characterization of the net flux and the surface gravity is accomplished through a model atmosphere approach.

The analysis of stellar spectra has been developed from the rudimentary curve of growth analysis, the relationship between the width of a line and the number of the effective absorbing atoms, by Minnaert and Slob (1931). This technique represents a specific method for the deduction of various atmospheric parameters such as the temperature, pressure and chemical composition, based on the approximation that formation of spectral lines can be assumed to originate in an atmosphere of some fixed density and temperature.

A model atmosphere technique was later developed by Strömgren (1940) which improved upon the treatment of spectral analysis and

has since been significantly improved by more recent investigators. Aller (1949) was the first to apply the model atmosphere technique to stars other than our own sun where he investigated γ Pegasi, a B2V star.

The determination of the chemical abundance of a stellar atmosphere using the fine analysis approach is merely a successive approximation procedure. First, a curve of growth analysis supplies a rough or crude estimate of the existing elemental abundances in the star, its surface gravity, and finally its effective temperature. Next, a grid of stellar atmospheres can be computed on the basis of this knowledge. Selection of the appropriate model for the stellar atmosphere finally is based upon a comparison between observational and theoretical values of the energy distribution in the continuous spectrum, the color temperature and the hydrogen line profiles of the star. Any correct stellar model should effectively reproduce the discontinuity at the Balmer limit of the energy distribution. The stratification of the pressure, temperature, and opacity can be used in conjunction with an assumed mechanism for the spectral line formation to theoretically predict the profile of the line and its equivalent width from the model atmosphere. Once agreement between the observed and calculated profiles has been reached the abundances can then be determined.

Purpose of the Study

The purpose of this investigation is to determine the chemical composition of the stellar atmosphere of the peculiar A-star Beta Coronae Borealis. The abundances of the elements are determined

from a detailed description of the structuring of the stellar atmosphere. Theoretical curves of growth, metal line profiles, and equivalent widths are employed to assess the effects of the various line broadening agents which are present in the stellar atmosphere.

Previous Investigations of Beta Coronae Borealis

Beta Coronae Borealis (1970: $\alpha=15^h26^m37^s.9$ $\delta=29^o12'17"$) has been classified in the Henry Draper Catalog as FOp and by Sargent and Searle in 1962 as A5p (Paschen Type). It has a photographic apparent magnitude of +3.93, a visual magnitude of +3.7 (Adelman, 1973a) and a variable color index (B-V) of +0.27 (Abt and Golson, 1962). This star is peculiar because it has more enhanced lines of europium, chromium, and strontium than so-called "normal" stars. The Sr-Cr-Eu star Beta Coronae Borealis (HD 137909) has one of the greatest known rare earth abundances (Hack, 1958; Hardorp and Shore, 1971; Adelman, 1973b). It is the brightest example of a sharp-lined cool magnetic Ap star with an apparent rotational velocity $\leq$ 3 km/sec (Adelman and Shore, 1973; Preston, 1971). Its lines are broadened somewhat by a magnetic field of 6 kilogauss (Preston, 1969). Spectroscopic studies reveal that it is not a spectrum variable; however it is both a magnetic and light variable (Wolff and Morrison, 1971). It is indeed a spectroscopic binary with a period of 10.5 years (Neubauer, 1944).

In 1945 W. A. Hiltner (University of Michigan) prepared one of the more definitive line identification lists which covered the spectral region $\lambda\lambda$3980-4638. This was done with a short-screw measuring engine directly on the spectrogram. An abundance determination was made by Hack in 1958. And, in 1965, a curve of

growth was made by Fowler, et al. J. Gruber (1972) extended this identification list to include the spectral region λλ3613-4863. Later, T. Jordan (1974) extended this region even further to include λλ3405-6959. Finally, R. M. Opitz (1974) completed a preliminary abundance analysis and microturbulence determination. It is with these extended line lists that one can carry out a fine analysis abundance determination of the various elements present in this peculiar A-star, Beta Coronae Borealis.

CHAPTER II

MODEL ATMOSPHERES

The Description of a Stellar Atmosphere

A stellar atmosphere can be described as that portion of a star capable of being observed. This would refer, in a general way, to the regions of a star in which its components of the electromagnetic spectrum are formed. This would also imply the layers of a star in which the continuous and absorption-line spectra are likewise formed. The present interpretation of a stellar atmosphere is a depth range from a few hundred to a few thousand kilometers; the sun's atmosphere, for example, has a geometrical depth of approximately 330 kilometers (Aller, 1963). One may deduce the physical properties of the stellar atmosphere from observations of the continuum and the strengths and shapes of the star's absorption lines. These properties are specified because the actual processes occurring within the stellar atmosphere determine the very nature of the radiant energy emitted.

The representation of a stellar atmosphere in terms of a model proceeds from a postulation of the dependence of the physical parameters - pressure, temperature, and opacity - upon a specified depth-dependent variable for the computation of the net flux emerging from the star and the shape of the spectral absorption lines.

When one compares the computed data with the observations the model can be adjusted to yield a best fit thereby defining the stellar atmosphere in terms of the model only to the extent of the agreement between the two.

Before a description of a stellar atmosphere can be made certain simplifying assumptions are introduced into the model governing the physical processes that are occurring in the star. The assumptions made in this investigation are common to most investigations in stellar atmospheres (Unsöld, 1955; Aller, 1963).

For the detailed analysis of Beta Coronae Borealis, the star was assumed to be spherically symmetric, non-rotating, and the range of depth of the atmosphere negligible compared to the radius of the star. It is also assumed that the atmosphere is to be partitioned in homogeneous, steady-state, plane-paralled layers of which the outer boundary is defined by the condition that no significant quantity of radiation flows inward across this boundary. It is also assumed that the atmosphere provides no significant sources or sinks of energy. A state of hydrostatic equilibrium exists at all times and at all points within the atmosphere under the influence of a uniform gravitational field. There are no provisions made for radiation, magnetic, or other mechanical forces. This will ensure that the total pressure at each homogeneous layer is equivalent to the gas pressure of the layer.

There are also assumptions made upon the mechanism of the interaction between the radiation and gravitational field. It is assumed that the gases in the stellar atmosphere are in local thermodynamic equilibrium (LTE). This merely implies that for

the continuous spectrum a replacement of the source function by the Planck function of the local electron temperature may be made since the ratio of the probability of the emission to absorption of a photon in a specified frequency interval would be unity. Pure absorption is then the only mechanism for the formation of the radiation field. In most cases this ratio is very close to unity except for the lines formed in high regions of the stellar atmosphere so that these assumptions are not by any means unrealistic for this problem (Böhm , 1960; Aller, 1963; Motz, 1970). Finally, the assertion is made that the formation of the line and continuous spectrum may be treated as separate entities.

Even though magnetic forces are formally neglected, they are, however, consolidated in an approximate fashion through the use of an effective surface gravity rather than of the dynamical quantity. Magnetic effects produce a distention in the atmosphere at its outermost layers and reduce the dynamical surface gravity in the process (Aller, 1963).

The method of computation of the corresponding pressure-opacity-flux model follows the computational procedure devised by Weidmann (1955) and later revised by Elste (1967) and Evans (1966,1972). The model atmosphere program will generate the electron and gas pressures as functions of a conveniently defined depth parameter for a given chemical composition, effective surface gravity, and temperature distribution. The logarithmic optical depth scale is used rather than the actual physical depth in the atmosphere itself (Elste,1955; Weidmann,1955). The scale of the logarithmic optical depth is approximately linearly proportional to the actual physical

depth of a layer in a stellar atmosphere. As the independent variable of depth, the logarithm of the continuum optical depth at 5000 $\mathring{A}$ is used. It can be related to the geometrical depth scale by the relation

$$X \equiv \log \tau_o = \log \left[\int_o^t \frac{K_o(t)}{m_o \sum_i \varepsilon_i \mu_i} \rho(t)dt\right], \qquad (2\text{-}1)$$

where

t = the physical depth in the atmosphere,

$K_o(t)$ = the continuous absorption coefficient per hydrogen particle at 5000$\mathring{A}$,

m_o = the gram mass of a unit atomic weight,

μ_i = the atomic weight of species i,

ε_i = the number abundance of species i relative to hydrogen,

$\rho(t)$ = the density of stellar material.

The quantity $1/m_o \sum_i \varepsilon_i \mu_i$ is the number of hydrogen particles per gram of material. The stellar atmosphere model was divided into twenty-seven layers each specified by a corresponding value of the logarithm of the optical depth ranging from $-4.00 \leq X \leq +1.20$. The theory developed for computing the pressure-opacity flux model used in this investigation has been discussed extensively by Evans (1966,1969) and Bulman (1971) and the necessary details are given in Appendix A.

The Temperature Distribution

The temperature is one of the thermodynamic parameters that specify the model atmosphere. In thermodynamic equilibrium, the temperature distribution is determined by the amount of energy incident at the bottom of the atmosphere from the deep interior of the star, the mechanism for energy transport, and the sources of continuous absorption. The assumption that the net flux must be constant at each layer in the atmosphere, the transport mechanisms being either strictly radiative or combined radiative and convective, is a sufficient criterion to determine the temperature with depth in the stellar atmosphere. The source of continuous opacity must also be known.

In the case of the solar photosphere, however, it is possible to use limb-darkening observations together with the energy distribution at the center of the solar disk to determine an empirical temperature distribution for $-1.00 \leq X \leq +0.30$ (Aller, 1963). In comparing such a temperature distribution with theoretical results, a discrepancy arises which is probably due to the blanketing by the absorption lines and temperature inhomogenities due to turbulent and convective velocity fields (Schmalberger, 1963). The region of formation for the observed radiation depends upon the depth variation of the number of absorbing atoms and their wavelength dependence for absorption. For most wavelengths, the continuum is formed between $-0.6 \leq X \leq +0.6$ so that the differences in the region $-4.0 \leq X \leq +1.2$ do not influence the continuum formation. Line centers which are, in general, formed higher than the continuum

are more sensitive to the differences between theoretical and empirical temperature distributions. The latter procedure is convenient for stars whose sources of continuous absorption coefficients and ionization equilibria are not far removed from those of the sun.

For the purpose of this study, however, the empirical solar temperature distribution used was one due to Elste (1955) with graphical modifications in deep layers to represent radiative transport and a combination of radiative and convective transport. The scaling of Elste's solar temperature distribution is accomplished by multiplying the empirical solar temperature at each optical depth by the ratio of the desired stellar to solar effective temperature for each layer of atmosphere [T_{eff} (solar) = 5780^{o}K; Aller, (1963)]. The resulting effective temperature, however, does not yield the total integrated flux since it has been empirically derived. It is only an approximation and will accordingly be referred to as the model temperature.

The detailed model atmosphere is shown in Table I. It represents the model atmosphere chosen for the computational analysis of Beta Coronae Borealis. Following the data table, the effective temperature, the surface gravity, the helium to hydrogen number density, B, and the logarithm of the number of hydrogen atoms to those of the metals, A = log N_H/Σ N metals are listed respectively. In consecutive columns, the logarithm of the continuum optical depth at 5000$\mathring{A}$, the temperature expressed as either θ = 5040/T(^{o}K) or as T(^{o}K), the logarithms of the electron pressure, gas pressure, and the ratio of the absorption coefficient to the electron pressure are given as

TABLE I

THE REPRESENTATIVE MODEL ATMOSPHERE FOR BETA CORONAE BOREALIS

Log Tau (5000)	Theta Model	Temp. (^{o}K)	Log PE	Log PG	Log K/PE (5000)	Mean Mol. Wt.	Log Density	Geometrical Depth (KM)
-4.00	0.8580	5874.	-0.4879	1.7687	-25.1882	1.2923	-9.8087	-6129.40
-3.80	0.8575	5878.	-0.4372	1.8608	-25.2125	1.2929	-9.7166	-5761.90
-3.60	0.8567	5883.	-0.3561	2.0082	-25.2458	1.2939	-9.5693	-5353.60
-3.40	0.8555	5891.	-0.2720	2.1557	-25.2736	1.2946	-9.4222	-4947.10
-3.20	0.8540	5902.	-0.1867	2.3012	-25.2967	1.2953	-9.2772	-4545.80
-3.00	0.8520	5915.	-0.0992	2.4437	-25.3163	1.2958	-9.1356	-4152.20
-2.80	0.8490	5936.	-0.0064	2.5825	-25.3343	1.2961	-8.9983	-3768.30
-2.60	0.8444	5969.	0.0954	2.7161	-25.3522	1.2964	-8.8669	-3396.40
-2.40	0.8392	6006.	0.1991	2.8451	-25.3693	1.2965	-8.7405	-3036.30
-2.20	0.8309	6066.	0.3221	2.9680	-25.3899	1.2965	-8.6219	-2689.80
-2.00	0.8204	6143.	0.4572	3.0837	-25.4130	1.2964	-8.5118	-2360.30
-1.80	0.8077	6240.	0.6047	3.1919	-25.4387	1.2961	-8.4105	-2047.50
-1.60	0.7926	6359.	0.7659	3.2925	-25.4678	1.2956	-8.3182	-1751.40
-1.40	0.7761	6494.	0.9342	3.3861	-25.4987	1.2949	-8.2341	-1470.60
-1.20	0.7574	6654.	1.1155	3.4727	-25.5315	1.2938	-8.1583	-1204.10
-1.00	0.7371	6838.	1.3058	3.5526	-25.5646	1.2921	-8.0909	- 952.20
-0.80	0.7146	7053.	1.5093	3.6254	-25.4974	1.2895	-8.0324	- 715.10
-0.60	0.6891	7314.	1.7317	3.6904	-25.6277	1.2852	-7.9846	- 495.90
-0.40	0.6598	7639.	1.9781	3.7460	-25.6503	1.2773	-7.9505	- 299.70
-0.20	0.6260	8051.	2.2519	3.7907	-25.6556	1.2619	-7.9339	- 132.90
0.00	0.5885	8564.	2.5442	3.8238	-25.6300	1.2313	-7.9384	0.00
0.20	0.5479	9199.	2.8442	3.8462	-25.5636	1.1702	-7.9691	99.50
0.40	0.5066	9949.	3.1208	3.8605	-25.4657	1.0632	-8.0305	173.10

TABLE I (Concluded)

Log Tau (5000)	Theta Model	Temp. (°K)	Log PE	Log PG	Log K/PE (5000)	Mean Mol. Wt.	Log Density	Geometrical Depth (KM)
0.60	0.4751	10608.	3.3016	3.8710	-25.3931	0.9501	-8.0968	237.70
0.80	0.4533	11118.	3.4036	3.8813	-25.3567	0.8689	-8.1456	313.10
1.00	0.4383	11499.	3.4640	3.8940	-25.3448	0.8195	-8.1730	416.50
1.20	0.4309	11696.	3.4938	3.9002	-25.3443	0.7988	-8.1852	519.90

T(eff) = 7700.00°K Log g = 3.50 B = 0.1000 A = 2.8487

functions of the optical depth at 5000Å. The mean molecular weights and logarithmic densities are also tabulated. The values located under the column for the geometrical depth have been initialized to zero since the geometrical depth was not used for calculation purposes.

CHAPTER III

THE THEORIES OF LINE FORMATION, CURVES OF GROWTH AND ABUNDANCE DETERMINATIONS

Stellar Absorption Lines

We may regard the physical processes of line formation from two extreme points of view. One method assumes that a unique temperature completely determines the emission and absorption processes in a given volume element, i.e., Kirchhoff's law holds. This condition is called local thermaldynamic equilibrium (LTE) and is sometimes referred to as absorption. From this point of view, the radiation from the center of a strong line will correspond to the temperature of the uppermost stratum since the line absorption coefficient is large at this wavelength and radiation reaches us only from the surface. The second method assumes that the atoms are not in temperature equilibrium with the radiation field at all but simply scatter quanta reaching them from greater depths in the interior. A particular light quantum may be absorbed and re-emitted many times on its way through the atmosphere, and since it may be scattered either forward, backward, or sideways, its chance of reaching the surface is small.

There is a tendency for resonance transitions to favor scattering, or at least a mixture of scattering and pure absorption, as a formation mechanism (Aller, 1963). The absorption lines that are

assumed to be formed in LTE have the Planck function as the line source function. This assumption is more valid for subordinate transitions than for the resonance transitions.

In order to extract the most information possible about the stellar atmosphere, there are two aspects of an absorption line to consider. The first is the intensity of the line which is generally expressed in terms of an equivalent width. And the second is the line shape or, as it is more commonly called, its profile. The former is just the total amount of energy extracted by the absorption line itself while the latter depends principally upon the residual energy distribution in the line as a function of frequency.

Line Depth in Flux

If we assume thermodynamic equilibrium for the line formation mechanism, then scattering processes may be neglected as compared to pure absorption processes so the net flux in the continuum is represented by Equation (A-14). The formulation of the equation specifying the line depth in flux was done by Gussman (1963). The line depth is defined as

$$R(\Delta\lambda) = 1 - \frac{F_T^{\ell}(0,\Delta\lambda)}{F_T^{c}(0,\lambda_m)} = \frac{F_T^{c}(0,\lambda_m) - F_T^{\ell}(0,\Delta\lambda)}{F_T^{c}(0,\lambda_m)}, \qquad (3\text{-}1)$$

where

λ_m = the defining wavelength of a 300Å wide region of the spectrum containing λ,

$F_T^c(0,\lambda_m)$ = the total continuum flux emerging from the atmosphere [see Equation (A-14)],

$F_T^\ell(0,\Delta\lambda)$ = the emergent flux in the line at a distance $\Delta\lambda$ from the center.

Both $F(0,\Delta\lambda)$ and $\tau_{\lambda m}(x)$ have been specified as details of the calculations of the model atmosphere. If the mechanisms for line formation are independent of those for the formation of the continuum, then the flux in the line is

$$F_T^\ell(0,\Delta\lambda) = 2 \int_o^\infty B_{\lambda m}(\tau^c + \tau^\ell)\, E_2(\tau^c + \tau^\ell)\, d(\tau^c + \tau^\ell). \qquad (3\text{-}2)$$

since the optical depth τ, is just the addition of the optical depth in the continuum, τ^c, and the optical depth in the line, τ^ℓ. The quantity $B_{\lambda m}(\tau^c + \tau^\ell)$ appearing in the integrand is the Planck function. $E_2(\tau^c + \tau^\ell)$ represents the exponential-integral function,

$$E_2(x) = \int_1^\infty e^{-xy} \frac{dy}{y^2} \quad .$$

The optical depth in the line is given by

$$\tau^\ell(x,\Delta\lambda) = \int_{-\infty}^{x} \frac{K^\ell}{K_o} \frac{\tau_o}{\log e} (1 - 10^{-\chi_{\lambda m}\theta(x)})dx, \qquad (3\text{-}3)$$

where

$K^\ell(x,\Delta\lambda)$ = the line absorption coefficient per hydrogen particle,

$\chi_{\lambda m} = 12397.67/\lambda_m$,

$1 - 10^{-\chi_{\lambda m}\theta(x)}$ = the factor needed to account for stimulated emission.

$K_o(x)$, $\tau_o(x)$ and $\theta(x)$ are parameters specified by the model atmosphere calculations.

Line Broadening Mechanisms

The absorption lines in stellar spectra are broadened through several different mechanisms in addition to instrumental imperfections. In recent years, a number of reviews on spectral line broadening have been published. Among them are Böhm (1960), Traving (1960), Mazing (1961), Breene (1961, 1964), Baranger (1962) and van Regemorter (1965).

There are several broadening mechanisms of importance in stellar atmospheres. They may be separated into two categories: microscopic broadening agents and macroscopic broadening agents

(a) Microscopic broadening agents include:

(i) Radiation or natural broadening, due to the existence of small but finite lifetimes of excited states of a gas atom;

(ii) Doppler broadening, due to the random thermal motions of the absorbing particles as well as a possible small scale mass motion;

(iii) Resonance broadening, due to interactions with atoms of the same kind as the absorber;

(iv) Stark broadening, due to the interaction of the absorber with surrounding electrons and ions;

(v) Isotopic broadening, a pseudo-broadening, due to isotopic variations between atoms;

(vi) van der Waals broadening, due to the interaction with neutral atoms or molecules of a different kind than the absorbing particle;

(vii) Zeeman broadening, due to line splitting in a magnetic field;

(viii) Microturblence, due to the mass motions of turbulent elements whose linear extent is small compared to the mean free path of a photon.

(b) Macroscopic broadening agents include:

(i) Rotational broadening, due to the contributions from different parts of a rotating stellar surface;

(ii) Macroturbulence, due to mass motions of turbulent elements whose linear extent is large compared to the mean free path of a photon.

Turbulence affects both the equivalent width and line profiles, but in a different manner depending on whether or not the size of the atmosphere is greater than or smaller than the thickness of the line-forming region. Microturbulence elements moving with different velocities absorb radiation from the continuous spectrum at different distances from the line center resulting in a broadening of the line profile and an increased equivalent width. The delaying of optical saturation then raises the flat portion of the curve of growth, as can be seen in Figure 1, for various microturbulent velocities

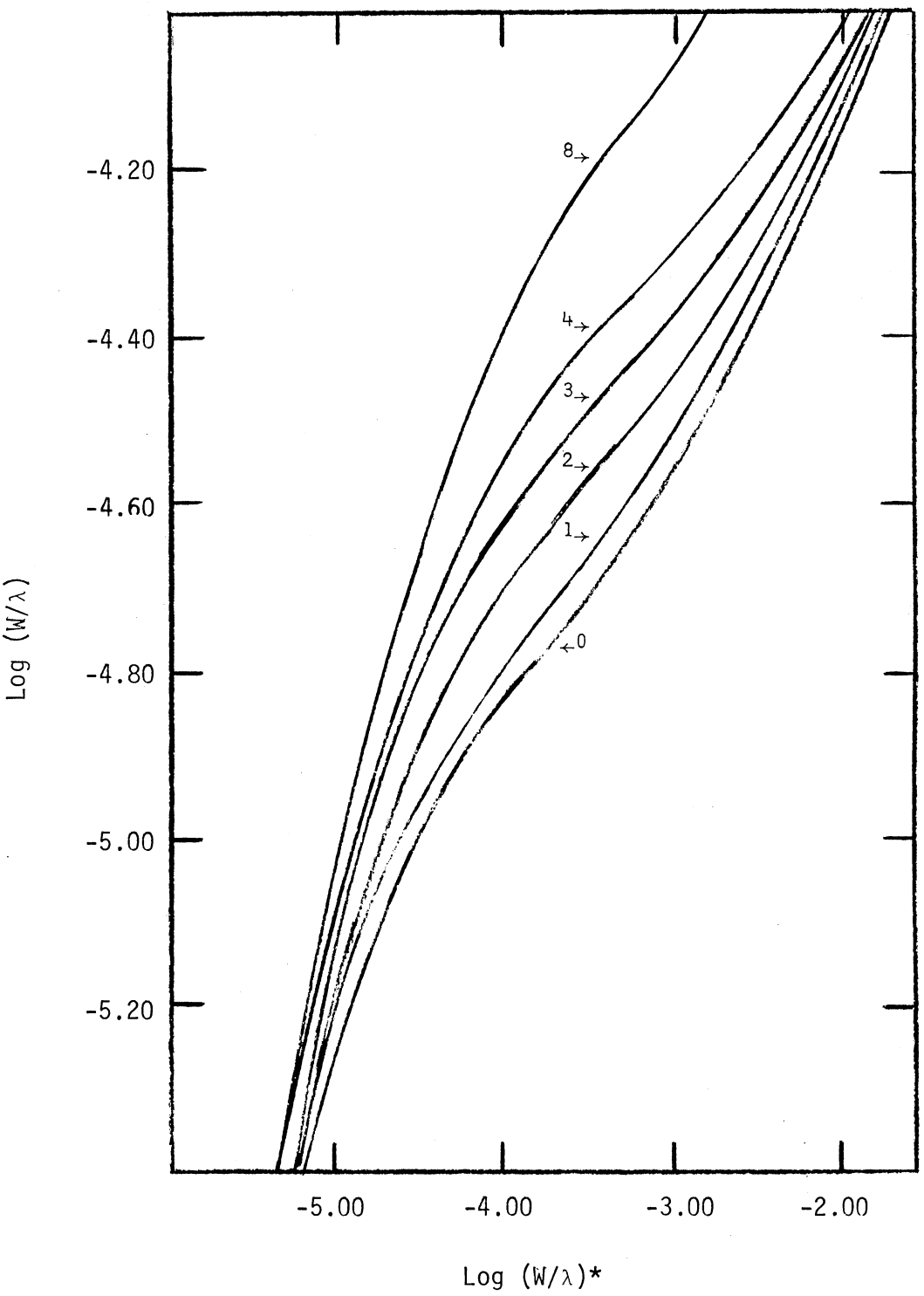

Figure 1. Theoretical Curve of Growth for Fe I with the Labeled Microturblent Velocities (km/s)

Macroturbulence and stellar rotation do not influence the equivalent width, since by definition they occur after the line has been formed. They simply round out the line profile.

Calculation of Theoretical Line Intensity and Flux

Consider a stellar atmosphere which contains mass motions, arising from cells whose thickness is greater than that of the region in which the line is formed, whose velocity along the line of sight has the tangential and radial components of

$$\varepsilon_i = \varepsilon_i^t \sin\theta + \varepsilon_i^r \cos\theta, \tag{3-4}$$

where

θ = the angle between the observer and the velocity component of the i^{th} cell.

If the continuum intensity of the i^{th} cell is I_i^c, and the line intensity of the i^{th} cell is I_i^ℓ, then the total continuum intensity arising from n distinct cells occupying an area A at a limb distance $\mu = \cos\theta$ is

$$I_T^c = \sum_{i=1}^{n} a_i I_i^c, \tag{3-5}$$

while the total line intensity is given by

$$I_T^\ell = \sum_{i=1}^{n} a_i I_i^\ell, \tag{3-6}$$

where

a_i = the fraction of area A occupied by cells with a velocity of ε_i.

The line depth expression for the emergent radiation from the region of interest is from Equations (3-5) and (3-6)

$$r_\lambda(\mu) = \frac{I_T^c - I_T^\ell}{I_T^c} = \sum_{i=1}^{n} a_i \left[\frac{I_i^c - I_i^\ell}{I_T^c}\right]. \qquad (3\text{-}7)$$

Now if the continuum is formed according to the mechanism of pure absorption, and LTE assumed, the equation for the specific intensity of a ray which emerges from the surface of the i^{th} cell at an angle θ with the normal is, where $\mu = \cos\theta$,

$$I_i^c(0,\mu) = \int_o^\infty s_i^c \, e^{-\tau_i^c/\mu} \frac{d\tau^c}{\mu} = \int_{-\infty}^{\infty} s_i^c \, e^{-\tau_i^c/\mu} \frac{K_i^c}{K_o^c} \left(\frac{10^x}{\log e}\right) \frac{dx}{\mu}, \qquad (3\text{-}8)$$

where

τ_i^c = the continuum optical depth,

$$= \int_{-\infty}^{x} \frac{K_i^c}{K_o^c} \left(\frac{10^x}{\log e}\right) dx,$$

x = the logarithm of the optical depth at $\lambda = 5000\text{Å}$, for a non-moving ambient photosphere,

S_i^c = the source function in the continuum of the i^{th} cell, which is in this case the Planck function.

Likewise the specific line intensity of the emergent ray is

$$I_i^\ell(0,\mu) = \int_o^\infty S_i \, e^{-\tau_i/\mu} \frac{d\tau_i}{\mu}, \qquad (3\text{-}9)$$

$$= \int_{-\infty}^{\infty} S_i \, e^{-\tau_i/\mu} \frac{K_i}{K_o^c} \left(\frac{10^x}{\log e}\right) \frac{dx}{\mu},$$

where

S_i = the source function of the i^{th} cell at a point in the line.

τ_i = the optical depth for a point in the line,

$= \tau_i^c + \tau_i^\ell$,

$$= \int_{-\infty}^{x} \frac{K_i^c + K_i^\ell}{K_o^c} \left(\frac{10^x}{\log e}\right) dx.$$

In Equation (3-9) the mechanism for the line formation has been assumed to be independent of that which produces the continuum (Motz, 1970), so that the source function S_i then becomes

$$S_i = \left[\frac{S_i^c + \rho_i S_i^\ell}{1 + \rho_i}\right] = S_i^c \left[\frac{1 + \rho_i \beta_i}{1 + \rho_i}\right], \qquad (3\text{-}10)$$

where

$$\rho_i = K_i^\ell / K_i^c \ , \quad \beta_i = S_i^\ell / S_i^c \ ,$$

and

$$K_i = K_i^\ell + K_i^c = K_i^c (1 + \rho_i).$$

Making use of Equations (3-8), (3-9), and (3-10), the line depth in intensity, from Equation (3-7), is

$$r_\lambda(\mu) = \sum_{i=1}^{n} \left\{ \frac{a_i}{I_T^c} \int_{-\infty}^{\infty} S_i^c \, e^{-\tau_i^c/\mu} \, \frac{K_i^c}{K_o^c} \left(\frac{10^x}{\log e}\right) \frac{dx}{\mu} \right\}$$

$$- \sum_{i=1}^{n} \frac{a_i}{I_T^c} \int_{-\infty}^{\infty} S_i^c \, e^{-\tau_i^c/\mu} \, e^{-\tau_i^\ell/\mu} \, \frac{(1 + \rho_i \beta_i)}{(1 + \rho_i)} (1 + \rho_i)$$

$$\cdot \frac{K_i^c}{K_o^c} \left(\frac{10^x}{\log e}\right) \frac{dx}{\mu} \ ,$$

or

$$r_\lambda(\mu) = \int_{-\infty}^{\infty} \left[\sum_{i=1}^{n} \frac{a_i S_i^c}{I_T^c} e^{-\tau_i^c/\mu} \{1-(1+\rho_i\beta_i)\, e^{-\tau_i^\ell/\mu}\} \right.$$

$$\left. \cdot \frac{K_i^c}{K_o^c} \frac{10^x}{\log e} \right] \frac{dx}{\mu} \quad . \qquad (3\text{-}11)$$

It is now beneficial to make necessary simplifying assumptions concerning Equation (3-11). The best observational evidence for the existence of macroturbulence appears in the granular structure of the photosphere of the sun. There the continuous radiation from the bright granules is not altogether different in intensity from that produced by the inter-granular region surrounding the cells (Evans, 1972). Therefore, it will be assumed that the intensity of the cells $I_i^c = I^c$ for all i. This implies that the total continuum intensity, summed over all cells, is just the total intensity I_T^c. Throughout the part of the line that makes the major contribution to the equivalent width, the source function in the line is not very different from that in the continuum and if LTE is invoked, they are identical. Further, Jugaku (1957) has shown that it is theoretically sound to assume the source function to be Planckian for main-sequence B stars. The last restriction is placed on the macroturbulent distribution itself. It will be assumed that all cells have the same temperature stratification and differ only in their velocity fields. This latter assumption constrains the Planck function and the optical depth in the continuum to be identical for all cells. With these conditions, Equation (3-11) for the line depth becomes

$$r_\lambda(\mu) = \int_{-\infty}^{\infty} \left[\frac{B\, e^{-\tau^c/\mu}}{I_T^c} \sum_{i=1}^{n} a_i \{1 - (1 + \rho_i)\, e^{-\tau_i^\ell/\mu}\}\right.$$

$$\left. \cdot \frac{K^c}{K_o^c}\right]\left(\frac{10^x}{\log e}\right) \frac{dx}{\mu}\,, \qquad (3\text{-}12)$$

where

$B = B_\lambda$ = the Planck function,

$K^c = K_\lambda^c$ = the continuous absorption coefficient,

K_o^c = the continuous absorption coefficient for $\lambda = 5000\text{Å}$,

τ_i^ℓ = the optical depth of a line occuring in the i^{th} cell of the stellar atmosphere.

If we use the identity

$$\sum_{i=1}^{n} a_i\,(1 - \psi_i) = 1 - \sum_{i=1}^{n} a_i\psi_i\,,$$

then Equation (3-12) may be written in the form

$$r_\lambda(\mu) = \int_{-\infty}^{\infty} \left[\frac{B\, e^{-\tau^c/\mu}}{I_T^c} \{1 - \sum_{i=1}^{n} a_i(1 + \rho_i)\, e^{-\tau_i^\ell/\mu}\} \frac{K^c}{K_o^c}\right.$$

$$\left. \cdot \left(\frac{10^x}{\log e}\right) \frac{dx}{\mu}\right] \cdot \qquad (3\text{-}13)$$

Except for the sun, it is impossible to observe separate portions of a stellar surface. The energy that is received from a star is then proportional to the total amount of energy emitted from each small segment of area. This energy or flux is then

obtained by integration of the specific intensity, Equations (3-5) and (3-6), over all possible solid angles. Hence, from Equations (3-8) and (3-9), the total flux in the continuum is

$$F_T^c(0,\lambda_m) = \frac{1}{\pi} \int_{\phi=0}^{\phi=2\pi} \int_{\theta=0}^{\theta=\pi/2} I_T^c(0,\mu) \cos\theta \sin\theta \, d\theta d\phi$$

or

$$F_T^c(0,\lambda_m) = 2 \sum_{i=1}^{n} a_i \{ \int_o^\infty S_i^c [\int_{y=1}^{y=\infty} e^{-\tau_i^c y} \frac{dy}{y^2}] d\tau_i^c \}, \qquad (3\text{-}14)$$

where $y = 1/\mu$. Likewise, the flux in the line becomes,

$$F_T^\ell(0,\Delta\lambda) = 2 \sum_{i=1}^{n} a_i \{ \int_o^\infty S_i [\int_{y=1}^{y=\infty} e^{-\tau_i y} \frac{dy}{y^2}] d\tau_i \}. \qquad (3\text{-}15)$$

The quantity in brackets is simply the second exponential integral function [see Equation (A-14)]. So Equation (3-14) and Equation (3-15) may now be written as

$$F_T^c(0,\lambda_m) = \sum_{i=1}^{n} 2a_i \int_{-\infty}^{\infty} S_i^c E_2(\tau_i^c) \frac{K_i^c}{K_o^c} (\frac{10^x}{\log e}) dx, \qquad (3\text{-}16)$$

and

$$F_T^\ell(0,\Delta\lambda) = \sum_{i=1}^{n} 2a_i \int_{-\infty}^{\infty} S_i E_2(\tau_i^c + \tau_i^\ell) \frac{K_i}{K_o^c} (\frac{10^x}{\log e}) dx . \qquad (3\text{-}17)$$

The line depth in flux is then

$$R_\lambda(\mu) = \frac{F_T^c(0,\lambda_m) - F_T^\ell(0,\Delta\lambda)}{F_T^c(0,\Delta\lambda_m)}, \text{ or}$$

$$R_\lambda(\mu) = \sum_{i=1}^{n} \frac{2a_i}{F_T^c(0,\Delta\lambda_m)} \int_{-\infty}^{\infty} [S_i^c \, E_2(\tau_i^c) \frac{K_i^c}{K_o^c} -$$

$$S_i \, E_2(\tau_i^c + \tau_i^\ell) \frac{K_i^c}{K_o^c}] \left(\frac{10^x}{\log e}\right) dx \, .$$

Using Equation (3-10) this expression becomes

$$R_\lambda(\mu) = \int_{-\infty}^{\infty} [\sum_{i=1}^{n} \frac{2a_i \, S_i^c \, E_2(\tau_i^c)}{F_T^c(0,\lambda m)} \{1 - \frac{(1+\rho_i\beta) \, E_2(\tau_i^c + \tau_i^\ell)}{E_2(\tau_i^c)}\}$$

$$\cdot \frac{K_i^c}{K_o^c} \left(\frac{10^x}{\log e}\right)] \, dx \, . \qquad (3\text{-}18)$$

The solution of the line depth Equation (3-18) is based upon the method of the Planckian gradient of Mugglestone (1958) and later modified by Evans (1969, 1971). The method uses an integration by parts of the flux Equations (3-14) and 3-15) for the line and the continuum. The general form of these equations is

$$\psi = 2 \int_o^\infty S(\tau) \, E_2(\tau) \, d\tau \, .$$

Letting $u = S(\tau)$, $dv = E_2(\tau)$

then $du = \frac{dS(\tau)}{d\tau} d\tau = \frac{d \, S(\tau)}{d \, (\log \tau)} \frac{d \, (\log \tau)}{d\tau} = \frac{dS(\tau)}{dx} dx,$

$$v = -E_3(\tau) \, .$$

The previous integral then becomes

$$\psi = S(0) + 2 \int_{-\infty}^{\infty} \frac{dS}{dx} \cdot E_3(\tau)\, dx \ . \qquad (3\text{-}19)$$

From the results of Equation (3-19), the Planckian gradient form of the line depth becomes

$$R_\lambda(\mu) = \sum_{i=1}^{n} \frac{a_i}{F_T^c(0,\lambda m)} \{(S_i^c(0) - S_i^\ell(0)) + 2 \int_{-\infty}^{\infty} \frac{dS_i^c}{dx} E_3(\tau_i^c) \left[1 - \Phi_i \frac{E_3(\tau_i^c + \tau_i^\ell)}{E_3(\tau_i^c)}\right] dx\} \ , \qquad (3\text{-}20)$$

where $\Phi_i = \frac{dS_i^\ell}{dx} / \frac{dS_i^c}{dx}$. Under the same restrictions used to calculate the intensity form of the line depth, the following conditions will be assumed: (a) the source function in the line and in the continuum is the Planck function; (b) the optical depth in the continuum is the same for all cells. Thus, the Planckian gradient form of the line depth, Equation (3-20), may be expressed as

$$R_\lambda(\mu) = \int_{-\infty}^{\infty} \{ \sum_{i=1}^{n} \frac{2a_i}{F_T^c(0,\lambda m)} \frac{dB}{dx} E_3(\tau^c)\left[1 - \frac{E_3(\tau^c + \tau_i^\ell)}{E_3(\tau_i^c)}\right]\} dx \ ,$$

or,

$$R_\lambda(\mu) = \frac{2}{F_T^c(0,\lambda m)} \int_{-\infty}^{\infty} \frac{dB}{dx} E_3(\tau^c)\left[1 - \sum_{i=1}^{n} \frac{a_i\, E_3(\tau^c + \tau_i^\ell)}{E_3(\tau^c)}\right] dx \ .$$

If the macroturbulent cells are assumed to produce a velocity dispersion function, the expression in the bracket may be replaced by a weighted mean for the line optical depth (Evans, 1971), so that the expression for the line depth becomes

$$R_\lambda(\mu) = \frac{2}{F_T^c(0,\lambda m)} \int_{-\infty}^{\infty} \frac{dB}{dx} E_3(\tau^c)\left[1 - \frac{E_3(\tau^c + \sum_{i=1}^{n} a_i \tau_i^{\ell})}{E_3(\tau^c)}\right]dx. \quad (3\text{-}21)$$

The Metal Line Absorption Coefficient

For the computation of the metal lines, turbulence pressure was ignored; only broadening mechanisms giving rise to Gaussian profiles or Lorentz profiles are included. Assuming an isotropic distribution of turbulent elements obeying a Maxwellian velocity distribution, microturbulence produces a Doppler broadening similar to thermal motions.

Besides the thermal and microturbulent Doppler broadening, the line absorption coefficient includes natural, Stark, and van der Waals broadening. Magnetic interactions have been neglected as well as rotational broadening although macroturbulence broadening could be made to simulate the latter effect. The profile of a line that results from a thermal Doppler effect is a Gaussian profile while that from natural or pressure broadening is a dispersion profile. Assuming a statistical independence of each broadening mechanism, the convolution of the Gaussian and dispersion profiles results in the Voight profile for the shape of the absorption coefficient per absorbing particle (Unsöld, 1955; Aller, 1963). Considering only Doppler broadening, the random thermal agitation in a stellar atmosphere is increased by any microturbulence, and the most probable velocity of the atoms is given by

$$v_{mp} = \sqrt{\varepsilon_{th}^2 + \varepsilon_{mt}^2}\ , \quad (3\text{-}22)$$

where

ε_{th} = the most probable thermal velocity,

$= \sqrt{2kT/m} = \sqrt{2RT/\mu_i} = \sqrt{83.83/(\mu_i \theta)}$.

ε_{mt} = the most probable velocity of the microturbulence.

The 1/e width of the resulting Gaussian profile is given by the Doppler width

$$\Delta\lambda_D = \frac{\lambda}{c} v_{mp} = \frac{\lambda}{c} \sqrt{\left(\frac{2kT}{m}\right) + \varepsilon_{mt}^2} . \qquad (3\text{-}23)$$

Since the convolution of two Lorentz profiles again yields a Lorentz profile whose width is equal to the sum of the widths of the convoluted functions, the half-width of the dispersion profile for the other broadening mechanisms is just the sum of the half-widths due to natural, Stark and van der Waals broadening,

$$\Gamma_T(x) = \Gamma_{rad} + \Gamma_{Stark} + \Gamma_{van\ der\ Waals} . \qquad (3\text{-}24)$$

The radiation damping constant is obtained through classical means while the Stark broadening due to hydrogen and helium as well as van der Waals broadening by ions and electrons are approximated using the Lindholm theory as a basis (Evans, 1966). The line absorption coefficient per hydrogen particle is computed from the absorption coefficient per absorbing particle by multiplying by the number of absorbing particles per hydrogen particle,

$$K^{\ell} = \left(\frac{n_{n,m}}{N_H}\right) K_{atomic} . \qquad (3\text{-}25)$$

For the case of doublets, the blending is calculated by adding the absorption coefficients for each line. More of the details of the metal line absorption coefficient can be found in Appendix B.

The Theoretical Curve of Growth

The curve of growth method is a concept representing the behavior of the equivalent width of a stellar spectral line as the number of effective absorbers in the stellar atmosphere changes. For computational ease, the theoretical curve of growth will be defined as a plot of the saturated equivalent width as a function of the unsaturated equivalent width (Aller, Elste, and Jugaku, 1957; Aller, 1960; Aller, 1963). The unsaturated equivalent width is defined as

$$\left(\frac{W}{\lambda}\right)^{*} = \int_{-\infty}^{\infty} \frac{K^{\ell c}}{K_{o}} \left(\frac{\tau_{o}}{\log e}\right)\left(1 - 10^{-\chi_{\lambda m}\theta}\right) G_{\lambda m}\, dx \,, \qquad (3\text{-}26)$$

where $K^{\ell c}$ = the absorption coefficient at the line center,

$G_{\lambda m}$ = the flux weight function (see Appendix B).

The flux weight function has the advantage that it depends only upon the model atmosphere chosen and so can be computed once and for all for the various wavelength regions covering the observed spectrum. For weak lines the logarithm of the saturated equivalent width is proportional to the logarithm of the unsaturated equivalent width so that it is more convenient to plot these quantities for the theoretical curve of growth. The relative abundance can be removed from Equation (3-26) to get

$$\log (W/\lambda)^* = \log \varepsilon + \log C_\lambda \ , \qquad (3\text{-}27)$$

where

$$\log C_\lambda = \log \{ \int_{-\infty}^{\infty} \frac{K^{\ell c}}{K_o^c \ \varepsilon} \left(\frac{\tau_o}{\log e}\right)\left(1 - 10^{-x_{\lambda m}\theta}\right) G_{\lambda m} dx \}, \qquad (3\text{-}28)$$

and

ε = the abundance of the element relative to hydrogen,

= N/N(H) .

The saturated equivalent width describes the total absorption of a spectral line and is represented by the area of a strip which removes the same amount of energy from the continuum as the spectral line. In the logarithmic form this can be expressed in terms of the line depth as

$$\log (W/\lambda) = \log \left[\frac{1}{\lambda} \int_o^{\infty} R_\lambda(\mu) \, d\lambda \right] , \qquad (3\text{-}29)$$

where $R_\lambda(\mu)$ is defined in Equation (3-21).

The Metal Line Program

For the analysis of the absorption lines, both the line profile and curve of growth are calculated with the aid of a computer program devised by Evans (1966, 1971, 1972). Details of the computations can be found in Appendix B. For each observed line, the program calculates from three to nine points on the curve of growth. The abundance for the observed equivalent width is then estimated from this curve of growth and the result is used to calculate the line depth and the median point of the line depth integrand for a range of different values of $\Delta\lambda$. In addition to this it also supplies the

optical depth in the line, the damping parameters, the Doppler width at the median point, the half-width of the line profile, a plot of the theoretical line profile, and the model atmosphere and turbulence model chosen for the analysis. For a model atmosphere consisting of from one to ten elements, the program can compute, element by element, equivalent width and line profiles for as many lines as are needed for the analysis.

Chemical Abundances and Empirical Curve of Growth

If one is provided with an equivalent width, a set of oscillator strengths and an atmospheric model, the stellar abundance of an element can be determined. The process is basically an interpolation between the observed equivalent width and the theoretically calculated value. From Equation (3-26), it is readily seen that it is most advantageous to define an empirical curve of growth as a plot of the logarithm of the saturated equivalent width as the ordinate and the quantity

$$\log C_\lambda = \log \{g_{r,s} f_{r,s} \lambda\} + \log L^*_\lambda(\chi_{r,s}), \qquad (3\text{-}30)$$

as the abscissa. Equation (3-30) is obtained directly from Equation (B-22) utilizing the fact that $L^*_\lambda(\chi_{r,s})$ is independent of the variable of integration and the definition of $\log L^*_\lambda(\chi_{r,s})$ is

$$\log L^*_\lambda(\chi_{r,s}) \equiv \log \frac{\pi}{c} \int_{-\infty}^{\infty} \left(\frac{\Delta\lambda_D}{\lambda}\right) M(x)\, N_i(x) \left[1-10^{-\chi_\lambda m^\theta}\right] dx + \Delta\chi\theta \, . \qquad (3\text{-}31)$$

The empirical curve of growth can be fitted to the theoretical curve of growth by a horizontal translation. The amount of displacement then yields the relative abundance, $\log \varepsilon = \log N/N(H)$. Each point on the theoretical curve of growth represents an observed spectral line; and each line has its own theoretical curve of growth; consequently, its own abundance. Because in practice the curves of growth for many lines in certain spectral regions have the same shape, it is of use to define a mean abundance, derived from a mean curve of growth. The mean curve of growth is determined by fitting the empirical curve of growth for all the observed spectral lines falling within a wavelength region to the theoretical curve of growth for a representative line of the group. For a solar-type star, this procedure can be applied over wavelength regions of hundreds of angstroms. To aid in this investigation, the abundance determination for an element was automatically produced by a computer program (Evans, 1971, 1974).

The Abundance Program

Basically an adaptation of the metal line program, the abundance program will compute, for a single theoretical curve of growth, the abundance of from one to fifty individual lines. A turbulence model incorporating both the line broadening effects due to macroturbulent and microturbulent motions can be varied at will to alter the abundance results. The program supplies the abscissa for the empirical curve of growth from which the empirical curve of growth can be constructed for the determination of the mean abundance. In addition a statistical weighting factor may be used for the computation of a mean weighted

abundance for an element. The details of this calculation may be found in Appendix B.

CHAPTER IV

OBSERVATIONAL MATERIAL

The Spectrograms

The spectrograms used in this study were made at the coudé focus of the 84-inch telescope at Kitt Peak National Observatory in June of 1971 by Drs. Leon Schroeder and Ronald Oines both of Oklahoma State University, and Dr. John Evans of George Mason University. Kitt Peak National Observatory is operated by the Association of Universities for Research in Astronomy, Inc. (AURA). Table II contains data on the spectrograms and on the spectrograph and cameras used to record them.

The spectrograms themselves are between 975Å and 1600Å wide and were exposed on 28 inches of photographic plate, each of which was divided into two ten-inch segments and one eight-inch segment. The first 28 inch plate (D2837) contains the absorption spectrum from about 3405Å to about 5000Å. The second plate (D2829) contains the absorption spectrum from about 3613Å to about 4950Å. Finally, the last plate (D2836) contains the absorption spectrum from about 4525Å to about 6959Å.

TABLE II

DATA FOR 84-INCH COUDÉ SPECTROGRAPH

Plate D2829:

Slit Width: 0.075 millimeter

Decker Dimensions: Decker 9

Stellar length: 1.16 millimeter or 3.6 seconds
Comparison length (inner): 1.78 millimeter
Comparison length (outer): 5.29 millimeter

Grating "C":

Bausch and Lomb No. 33-53-36-35, ruled with two diamonds
Ruled area: 204 x 254 millimeter
Grooves per millimeter: 600
Blaze: 8000Å (1st order)
Ghost intensity: 0.06% of parent line

CAMERA: 6

Grating tilt: 7935
Plate position: 46.0
Central wavelength: 4400Å
Focus: 60.60
Tilt: 4.15
Emulsion: II a-O
Exposure meter count: 15988
Calibration: Sensitometer, 5-74 filter; Neutral density factor x 100; Exposure time 21 minutes.
Developer: D-19 for 4 minutes

f-ratio: f/16
Focal length: 143.8 inches
Demagnification from slit to plate: 1.88
Dispersion (2nd order blue): 2.2 Å/mm
Plate width: 27/32 inches
Plate length: 28 inches
Starlight exposure time: 39 minutes
Iron arc comparison exposure time: 10 sec (no filter)
Temperature in spectrograph room: 61°F

POSITION OF STAR:

$\alpha(1970) = 15^h26^m35^s$
$\delta(1970) = 29^o12'$

OBSERVING CONDITIONS:

Seeing: 1
Trans: 4
Photographic apparent magnitude: +3.93

TABLE II (Continued)

Plate D2836:

Slit Width: 0.075 millimeter

Decker Dimensions: Decker 9

Stellar length: 1.16 millimeter or 3.6 seconds
Comparison length (inner): 1.78 millimeter
Comparison length (outer): 5.29 millimeter

Grating "C":

Bausch and Lomb No. 33-53-36-35, ruled with two diamonds
Ruled area: 204 x 254 millimeter
Grooves per millimeter: 600
Blaze: 8000Å (1st order)
Ghost intensity: 0.06% of parent line

CAMERA: 6

Grating tilt: 8056
Plate position: 46.0 (low)
Central wavelength: 5400Å
Focus: 60.60
Tilt: 4.15
Emulsion: II a-F
Exposure meter count: 50981
Calibration: Sensitometer, 4-102 filter; Neutral density factor x 100; Exposure time 34 minutes
Developer: D-19 for 4 minutes
f-ratio: f/16
Focal length: 143.8 inches
Demagnification from slit to plate: 1.88
Dispersion (1st order blue): 4.4 Å/mm
Plate width: 27/32 inches
Plate length: 28 inches
Starlight exposure time: 2^h03^m
Neon arc comparison exposure time: 120 seconds
Iron arc comparison exposure time: 10 seconds (no filter)
Temperature in spectrograph room: 61^oF

POSITION OF STAR:

$\alpha(1970) = 15^h26^m35^s$
$\delta(1970) = 29^o12'$

OBSERVING CONDITIONS:

Seeing: 0.8-1
Trans: 2-3
Photographic apparent magnitude: +3.93

TABLE II (Concluded)

Plate D2837:

Slit Width: 0.075 millimeter

Decker Dimensions: Decker 9

Stellar length: 1.16 millimeter or 3.6 seconds
Comparison length (inner): 1.78 millimeter
Comparison length (outer): 5.29 millimeter

Grating "C":

Bausch and Lomb No. 33-53-36-35, ruled with two diamonds
Ruled area: 204 x 254 millimeter
Grooves per millimeter: 600
Blaze: 8000Å (1st order)
Ghost intensity: 0.06% of parent line

CAMERA: 6

Grating tilt: 7949
Plate position: 46.0 (low)
Central wavelength: 4200Å
Focus: 60.60
Tilt: 4.15
Emulsion: II a-O
Exposure meter count: 18574
Calibration: Sensitometer, 5-74 filter; Neutral density factor x 100; Exposure time 21 minutes
Developer: D-19 for 4 minutes

f-ratio: f/16
Focal length: 143.8 inches
Demagnification from slit to plate: 1.88
Dispersion (2nd order blue): 2.2 Å/mm
Plate width: 27/32 inches
Plate length: 28 inches
Starlight exposure time: 42 minutes
Iron arc comparison exposure
Temperature in spectrograph room: 61°F

POSITION OF STAR:

$\alpha(1970) = 15^h26^m35^s$
$\delta(1970) = 29^o12'$

OBSERVING CONDITIONS:

Seeing: 0.8-1
Trans: 2-3
Photographic apparent magnitude: +3.93

The Intensity Tracings

Nine intensity tracings covering the wavelength range λλ3405-6959 were made by the author in May 1972 with the Hilger-Watts Direct Intensity Microphotometer (Model L-470) at Kitt Peak National Headquarters in Tucson, Arizona at a carriage speed of 0.50 mm/minute resulting in a plate-to-chart magnification of 102.5/1. Table III below gives the pertinent data for the settings on the microphotometer when the tracings were made.

TABLE III

DATA FOR MICROPHOTOMETER (D2829,D2836,D2837)

Reference Current:	0.60 milliamps
Slit Rotation Setting:	28.5
Slit Length Setting:	2.75
Slit Width Setting:	12
Brown Recorder Gear Ratio:	80/40

Location of the Continuum

The continuum was drawn directly on the intensitometer tracings as an average of the galvanometer deflections due to the plate grain in the regions between the spectral lines. Figure 2 is a small portion of one of the direct intensity tracings (D2829) and shows the location of the continuum. The microphotometer automatically sets the reference level which is displayed as the zero level at the bottom of the tracings.

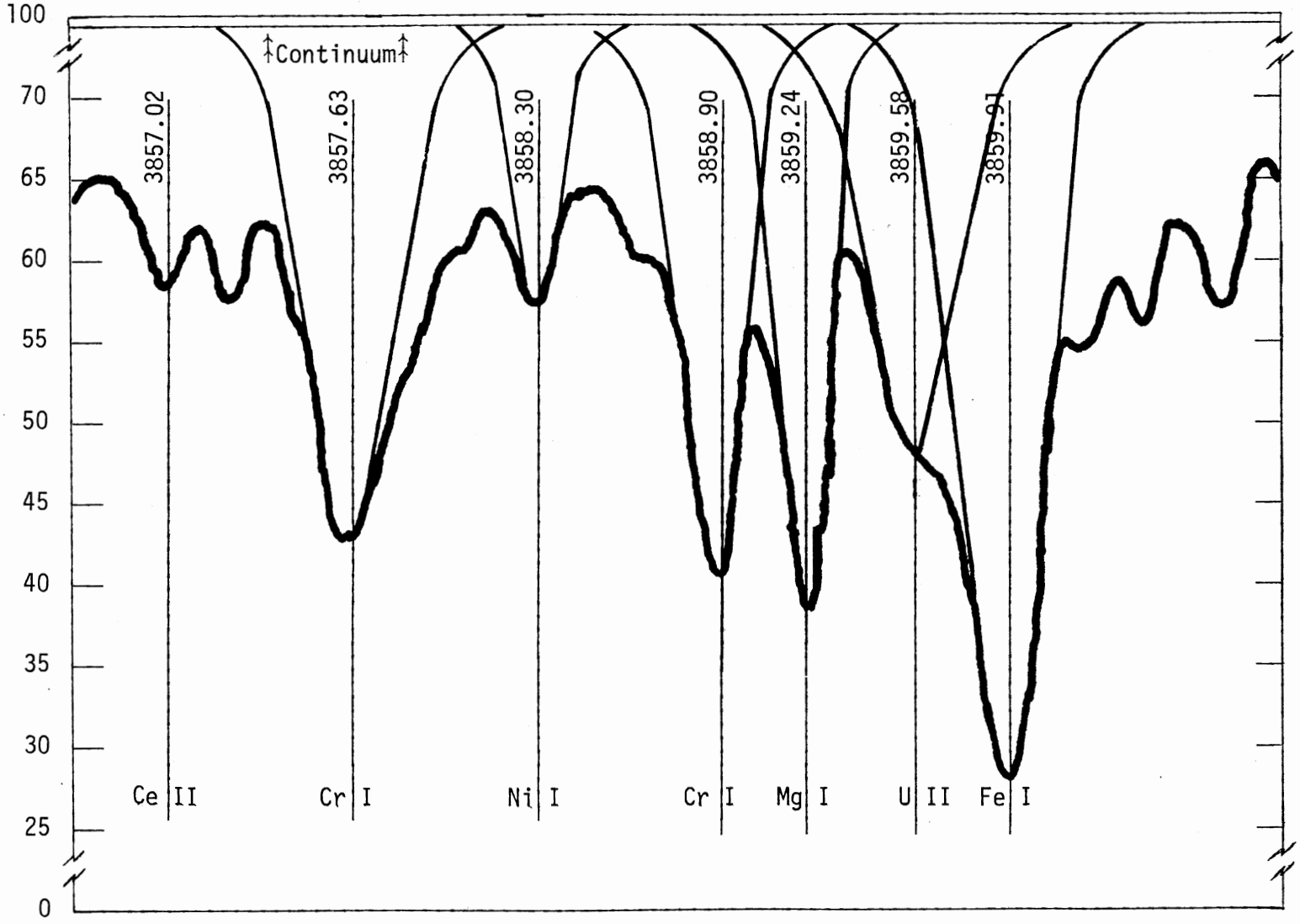

Figure 2. Scale Drawing of Microphotometer Tracing

Approximation of the Profiles

Theory indicated that the shape of the wings exhibited by the stronger lines should be inversely proportional to the square of ν_D, the distance from the line center in units of the Doppler width. An attempt was made to take this into account when drawing the profiles of the stronger lines as shown in Figure 2. The shapes of the wings were readily apparent for very strong lines, especially when there were no nearby lines to produce blending effects in the wings. When blending was serious, however, the wings were roughly approximated.

Identification of the Spectral Lines

The line listing used in this investigation was compiled by the author in 1974. The list was prepared from the work of W. A. Hiltner (1945), J. Gruber (1972) and T. Jordan (1974). The sources used in their investigations were A Multiplet Table of Astrophysical Interest, Revised Edition; National Bureau of Standards Monograph 32; MIT Wavelength Tables; Optical Society of America, Journal; National Bureau of Standards Journal of Research; Spectrochimica Acta; Joint Establishment for Nuclear Energy Research; Adelman (1974) and others.

Determination of Equivalent Widths

The determination of equivalent widths first involves measurement of the area enclosed by the line profile and the continuum. These areas were obtained using an Ott rolling disc planimeter. The continuum height (H_c) was taken as the average of the values

adjacent to the line. For each tracing the dispersion was taken at various points along the spectrum and a straight line fitted to a plot of dispersion versus wavelength. For the calculation of equivalent widths the dispersion was then read from these plots. The profile of a line is the plot of the flux at each point in the line versus the wavelength. Hence, the area enclosed by the profile and the continuum is the total amount of energy absorbed in the line. The equivalent width, then, is the width of a rectangle having the same area and with a height equal to that of the averaged adjacent continuum. These relationships are shown in Figure 3. The equivalent width was calculated in milliangstroms. Due to overlapping and duplication of the spectrograms, some lines were represented by as many as four profiles, a few by only one. The equivalent width, in all cases, was taken as the average with all measures assigned equal weight.

Figure 4 displays the various measured parameters with respect to the spectral line profiles. They are: H_c, the continuum height; h, the half-width; d_1, the central depth of the absorption line; and R_1, the residual line intensity at the line center with respect to the reference level, i.e. $R_1 = H_c - d_1$. For a representative group of lines Figure 5 compares the equivalent widths measured on different tracings. Theoretically all of the data points in Figure 5 should lie on the straight diagonal line displayed. Since the data points appear to be consistently below this line, this suggests that the estimation of the continuum was either slightly too high on tracing D2837 or slightly too low on tracing D2829.

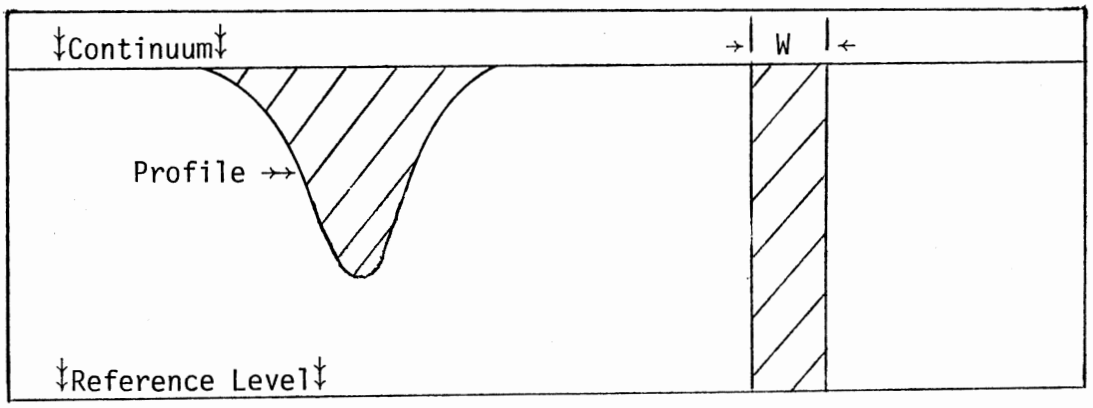

Figure 3. The Equivalent Width, W, of a Spectral Line

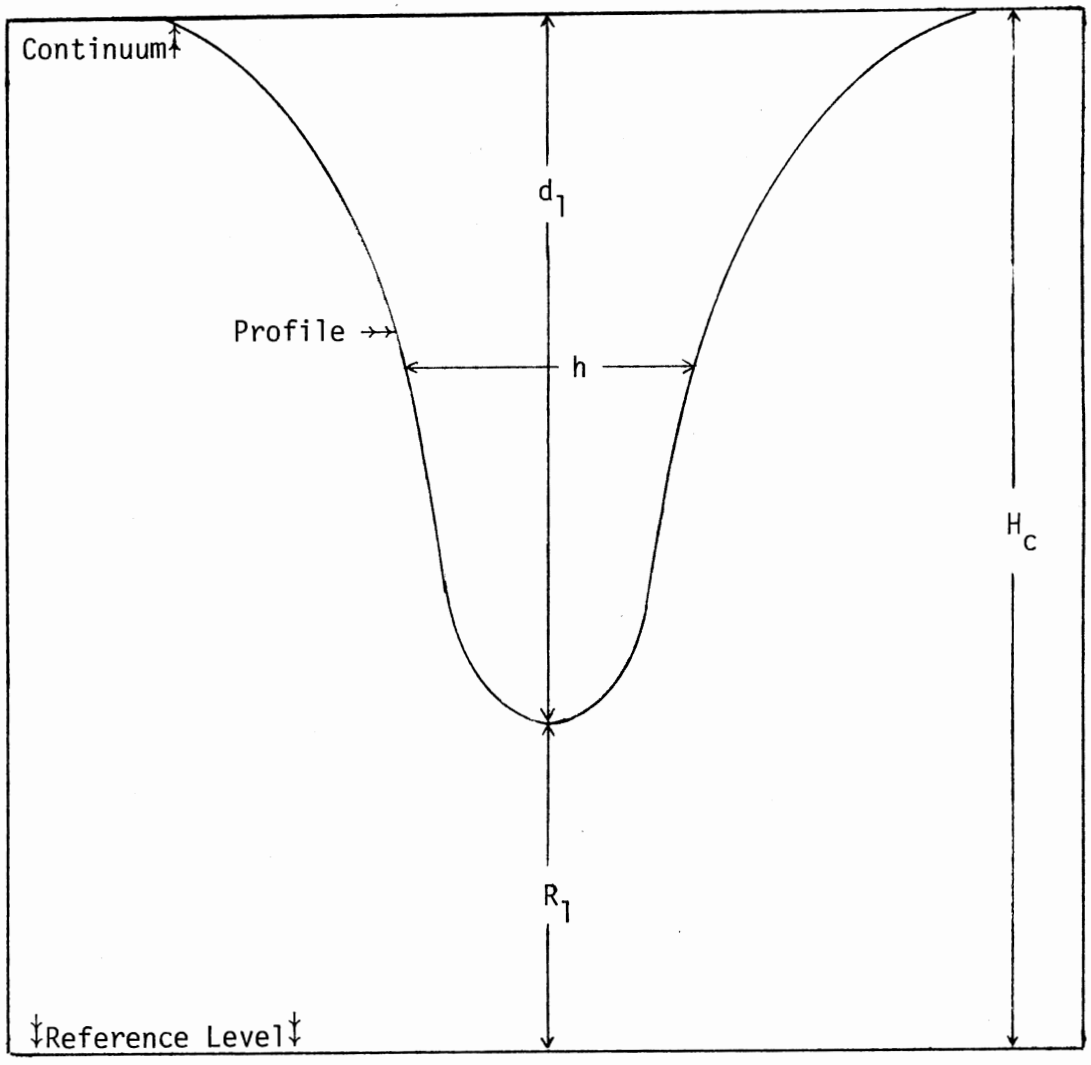

Figure 4. Measured Lines Parameters

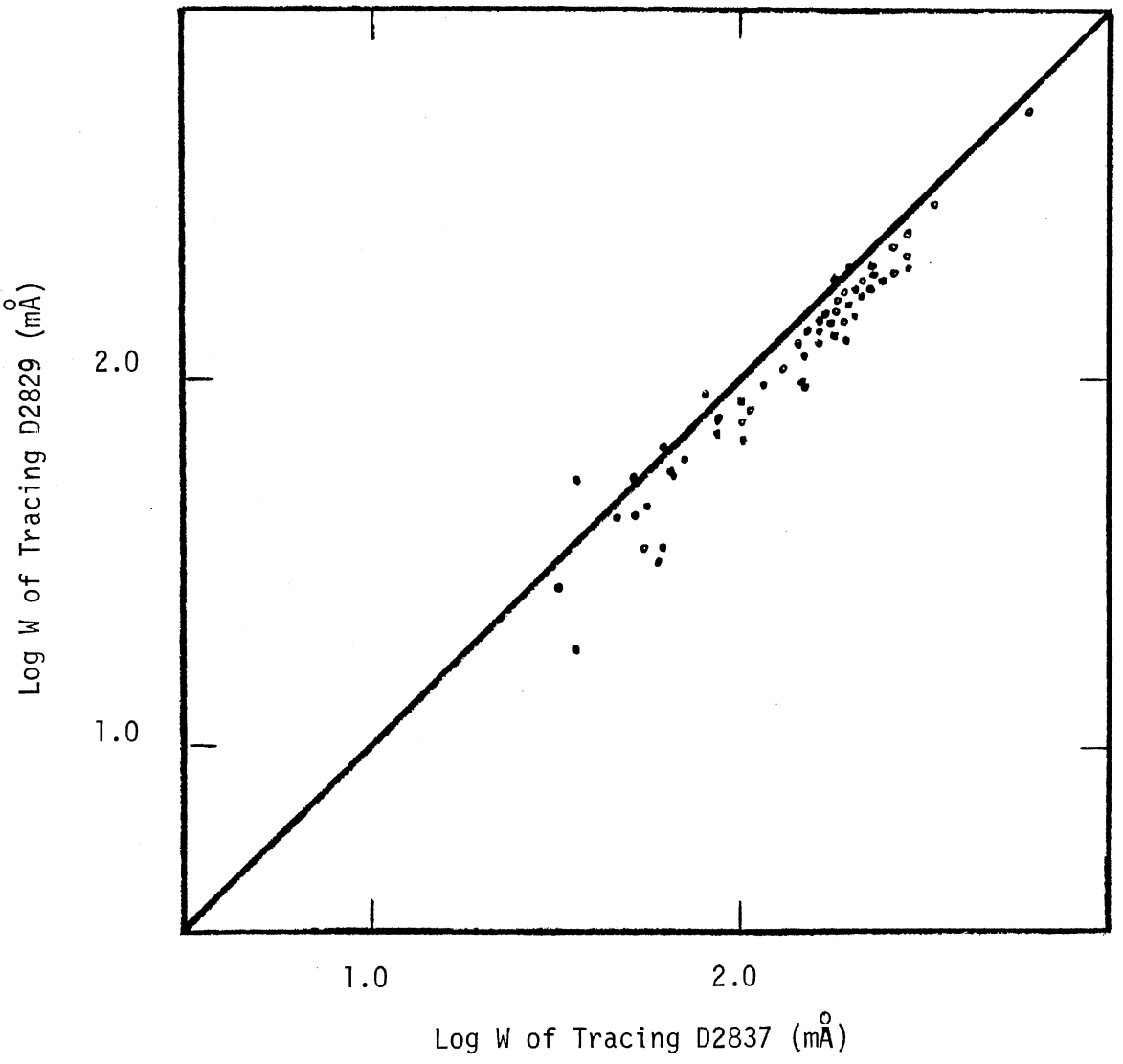

Figure 5. Comparsion of Observed Equivalent Widths Measured on Different Tracings

Raising the continuum would effectively increase the measured area contained between the profile and the continuum, thus increasing the apparent equivalent width of that spectral line.

Thackeray's (1936) relation was applied to increase the measured equivalent widths of the lines located in the wings of the Balmer lines. This relationship is given by:

$$W = W_b / r_w \ , \qquad (4\text{-}1)$$

where

W is the equivalent width of the line if no blending occurred,

W_B is the measured equivalent width referred to the wing as the continuum,

r_w is the ratio of the intensity of the wing to the intensity of the true continuum at the center of the line being studied.

Assessment of Errors

The sources of error which arise from the spectrophotometric techniques are discussed in some detail by Wright (1948). Errors due to improper focus, ghosts, calibration of the photographic plate, finite slit width of the microphotometer and the development process of the spectrograms can all be important but probably not as much as errors introduced during the reduction of the intensity tracings themselves. The location of the continuum and the treatment of blending effects are probably the most significant constituents affecting uncertainty in the equivalent width data. Typically,

the uncertainty in the equivalent widths of weak lines (on the order of 20 mÅ) can be as great as twenty percent; for moderately strong lines, the error may drop to about ten percent.

The Physical Constants

Abundances derived from the model atmosphere technique can be no better than the reliability of the system of physical constants used for the analysis. At the present time knowledge of the damping constants and oscillator strengths is still somewhat uncertain and at times conflicting. In the last few years the number of reliable oscillator strength measurements has increased dramatically, relieving some of the difficulty in the computation of stellar abundances.

The necessary atomic data, the partition functions, atomic weights, and ionization potentials were obtained from the results published by Evans (1966). The damping constants used for this analysis have been discussed elsewhere in this study (See Appendix B).

A number of authors have published results of both theoretically or experimentally determined oscillator strengths and extensive lists have been prepared in bibliographical form by Glennon and Wiese (1962) and by Miles and Wiese (1970) and by Fuhr and Wiese (1971), and more recently by Fuhr and Wiese (1973). For this study, oscillator strengths were used extensively from the work of Corliss and Bozman (1962), Corliss and Tech (1968), Warner (1967, 1968), Wiese, Smith, and Miles (1969), and Fuhr and Wiese (1973).

The results of recent investigations have given evidence for an excitation potential dependence in the log gf values reported by Corliss and Bozman (Takens, 1970) and by Corliss and Tech (Wolnik, Berthel, and Wares, 1970; Evans, Weems, and Schroeder, 1970). As a result, correction factors were employed to remove any traces of a systematic error due to the excitation level of the transition.

Wavelengths and Excitation Potentials

The wavelengths for the observed lines in the spectrum of Beta Coronae Borealis, as mentioned earlier in this study, were primarily identified from Charlotte Moore's tabulation A Multiplet Table of Astrophysical Interest, Revised Edition (1959). In addition, the excitation potential of the lower level of a transition was also obtained from the same source.

CHAPTER V

ANALYSIS OF THE OBSERVATIONAL DATA

The shape and breadth of the Fraunhofer lines in the spectrum of Beta Coronae Borealis are affected by the various line broadening agents mentioned in Chapter III. For Beta Coronae Borealis, one important contributor is atmospheric turbulence. The existence of microturbulence can best be determined from the curve of growth. Microturbulence produces an effective Doppler broadening which tends to delay the onset of optical saturation and affects the transition region of the curve of growth. Huang and Struve (1960) discuss this effect in some detail in their reviews on atmospheric turbulence. On the other hand, if the scale of the turbulence is large the effect upon the equivalent width is negligible but the line profile will be altered as by stellar rotation.

From the analysis of the profile of a line, Huang and Struve (1952) first developed a method for the separation of these two broadening mechanisms. Through a curve of half-width correlation, a plot of the functional dependence of the half-width of a spectral line upon its equivalent width, they developed a procedure whereby a shift in the vertical and horizontal axes necessary to fit the empirical to the theoretical curve could be used to derive a value for both large and small scale turbulent effects. Van den Heuvel (1963) and Elste (1967) have employed a similar curve to distinguish

between macroturbulence and microturbulence. However, their approach calculates the theoretical relation using a model atmosphere, and so gives a more exact relationship between log (h/λ) and log (W/λ) than did Huang and Struve. This approach will be used here with a model atmosphere provided by Dr. John C. Evans of George Mason University for a similar A-star, Gamma Equulei. One might note here again that Beta Coronae Borealis has a slow rotational velocity of less than or equal to three (3) kilometers per second (Adelman and Shore, 1973; Preston, 1971) and consequently has very sharp spectral lines. This would suggest that the velocity broadening effects would be of negligible importance for macroturbulence as compared to the thermal and microturbulent broadening effects.

The Microturbulence Analysis

Line intensities for sixty-four neutral and singly ionized lines of iron were used for the curve of growth analysis. The results have been incorporated into Table XXI and Table XXII for convenience.

The f-values for the neutral iron lines were taken from the compilation of Corliss and Tech (1968). Since these f-values have been shown to contain a systematic dependence upon the excitation potential (Wolnik, Berthel, and Wares, 1970; Evans, Weems, and Schroeder, 1970) an attempt was made to correct for this uncertainty using the results of Evans, Weems, and Schroeder. For multiplets of Fe I falling within the wavelength region of λ4200, the f-values were lowered by 0.5 dex* for those multiplets with χ_ℓ greater than

*The notation 0.5 dex corresponds to the quantity log x = 0.5.

2.2 eV. Multiplets with χ_ℓ less than 1.5 eV were left unchanged. The correction factor for all cases was determined by decreasing or increasing the f-values of all multiplets until the data defined a single curve of growth. The oscillator strengths for the Fe II lines were obtained from the results published by Warner (1967, 1968).

The curves of growth for iron are shown in Figures 6 through 8. All curves of growth have been computed for the center of the star's disk.

In Figures 6 and 7 the lower curves represent the curves of growth for Fe I for the wavelength regions λ4200 and λ5150 respectively, broadened only by the random thermal motion of the atoms in the stellar atmosphere, i.e., with zero microturbulence. The fact that the data lies on both sides of this curve indicates that the macroturbulent velocity of the region is small, if it exists at all. The upper curve, which is labeled with a 1.50 kilometer per second microturbulent velocity, seems to represent the average value over this wavelength range.

Figure 8 represents the curve of growth of Fe II for the wavelength region λ4600. In this figure the curve of growth has been calculated for a thermally broadened line (lower curve) and a curve incorporating a 1.50 kilometer per second microturbulent velocity (upper line). Again the data suggest that a value closer to 1.50 kilometers per second represents the best estimate for all lines in this region due to small scale eddies. The microturbulent velocity fields used for the computation of the theoretical curves of growth were based upon a thermally homogeneous model independent of the optical depth in the stellar atmosphere. This procedure eliminates

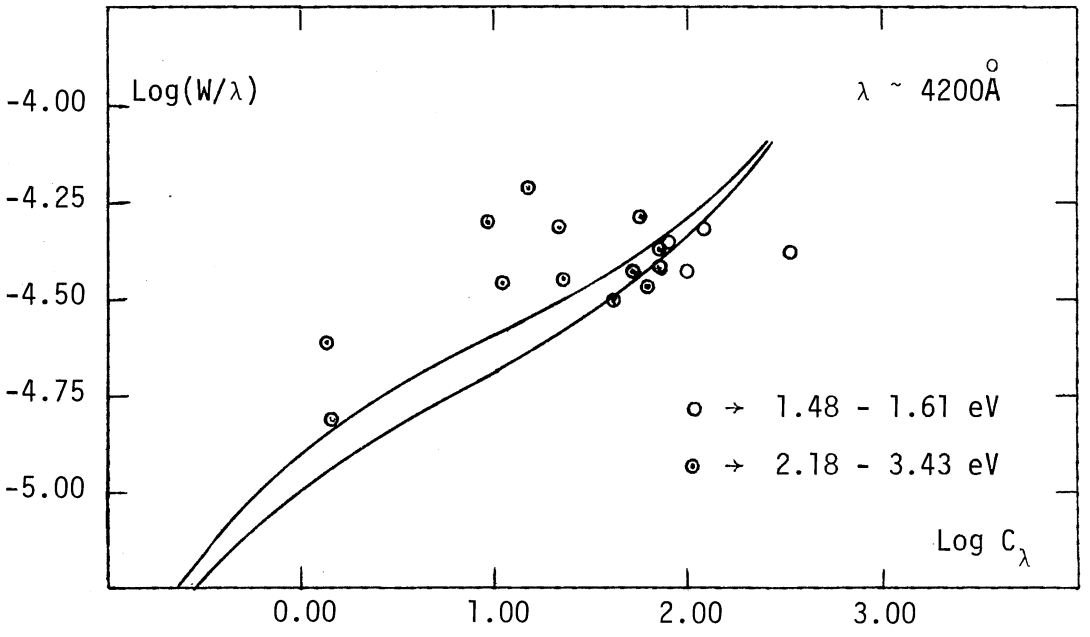

Figure 6. The Observed and Theoretical Center-of-the Disk Curves of Growth for Lines in the Wavelength Region λ4200 for Fe I

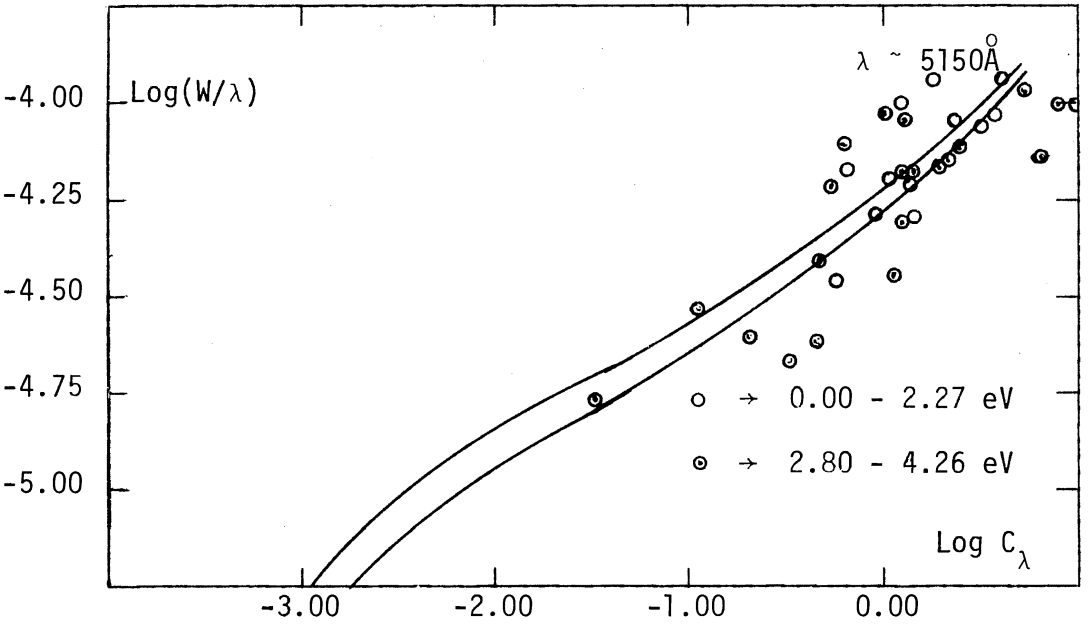

Figure 7. The Observed and Theoretical Center-of-the Disk Curves of Growth for Lines in the Wavelength Region λ5150 for Fe I

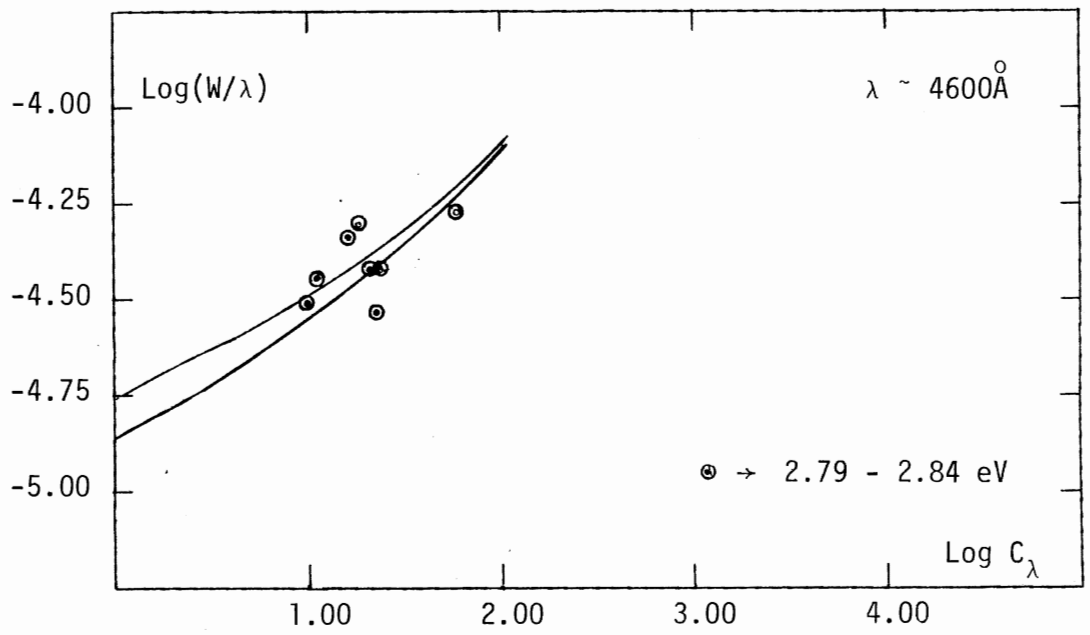

Figure 8. The Observed and Theoretical Center-of-the-Disk Curves of Growth for Lines in the Wavelength Region λ4600 for Fe II

any microturbulent velocity stratification in the stellar atmosphere and so the microturbulent velocity, as evaluated from the curve of growth technique, represents a value averaged over all layers of the atmosphere. A microturbulence value of 1.50 kilometers per second is incorporated in all subsequent calculations.

The Abundance Analysis

The ratio of the abundance of an element to hydrogen was computed for each individual observation according to the procedures outlined in Chapter III. The solar-type model atmosphere, (see Chapter II) with an effective temperature of 7700 ^{o}K and log g = 3.5, was used for the analysis employing a turbulence model having a depth independent microturbulent velocity of 1.50 kilometers per second.

The observational and calculated data are listed in Tables IV through XXXI in increasing order of ionization and atomic number. In order, the captions list element, multiplet number, wavelength in angstroms, excitation potential of the lower level in eV, the logarithm of the product of the statistical weight and the oscillator strength, the abscissa for the empirical curve of growth, the calculated value of the logarithm of the unsaturated equivalent width, the logarithm of the observed saturated equivalent width, the weight assigned to the line, and the calculated logarithm of the abundance of the element relative to hydrogen. The application of a weighting procedure allows for the computation of a weighted mean abundance for all lines of an element.

The following criteria were used to assign weighting factors to the spectral lines for the purpose of calculating the mean abundances.

TABLE IV

ABUNDANCE RESULTS FOR Na I

Element	RMT	λ	χ(R,S)	Log gf	Log gfλ	Log C	Log (W/λ)*	Log (W/λ)	Wt.	Log N/N(H)
Na I	1	5889.95	0.00	+0.12	-4.1099	3.0745	-2.1542	-4.2561	3.	-5.2287
Na I	1	5895.92	0.00	-0.18	-4.4094	2.7749	-2.4020	-4.3488	3.	-5.1769
Na I	6	5688.19	2.10	-1.37	-5.6150	0.0703	-2.6751	-4.3895	2.	-2.7455
Na I	6	5688.20	2.10	-0.42	-4.6650	1.0203	-2.6751	-4.3895	2.	-3.6955

TABLE V

ABUNDANCES RESULTS FOR Mg I

Element	RMT	λ	χ(R,S)	Log gf	Log gfλ	Log C	Log (W/λ)*	Log (W/λ)	Wt.	Log N/N(H)
Mg I	2	5167.32	2.70	-0.86	-5.1467	1.6939	-1.5085	-3.9133	3.	-3.2024
Mg I	2	5172.68	2.70	-0.38	-4.6663	2.1744	-1.5132	-3.9153	3.	-3.6876
Mg I	2	5183.60	2.70	-0.16	-4.4454	2.3953	-1.5199	-3.9181	3.	-3.9151
Mg I	3	3829.35	2.70	-0.21	-4.6269	2.4103	-2.2473	-4.1559	1.	-4.6576
Mg I	3	3832.30	2.70	-0.33	-4.7465	2.2907	-2.1046	-4.0981	1.	-4.3952
Mg I	10	4730.03	4.33	-0.12	-4.4451	1.2972	-4.4184	-4.8451	2.	-5.7156

TABLE VI

ABUNDANCE RESULTS FOR Mg II

Element	RMT	λ	χ(R,S)	Log gf	Log gfλ	Log C	Log (W/λ)*	Log (W/λ)	Wt.	Log N/N(H)
Mg II	5	3850.40	8.83	-1.81	-0.7928	-0.7928	-4.2666	-4.7802	1.	-3.4738
Mg II	10	4390.58	9.96	-0.53	-4.8875	-0.3192	-3.7726	-4.6325	3.	-3.4534

TABLE VII

ABUNDANCE RESULTS FOR Si I

Element	RMT	λ	χ(R,S)	Log gf	Log gfλ	Log C	Log (W/λ)*	Log (W/λ)	Wt.	Log N/N(H)
Si I	2	3905.53	1.90	-1.00	-5.4083	2.0900	-4.7261	-4.9662	2.	-6.8161
Si I	9	5793.13	4.91	-1.48	-5.7171	-0.7162	-3.0834	-4.5506	1.	-2.3673
Si I	10	5690.47	4.91	-1.86	-6.1049	-1.0528	-3.0155	-4.5078	1.	-1.9627
Si I	16	5948.58	5.06	-1.24	-5.4656	-0.5742	-3.0240	-4.5322	3.	-2.4498

TABLE VIII

ABUNDANCE RESULTS FOR Si II

Element	RMT	λ	χ(R,S)	Log gf	Log gfλ	Log C	Log (W/λ)*	Log (W/λ)	Wt.	Log N/N(H)
Si II	1	3853.66	6.83	-1.61	-6.0241	0.1882	-3.0659	-4.3629	2.	-3.2541
Si II	1	3862.59	6.83	-0.90	-5.3131	0.8992	-3.0959	-4.3722	2.	-3.9952
Si II	3	4130.88	9.80	+0.46	-3.9240	0.4011	-2.5562	-4.1310	1.	-2.9572

TABLE IX

ABUNDANCE RESULTS FOR Ca I

Element	RMT	λ	χ(R,S)	Log gf	Log gfλ	Log C	Log (W/λ)*	Log (W/λ)	Wt.	Log N/N(H)
Ca I	3	6122.22	1.88	-0.41	-4.6231	1.4271	-2.6606	-4.4742	3.	-4.0877
Ca I	3	6162.17	1.89	-0.22	-4.4303	1.6124	-2.3030	-4.3385	3.	-3.9155
Ca I	4	4454.78	1.89	+0.25	-4.1012	2.1447	-2.5107	-4.3212	3.	-4.6554
Ca I	4	4455.89	1.89	-0.51	-4.8611	1.3848	-2.8669	-4.4453	3.	-4.2517
Ca I	4	4456.61	1.89	-1.66	-6.0110	0.2349	-2.9077	-4.4584	2.	-3.1426
Ca I	9	3630.75	1.88	-0.53	-4.9700	1.4306	-2.6714	-4.3277	1.	-4.1020
Ca I	9	3644.41	1.89	-0.30	-4.7384	1.6550	-3.1809	-4.4787	1.	-4.8359
Ca I	9	3644.76	1.89	-1.03	-5.4683	0.9250	-3.3076	-4.5095	1.	-4.2327
Ca I	20	6163.76	2.51	-1.02	-5.2302	0.3501	-2.8539	-4.5360	2.	-3.2041
Ca I	20	6166.44	2.51	-0.90	-5.1100	0.4703	-2.9899	-4.5716	2.	-3.4602
Ca I	21	5581.97	2.51	-0.71	-4.9632	0.6844	-1.9938	-4.1538	2.	-2.6782
Ca I	21	5588.76	2.51	+0.21	-4.0427	1.6050	-1.9940	-4.1539	3.	-3.5989
Ca I	21	5590.12	2.51	-0.71	-4.9626	0.6851	-1.9805	-4.1468	3.	-2.6656
Ca I	21	5594.47	2.51	-0.05	-4.3022	1.3454	-1.8935	-4.1019	3.	-3.2389
Ca I	21	5598.49	2.51	-0.22	-4.4719	1.1757	-1.8672	-4.0998	3.	-3.0429
Ca I	21	5601.28	2.51	-0.69	-4.9417	0.7059	-1.7803	-4.0511	3.	-2.4862
Ca I	21	5602.85	2.51	-0.70	-4.9516	0.6961	-1.8742	-4.0930	3.	-2.5702
Ca I	23	4578.56	2.51	-0.56	-4.8993	0.8932	-3.4981	-4.6201	2.	-4.3913
Ca I	23	4581.40	2.51	-0.34	-4.6790	1.1135	-2.9302	-4.4655	2.	-4.0437
Ca I	23	4585.87	2.51	-0.19	-4.5286	1.2639	-3.4344	-4.6039	2.	-4.6982
Ca I	23	4585.92	2.51	-1.26	-5.5986	0.1939	-3.4344	-4.6039	2.	-3.6282
Ca I	48	5512.98	2.92	-0.29	-4.5486	0.7972	-1.8905	-4.1005	2.	-2.6876

TABLE X

ABUNDANCE RESULTS FOR Ca II

Element	RMT	λ	χ(R,S)	Log gf	Log gfλ	Log C	Log (W/λ)*	Log (W/λ)	Wt.	Log N/N(H)
Ca II	1	3933.66	0.00	+0.14	-4.2652	7.1792	0.9374	-2.7705	3	-6.2418
Ca II	1	3968.47	0.00	-0.16	-4.5614	6.8830	-1.0805	-3.7501	1	-7.9634
Ca II	3	3706.03	3.11	-0.46	-4.8911	4.2214	-2.1918	-4.1608	1.	-6.4132
Ca II	3	3736.90	3.14	-0.16	-4.5875	4.5031	-2.5481	-4.2971	1.	-7.0512
Ca II	15	5001.49	7.47	-0.52	-4.8209	0.9827	-2.3294	-4.2066	3.	-3.3121
Ca II	15	5019.98	7.48	-0.28	-4.5793	1.2174	-2.3806	-4.2256	3.	-3.5980
Ca II	15	5021.14	7.48	-1.22	-5.5192	0.2775	-2.7534	-4.3598	3.	-3.0308

TABLE XI

ABUNDANCE RESULTS FOR Sc I

Element	RMT	λ	χ(R,S)	Log gf	Log gfλ	Log C	Log (W/λ)*	Log (W/λ)	Wt.	Log N/N(H)
Sc I	7	4020.40	0.00	+0.39	-4.0057	2.8432	-4.3907	-4.8343	2.	-7.2339
Sc I	7	4023.69	0.02	+0.41	-3.9854	2.8485	-4.1251	-4.7515	3.	-6.9736
Sc I	7	4047.79	0.02	-0.48	-4.8728	1.9611	-3.5680	-4.6171	2.	-5.5291
Sc I	8	39.07.48	0.00	+0.44	-3.9681	2.8808	-3.8483	-4.6843	1.	-6.7292
Sc I	14	4741.02	1.43	+0.18	-4.1441	1.5152	-3.7232	-4.7014	2.	-5.2384
Sc I	21	3419.36	1.93	+0.02	-4.4461	0.5951	-2.4675	-4.4908	2.	-3.0627
Sc I	21	3429.21	1.95	+0.51	-3.9548	1.0708	-2.2652	-4.4269	2.	-3.3361
Sc I	21	3435.55	1.98	+0.96	-3.5040	1.4984	-2.5566	-4.5166	2.	-4.0550
Sc I	21	3439.41	1.95	+0.15	-4.3135	0.7121	-2.6678	-4.5464	2.	-3.3799

TABLE XII

ABUNDANCE RESULTS FOR Sc II

Element	RMT	λ	χ(R,S)	Log gf	Log gfλ	Log C	Log (W/λ)*	Log (W/λ)	Wt.	Log N/N(H)
Sc II	2	3613.84	0.02	+0.45	-3.9920	5.9229	-1.3874	-4.1876	1.	-7.3103
Sc II	2	3630.74	0.01	+0.28	-4.1600	5.7629	-1.7257	-4.3277	1.	-7.4886
Sc II	2	3642.78	0.00	+0.09	-4.3486	5.5824	-1.3526	-4.1698	2.	-6.9350
Sc II	2	3645.31	0.02	-0.38	-4.8183	5.0966	-1.6459	-4.2992	1.	-6.7425
Sc II	3	3558.54	0.01	-0.15	-4.5987	5.3242	-1.2424	-4.1104	3.	-6.5666
Sc II	3	3576.34	0.01	+0.01	-4.4366	5.4864	-1.3219	-4.1536	3.	-6.8082
Sc II	3	3580.93	0.00	-0.15	-4.5960	5.3349	-1.2880	-4.1354	3.	-6.6230
Sc II	3	3589.63	0.01	-0.63	-5.0750	4.8480	-1.5574	-4.2644	2.	-6.4054
Sc II	3	3590.47	0.02	-0.62	-5.0648	4.8500	-1.0939	-4.0306	3.	-5.9440
Sc II	7	4246.83	0.31	+0.19	-4.1819	5.7732	-2.4591	-4.3757	3.	-8.2323
Sc II	14	4374.45	0.62	-0.45	-4.8091	4.9075	-2.6518	-4.4353	3.	-7.5592
Sc II	14	4400.35	0.60	-0.72	-5.0765	4.6554	-2.7826	-4.4709	3.	-7.4380
Sc II	14	4415.56	0.59	-0.84	-5.1950	4.5445	-3.7224	-4.6665	3.	-8.2669
Sc II	15	4294.77	0.60	-1.27	-5.6371	4.0948	-2.9680	-4.5147	3.	-7.0628
Sc II	15	4314.08	0.62	-0.10	-4.4651	5.2514	-2.5629	-4.4090	2.	-7.8143
Sc II	15	4320.74	0.60	-0.22	-4.5844	5.1474	-2.1185	-4.2511	1.	-7.2660
Sc II	15	4325.01	0.59	-0.37	-4.7340	5.0055	-2.5477	-4.4043	1.	-7.5532
Sc II	23	5031.02	1.35	-0.38	-4.6783	4.3809	-1.9048	-4.1816	2.	-6.2858
Sc II	25	5552.25	1.45	-2.38	-6.6355	2.2985	-1.9602	-4.2223	2.	-4.2587
Sc II	26	5239.82	1.45	-0.50	-4.7807	4.2017	-1.4794	-3.9795	2.	-5.6811
Sc II	29	5684.19	1.50	-1.09	-5.3353	3.5600	-2.1495	-4.3063	3.	-5.7095
Sc II	31	5526.81	1.76	+0.03	-4.2275	4.4681	-1.9386	-4.2117	3.	-6.4066

TABLE XIII

ABUNDANCE RESULTS FOR Ti I

Element	RMT	λ	χ(R,S)	Log gf	Log gfλ	Log C	Log (W/λ)*	Log (W/λ)	Wt.	Log N/N(H)
Ti I	5	5064.65	0.05	-1.05	-5.3455	1.3492	-2.2455	-4.3156	1.	-3.5947
Ti I	6	4681.91	0.05	-1.02	-5.3496	1.4142	-2.9374	-4.5061	1.	-4.3516
Ti I	12	3998.63	0.05	-0.07	-4.4681	2.3908	-2.8496	-4.4462	3.	-5.2404
Ti I	13	3924.53	0.02	-0.96	-5.3662	1.5150	-4.5749	-4.9091	1.	-6.0899
Ti I	13	3929.87	0.00	-1.00	-5.4056	1.4905	-3.6152	-4.6245	1.	-5.1057
Ti I	13	3958.21	0.05	-0.15	-4.5525	2.3064	-3.5101	-4.5991	1.	-5.8165
Ti I	17	3741.06	0.02	-0.25	-4.6770	2.2042	-3.8910	-4.6921	1.	-6.0952
Ti I	38	5016.16	0.84	-0.62	-4.9196	1.1776	-3.7845	-4.7430	2.	-4.9622
Ti I	38	5022.87	0.82	-0.51	-4.8090	1.3033	-2.3957	-4.3668	3.	-3.6990
Ti I	42	4512.73	0.83	-0.54	-4.8856	1.2923	-5.2700	-5.3876	2.	-6.5623
Ti I	77	4675.12	1.06	-1.29	-5.6202	0.3858	-4.5100	-4.9210	1.	-4.8958
Ti I	145	4617.27	1.74	+0.20	-4.1356	1.3659	-4.7143	-5.0183	1.	-6.0802
Ti I	145	4623.10	1.73	-0.07	-4.4051	1.1038	-4.9537	-5.1530	2.	-6.0576
Ti I	145	4629.34	1.73	-0.44	-4.7745	0.7344	-2.9677	-4.5014	3.	-3.7021
Ti I	157	4885.08	1.88	+0.18	-4.1311	1.2276	-3.2424	-4.5887	1.	-4.4700
Ti I	173	4968.57	1.97	-0.60	-4.9038	0.3882	-3.8507	-4.7399	1.	-4.2389
Ti I	241	4836.12	2.26	-0.57	-4.8855	0.1927	-3.9740	-4.7697	1.	-4.1667
Ti I	260	4792.48	2.32	-0.25	-4.5694	0.4645	-2.9467	-4.5033	2.	-3.4112
Ti I	283	4975.34	2.49	+0.04	-4.2632	0.6456	-4.3181	-4.8668	1.	-4.9637
Ti I	288	5120.42	2.57	+0.23	-4.0607	0.7478	-2.3828	-4.3167	3.	-3.1306

TABLE XIV

ABUNDANCE RESULTS FOR Ti II

Element	RMT	λ	χ(R,S)	Log gf	Log gfλ	Log C	Log (W/λ)*	Log (W/λ)	Wt.	Log N/N(H)
Ti II	1	3407.20	0.05	-2.00	-6.4676	3.2796	-1.7562	-4.2935	1.	-5.0358
Ti II	1	3409.83	0.03	-1.92	-6.3873	3.3758	-2.2532	-4.4664	1.	-5.6290
Ti II	6	3461.50	0.13	-0.87	-5.3307	4.3528	-1.6866	-4.2665	3.	-6.0393
Ti II	6	3477.18	0.12	-0.95	-5.4088	4.2827	-1.3898	-4.1535	2.	-5.6725
Ti II	6	3491.05	0.11	-1.09	-5.5470	4.1524	-1.6205	-4.2413	3.	-5.7729
Ti II	6	3500.34	0.12	-2.13	-6.5859	3.1056	-1.7084	-4.2750	3.	-4.8140
Ti II	15	3561.57	0.57	-2.34	-6.7884	2.8667	-2.3441	-4.2624	3.	-5.2108
Ti II	15	3573.74	0.57	-1.71	-6.1569	3.4981	-2.5566	-4.3291	2.	-6.0547
Ti II	15	3587.13	0.60	-1.81	-6.2553	3.3772	-1.8591	-4.0636	2.	-5.2363
Ti II	15	3596.05	0.60	-1.31	-5.7542	3.8783	-2.1356	-4.1836	3.	-6.0139
Ti II	18	4493.53	1.08	-2.66	-7.0074	2.1409	-3.3685	-4.6113	3.	-5.5094
Ti II	19	4450.49	1.08	-1.59	-5.9416	3.2067	-2.4368	-4.3558	2.	-5.6435
Ti II	20	4287.89	1.08	-1.96	-6.3278	2.8733	-2.9610	-4.4797	3.	-5.8343
Ti II	31	4468.49	1.13	-0.77	-5.1198	3.9905	-2.5118	-4.3823	3.	-6.5023
Ti II	31	4501.27	1.11	-0.86	-5.2067	3.9189	-2.5554	-4.3972	2.	-6.4743
Ti II	38	4636.34	1.16	-2.73	-7.0638	2.0238	-4.7474	-5.0241	2.	-6.7712
Ti II	41	4300.05	1.18	-0.81	-5.1765	3.9492	-2.1607	-4.2075	3.	-6.1099
Ti II	41	4301.93	1.16	-1.49	-5.8563	3.2845	-2.6214	-4.3780	3.	-5.9058
Ti II	41	4312.86	1.18	-1.37	-5.7352	3.3905	-2.2821	-4.2555	3.	-5.6725
Ti II	42	3561.91	1.16	-2.31	-6.7583	2.4538	-2.6627	-4.3619	1.	-5.1165
Ti II	42	3566.00	1.16	-1.83	-6.2778	2.9343	-2.0089	-4.1287	1.	-4.9432
Ti II	49	4708.66	1.23	-2.63	-6.9571	2.0774	-4.0503	-4.7614	2.	-6.1277
Ti II	50	4533.97	1.23	-0.71	-5.0535	3.9810	-2.1628	-4.2513	2.	-6.1437
Ti II	50	4563.76	1.22	-0.90	-5.2407	3.8014	-2.8127	-4.4779	3.	-6.6141
Ti II	52	3624.83	1.22	-0.94	-5.3807	3.7866	-2.2403	-4.2254	1.	-6.0269
Ti II	52	3641.33	1.23	-0.71	-5.1487	4.0111	-2.1275	-4.1802	1.	-6.1386

TABLE XIV (Concluded)

Element	RMT	λ	χ(R,S)	Log gf	Log gfλ	Log C	Log (W/λ)*	Log (W/λ)	Wt.	Log N/N(H)
Ti II	70	5188.70	1.57	-1.15	-5.4349	3.2714	-1.6130	-4.0147	3.	-4.8844
Ti II	70	5226.56	1.56	-1.24	-5.5218	3.1921	-1.6161	-4.0160	3.	-4.8083
Ti II	86	5129.14	1.88	-1.51	-5.8000	2.6710	-1.7006	-4.0517	3.	-4.3716
Ti II	86	5185.90	1.88	-1.56	-5.8452	2.6258	-1.6058	-4.0117	0.	-4.2316
Ti II	88	3504.89	1.88	+0.03	-4.4253	3.8720	-1.8865	-4.3256	3.	-5.7886
Ti II	88	3505.90	1.88	-2.07	-6.5252	1.7722	-1.9048	-4.3324	3.	-3.6770
Ti II	88	3510.84	1.88	-0.01	-4.4646	3.8328	-1.5435	-4.1809	3.	-5.3763
Ti II	98	3520.25	2.04	-0.46	-4.9034	3.2680	-1.6994	-4.2515	3.	-4.9673
Ti II	98	3533.87	2.05	-1.67	-6.1217	2.0418	-1.5100	-4.1643	1.	-3.5518
Ti II	98	3535.41	2.05	-0.21	-4.6616	3.5020	-1.4941	-4.1562	3.	-4.9961
Ti II	99	3456.39	2.05	-0.16	-4.6214	3.5422	-2.0054	-4.3687	3.	-5.5476
Ti II	99	3465.56	2.05	-1.00	-5.4602	2.7033	-1.5289	-4.1737	3.	-4.2322
Ti II	105	4163.64	2.58	-0.40	-4.7805	3.3006	-2.4644	-4.3238	2.	-5.7650

TABLE XV

ABUNDANCE RESULTS FOR V I

Element	RMT	λ	χ(R,S)	Log gf	Log gfλ	Log C	Log (W/λ)*	Log (W/λ)	Wt.	Log N/N(H)
V I	4	4577.17	0.00	-1.37	-5.7094	1.1085	-5.7961	-5.8426	1.	-6.9045
V I	4	4580.39	0.02	-1.25	-5.5891	1.2137	-4.6147	-4.9660	2.	-5.8284
V I	5	4355.94	0.02	-1.80	-6.1609	0.6952	-5.0561	-5.2154	1.	-5.7513
V I	5	4384.72	0.07	+0.12	-4.2381	2.5806	-3.4590	-4.6067	2.	-6.0396
V I	22	4384.72	0.29	+0.12	-4.2381	2.3966	-3.3926	-4.6067	2.	-5.7892
V I	22	4406.64	0.30	-0.36	-4.7159	1.9112	-3.8986	-4.7172	3.	-5.8098
V I	22	4407.64	0.29	-0.29	-4.6458	1.9888	-3.3948	-4.6072	3.	-5.3836
V I	27	4099.80	0.27	-0.19	-4.5772	2.0915	-3.6644	-4.6539	1.	-5.7560
V I	27	4109.79	0.26	-0.29	-4.6762	2.0001	-2.3287	-4.2918	1.	-4.3288
V I	27	4111.78	0.30	+0.34	-4.0460	2.6003	-3.2264	-4.5590	1.	-5.8267
V I	27	4132.02	0.29	-0.15	-4.5338	2.1199	-1.9679	-4.1435	3.	-4.0879
V I	27	4134.49	0.30	-0.26	-4.6436	2.0027	-3.4744	-4.6101	3.	-5.4771
V I	87	4452.01	1.86	+0.52	-3.8314	1.5973	-5.6542	-5.7180	1.	-7.2514
V I	87	4462.36	1.85	+0.51	-3.8404	1.5956	-5.8806	-5.9254	1.	-7.4763
V I	87	4468.01	1.84	-0.23	-4.5799	0.8636	-5.0990	-5.2562	1.	-5.9626
V I	87	4469.71	1.85	+0.29	-4.0597	1.3764	-5.2688	-5.3933	1.	-6.6452
V I	100	4540.01	1.88	-0.69	-5.0329	0.3810	-4.4083	-4.8855	2.	-4.7893

TABLE XVI

ABUNDANCE RESULTS FOR V II

Element	RMT	λ	χ(R,S)	Log gf	Log gfλ	Log C	Log (W/λ)*	Log (W/λ)	Wt.	Log N/N(H)
V II	4	3592.01	1.09	-0.65	-5.0947	4.2461	-2.1848	-4.1895	2.	-6.4309
V II	5	3499.82	1.07	-2.64	-7.0960	2.2598	-3.4798	-4.5852	1.	-5.7396
V II	5	3520.02	1.07	-1.58	-6.0335	3.3223	-2.2191	-4.2023	2.	-5.5414
V II	5	3530.76	1.07	-0.97	-5.4221	3.9336	-2.9232	-4.4410	2.	-6.8567
V II	6	3517.30	1.12	-0.73	-5.1838	4.1346	-2.5104	-4.3105	3.	-6.6450
V II	14	4056.27	1.57	-2.85	-7.2419	1.6668	-2.8541	-4.4445	2.	-4.5209
V II	15	3715.48	1.57	-0.44	-4.8700	4.1125	-2.5790	-4.3344	1.	-6.6914
V II	25	4178.39	1.68	-1.70	-6.0790	2.7473	-3.9825	-4.7223	2.	-6.7298
V II	25	4220.05	1.67	-2.97	-7.3447	1.4891	-3.4877	-4.6060	3.	-4.9768
V II	37	4183.43	2.04	-1.36	-5.7385	2.8184	-3.7012	-4.6564	3.	-6.5196
V II	57	3514.42	2.26	-1.89	-6.3441	2.1289	-2.7342	-4.3474	2.	-4.8631
V II	57	3521.84	2.27	-1.23	-5.6832	2.7825	-2.4055	-4.2384	2.	-5.1880
V II	78	3574.34	2.36	-1.41	-5.8568	2.5428	-2.2899	-4.1921	3.	-4.8327
V II	78	3588.13	2.37	-1.88	-6.3251	2.0672	-2.8034	-4.3687	2.	-4.8706
V II	146	3497.03	2.59	-0.42	-4.8763	3.3552	-2.3441	-4.2145	1.	-5.6993
V II	192	3532.28	3.31	-0.75	-5.2019	2.5086	-2.6996	-4.3367	2.	-5.2081
V II	200	4234.55	3.74	-0.47	-4.8432	2.4656	-3.8560	-4.6835	2.	-6.3216
V II	225	4065.07	3.78	-0.93	-5.3209	1.9589	-3.4663	-4.5851	2.	-5.4252

TABLE XVII

ABUNDANCE RESULTS FOR Cr I

Element	RMT	λ	χ(R,S)	Log gf	Log gfλ	Log C	Log (W/λ)*	Log (W/λ)	Wt.	Log N/N(H)
Cr I	10	4496.86	0.94	-1.19	-5.5371	0.7669	-3.2457	-4.5854	3.	-4.0126
Cr I	10	4545.96	0.94	-1.37	-5.7124	0.5916	-3.1502	-4.5621	3.	-3.7418
Cr I	10	4580.06	0.94	-1.62	-5.9591	0.3448	-2.7937	-4.4601	3.	-3.1386
Cr I	21	4600.75	1.00	-1.21	-5.5472	0.7119	-2.9452	-4.5063	2.	-3.6571
Cr I	21	4616.14	0.98	-1.21	-5.5457	0.7283	-2.4615	-4.3472	2.	-3.1898
Cr I	21	4646.17	1.03	-0.72	-5.0529	1.1838	-2.6408	-4.4090	3.	-3.8246
Cr I	21	4651.28	0.98	-1.52	-5.8524	0.4216	-3.2923	-4.5965	3.	-3.7139
Cr I	21	4652.16	1.00	-1.23	-5.5623	0.6967	-3.0677	-4.5406	3.	-3.7644
Cr I	22	4359.63	0.98	-1.31	-5.6706	0.6610	-2.8547	-4.4472	1.	-3.5156
Cr I	22	4371.28	1.00	-1.31	-5.6694	0.6473	-3.2569	-4.5566	3.	-3.9042
Cr I	22	4384.98	1.03	-1.46	-5.8180	0.4764	-2.8738	-4.4529	3.	-3.3502
Cr I	22	4391.75	1.00	-2.13	-6.4874	-0.1707	-2.4744	-4.3318	3.	-2.3036
Cr I	33	4526.47	2.53	-0.22	-4.5642	0.5650	-2.6318	-4.3570	3.	-3.1968
Cr I	33	4544.62	2.53	-0.52	-4.8625	0.2667	-3.7538	-4.6948	3.	-4.0205
Cr I	35	4203.59	2.53	-1.26	-5.6364	-0.4419	-4.4789	-4.8961	2.	-4.0370
Cr I	62	4697.06	2.70	-1.06	-5.3882	-0.3828	-4.0169	-4.7651	2.	-3.6341
Cr I	62	4700.61	2.70	-1.27	-5.5978	-0.5925	-4.6745	-5.0054	1.	-4.0820
Cr I	95	4473.34	2.88	-1.10	-5.4492	-0.5749	-4.1489	-4.8060	3.	-3.5740
Cr I	96	4293.56	2.90	-1.10	-5.4672	-0.5401	-4.7916	-5.0488	1.	-4.2515
Cr I	99	4693.95	2.97	-0.96	-5.2885	-0.4797	-4.1042	-4.7918	1.	-3.6245
Cr I	133	4211.35	3.00	-0.82	-5.1956	-0.3407	-3.8075	-4.6744	2.	-3.4668
Cr I	145	4724.42	3.07	-0.85	-5.1757	-0.4393	-4.5493	-4.9484	2.	-4.1100
Cr I	145	4730.71	3.07	-0.47	-4.7951	-0.0587	-3.5859	-4.6541	2.	-3.5271
Cr I	150	4540.72	3.09	+0.10	-4.2429	0.4790	-3.1177	-4.5232	3.	-3.5967
Cr I	171	4632.18	3.10	-0.92	-5.2542	-0.5396	-3.9439	-4.7439	2.	-3.4043
Cr I	186	4689.37	3.11	-0.55	-4.8789	-0.1715	-3.2395	-4.5600	3.	-3.0680

TABLE XVII (Concluded)

Element	RMT	λ	χ(R,S)	Log gf	Log gfλ	Log C	Log (W/λ)*	Log (W/λ)	Wt.	Log N/N(H)
Cr I	186	4718.43	3.18	+0.08	-4.2462	0.4106	-3.5083	-4.6342	3.	-3.9189
Cr I	209	4626.81	3.42	-1.85	-6.1847	-1.7014	-4.8219	-5.0825	1.	-3.1206
Cr I	251	4058.77	3.83	+0.28	-4.1116	0.1502	-3.0334	-4.4537	3.	-3.1836
Cr I	286	4595.59	4.17	+0.15	-4.1877	-0.2417	-3.0210	-4.4925	2.	-2.7793
Cr I	288	4506.85	4.17	-0.18	-4.5261	-0.5802	-3.7755	-4.7001	2.	-3.1953
Cr I	305	4161.41	4.44	+0.36	-4.0208	-0.1900	-2.9663	-4.4305	3.	-2.7763
Cr I	305	4165.52	4.43	+0.28	-4.1003	-0.2625	-2.8150	-4.3758	3.	-2.5525

TABLE XVIII

ABUNDANCE RESULTS FOR Cr II

Element	RMT	λ	χ(R,S)	Log gf	Log gfλ	Log C	Log (W/λ)*	Log (W/λ)	Wt.	Log N/N(H)
Cr II	3	3408.76	2.47	-0.24	-4.7074	3.3778	-2.0172	-4.3713	2.	-5.3950
Cr II	3	3421.20	2.41	-0.42	-4.8858	3.2465	-1.7826	-4.2827	3.	-5.0291
Cr II	19	4087.63	3.09	-3.03	-7.4185	0.5365	-3.1919	-4.5130	1.	-3.7285
Cr II	19	4088.90	3.09	-3.43	-7.8184	0.1367	-2.7957	-4.3859	1.	-2.9324
Cr II	26	4086.14	3.70	-2.22	-6.6087	0.9031	-3.1150	-4.4903	1.	-4.0181
Cr II	30	4824.13	3.85	-1.01	-5.3266	1.9643	-2.3638	-4.2859	3.	-4.3281
Cr II	30	4848.24	3.85	-1.13	-5.4444	1.8464	-2.5334	-4.3523	1.	-4.3798
Cr II	30	4876.41	3.84	-1.56	-5.8719	1.4263	-2.1716	-4.2050	3.	-3.5979
Cr II	30	4876.48	3.85	-1.94	-6.2519	1.0390	-2.1716	-4.2050	3.	-3.2105
Cr II	31	4246.41	3.84	-3.05	-7.4220	-0.0113	-3.0255	-4.4627	3.	-3.0143
Cr II	31	4252.62	3.84	-1.85	-6.2213	1.1894	-2.8312	-4.3983	3.	-4.0206
Cr II	31	4261.92	3.85	-1.21	-5.5804	1.8231	-2.5005	-4.2763	3.	-4.3236
Cr II	31	4269.28	3.84	-2.06	-6.4296	0.9811	-2.6925	-4.3490	3.	-3.6736
Cr II	31	4275.57	3.84	-1.33	-5.6990	1.7117	-2.8326	-4.3988	3.	-4.5444
Cr II	44	4558.66	4.06	-0.31	-4.6512	2.5304	-1.9796	-4.0871	3.	-4.5100
Cr II	44	4588.22	4.05	-0.65	-4.9884	2.2004	-2.2322	-4.2070	3.	-4.4327
Cr II	44	4292.09	4.06	-1.37	-5.7080	1.4736	-2.4375	-4.2888	3.	-3.9110
Cr II	44	4616.64	4.05	-1.51	-5.8457	1.3431	-2.6173	-4.3490	3.	-3.9604
Cr II	44	4618.83	4.06	-0.98	-5.3155	1.8661	-2.6228	-4.3508	3.	-4.4889
Cr II	44	4634.11	4.05	-1.19	-5.5240	1.6648	-2.8552	-4.4276	3.	-4.5200
Cr II	165	4082.30	5.30	-1.13	-5.5191	0.8550	-3.0575	-4.4727	1.	-3.9124

TABLE XIX

ABUNDANCE RESULTS FOR Mn I

Element	RMT	λ	χ(R,S)	Log gf	Log gfλ	Log C	Log (W/λ)*	Log (W/λ)	Wt.	Log N/N(H)
Mn I	2	4034.49	0.00	-1.24	-5.6342	2.5502	-3.3181	-4.5706	3.	-5.8683
Mn I	5	4055.54	2.13	-0.01	-4.4020	2.1929	-3.6027	-4.6392	3.	-5.7956
Mn I	5	4070.28	2.18	-0.78	-5.1704	1.3878	-2.7570	-4.4182	2.	-4.1448
Mn I	16	4754.04	2.27	-0.41	-4.7329	1.6452	-4.3579	-4.8887	2.	-6.0031
Mn I	21	4739.11	2.93	-0.66	-4.9843	0.9054	-4.1879	-4.8355	2.	-5.0933
Mn I	21	4762.38	2.88	+0.06	-4.2622	1.6644	-3.8499	-4.7488	3.	-5.5143
Mn I	23	4235.14	2.91	-0.07	-4.4431	1.5813	-4.1364	-4.7719	2.	-5.7177
Mn I	23	4235.29	2.88	+0.04	-4.3331	1.7131	-4.3941	-4.8581	2.	-6.1073
Mn I	23	4239.73	2.93	-0.35	-4.7227	1.2872	-2.5895	-4.3270	3.	-3.8767
Mn I	29	4059.39	3.06	-0.36	-4.7515	1.1639	-3.7002	-4.6510	1.	-4.8641
Mn I	33	3986.83	3.12	-0.20	-4.5994	1.2727	-3.0728	-4.4908	1.	-4.3454

TABLE XX

ABUNDANCE RESULTS FOR Mn II

Element	RMT	λ	χ(R,S)	Log gf	Log gfλ	Log C	Log (W/λ)*	Log (W/λ)	Wt.	Log N/N(H)
Mn II	1	3460.04	1.17	-1.47	-5.9309	3.7840	-1.7680	-4.2919	1.	-5.5520
Mn II	3	3441.98	1.77	+0.05	-4.4132	4.8279	-2.4108	-4.5053	2.	-7.2387
Mn II	3	3460.31	1.80	-0.23	-4.6909	4.5266	-1.3840	-4.1158	3.	-5.9106
Mn II	3	3474.06	1.80	-0.44	-4.8992	4.3183	-1.5202	-4.1851	2.	-5.8385
Mn II	3	3474.12	1.82	-0.50	-4.9592	4.2425	-1.5202	-4.1851	2.	-5.7627
Mn II	3	3482.90	1.82	-0.32	-4.7781	4.4236	-1.3716	-4.1090	3.	-5.7953
Mn II	3	3488.68	1.84	-0.51	-4.9673	4.2186	-1.3862	-4.1170	2.	-5.6048
Mn II	3	3496.81	1.82	-1.04	-5.4963	3.7054	-1.6835	-4.2576	2.	-5.3888
Mn II	3	3497.53	1.84	-0.73	-5.1862	3.9997	-1.4651	-4.1582	2.	-5.4648

TABLE XXI

ABUNDANCE RESULTS FOR Fe I

Element	RMT	λ	χ(R,S)	Log gf	Log gfλ	Log C	Log (W/λ)*	Log (W/λ)	Wt.	Log N/N(H)
Fe I	1	5110.41	0.00	-3.25	-7.5415	0.1053	-2.0024	-4.2224	3.	-2.1077
Fe I	4	3856.37	0.05	-1.20	-5.6138	2.1343	-1.7453	-4.0547	3.	-3.8795
Fe I	4	3859.91	0.00	-0.60	-5.0134	2.7725	-2.0517	-4.1923	3.	-4.8242
Fe I	5	3679.91	0.00	-1.51	-5.9442	1.8823	-2.9621	-4.4669	1.	-4.8444
Fe I	5	3683.05	0.05	-1.95	-6.3838	1.4050	-3.5538	-4.6134	1.	-4.9589
Fe I	5	3705.57	0.05	-1.27	-5.7011	2.0877	-3.1676	-4.5213	1.	-5.2553
Fe I	15	5269.54	0.86	-1.39	-5.6682	1.3212	-1.8119	-4.1242	3.	-3.1331
Fe I	16	4994.13	0.91	-2.82	-7.1215	-0.1702	-2.6713	-4.4678	2.	-2.5010
Fe I	16	5012.07	0.86	-2.55	-6.8500	0.1394	-1.9981	-4.2204	3.	-2.1375
Fe I	16	5051.64	0.91	-2.62	-6.9166	0.0347	-2.1880	-4.3018	3.	-2.2227
Fe I	16	5083.34	0.95	-2.74	-7.0339	-0.1130	-1.9185	-4.1810	3.	-1.8054
Fe I	20	3849.97	1.01	-0.71	-5.1245	1.9000	-2.4780	-4.3572	1.	-4.3780
Fe I	23	3581.19	0.86	+0.64	-3.8060	3.3749	-1.9045	-4.0957	3.	-5.2794
Fe I	23	3585.32	0.95	-0.49	-4.9355	2.1781	-1.7476	-4.0271	2.	-3.9257
Fe I	23	3586.98	0.99	-0.41	-4.8553	2.2284	-1.7724	-4.0384	2.	-4.0008
Fe I	24	3513.82	0.86	-0.50	-4.9542	2.2267	-2.1084	-4.1752	3.	-4.3350
Fe I	24	3558.52	0.99	-0.18	-4.6287	2.4549	-1.9490	-4.1136	3.	-4.4040
Fe I	24	3565.38	0.95	+0.17	-4.2779	2.8357	-2.0512	-4.1534	2.	-4.8868
Fe I	24	3570.10	0.91	+0.50	-3.9173	3.2262	-1.9792	-4.1255	2.	-5.2053
Fe I	36	5171.60	1.48	-1.80	-6.0864	0.4326	-1.7081	-4.0684	3.	-2.1406
Fe I	36	5194.94	1.55	-1.55	-5.8344	0.6317	-1.6028	-4.0173	3.	-2.2345
Fe I	36	5216.28	1.60	-1.58	-5.8626	0.5658	-1.7206	-4.0750	3.	-2.2863
Fe I	37	5341.03	1.60	-2.00	-6.2724	0.1560	-1.5226	-3.9813	3.	-1.6787
Fe I	42	4202.03	1.48	-0.57	-4.9465	1.7130	-2.5926	-4.3766	3.	-4.3056
Fe I	42	4250.79	1.55	-0.54	-4.9115	1.6959	-2.4881	-4.3390	3.	-4.1840
Fe I	43	4045.81	1.48	+0.43	-3.9630	2.6965	-1.8802	-4.0870	2.	-4.5767

TABLE XXI (Continued)

Element	RMT	λ	χ(R,S)	Log gf	Log gfλ	Log C	Log (W/λ)*	Log (W/λ)	Wt.	Log N/N(H)
Fe I	43	4071.74	1.60	+0.17	-4.2202	2.3501	-2.4525	-4.3258	1.	-4.8025
Fe I	43	4143.87	1.55	-0.42	-4.8026	1.8048	-2.4211	-4.3140	3.	-4.2259
Fe I	48	3549.87	1.60	-2.32	-6.7698	-0.1386	-2.6646	-4.3796	2.	-2.5261
Fe I	66	5098.70	2.17	-1.40	-5.6925	0.3071	-1.4293	-3.9411	3.	-1.7364
Fe I	66	5202.34	2.17	-1.02	-5.3038	0.6959	-1.4406	-3.9459	3.	-2.1365
Fe I	71	4282.41	2.18	-0.16	-4.5283	1.5977	-3.0063	-4.4900	3.	-4.6040
Fe I	114	5049.82	2.27	-1.40	-5.6967	0.2281	-2.2471	-4.3247	3.	-2.4752
Fe I	130	3506.50	2.27	-0.41	-4.8651	1.2737	-2.4631	-4.3106	2.	-3.7368
Fe I	152	4187.04	2.45	+0.17	-4.2081	1.7185	-2.4062	-4.2800	3.	-4.1247
Fe I	152	4210.35	2.48	-0.19	-4.5657	1.3388	-2.8150	-4.4300	3.	-4.1537
Fe I	152	4235.94	2.42	+0.31	-4.0631	1.8857	-2.6152	-4.3600	3.	-4.5009
Fe I	152	4250.12	2.47	+0.25	-4.1216	1.7902	-2.9078	-4.4600	3.	-4.6980
Fe I	152	4271.16	2.45	+0.25	-4.1195	1.8071	-2.7852	-4.4200	3.	-4.5923
Fe I	177	3760.05	2.39	-0.43	-4.8548	1.1963	-3.0419	-4.4882	1.	-4.2382
Fe I	318	4957.60	2.80	+0.25	-4.0547	1.4745	-2.2948	-4.2916	2.	-3.7693
Fe I	318	5006.13	2.82	-0.83	-5.1305	0.3839	-1.9919	-4.1455	2.	-2.3757
Fe I	322	3594.63	2.84	-0.41	-4.8543	0.8696	-2.1421	-4.1271	2.	-3.0116
Fe I	322	3595.29	2.86	-0.93	-5.3743	0.3351	-2.7112	-4.3542	2.	-3.0464
Fe I	326	3533.20	2.87	+0.13	-4.3218	1.3803	-2.6452	-4.3303	2.	-4.0256
Fe I	326	3536.56	2.86	+0.52	-3.9314	1.7780	-2.5738	-4.3035	2.	-4.3518
Fe I	326	3541.08	2.84	+0.59	-3.8609	1.8631	-2.1823	-4.1443	2.	-4.0453
Fe I	326	3542.08	2.85	+0.56	-3.8907	1.8259	-2.3893	-4.2309	2.	-4.2152
Fe I	326	3554.92	2.82	+0.64	-3.8092	1.9293	-1.8554	-3.9952	2.	-3.7847
Fe I	383	5068.77	2.93	-1.00	-5.2951	0.1374	-2.0689	-4.1869	3.	-2.2062
Fe I	383	5139.47	2.93	-0.36	-4.6491	0.7834	-1.5738	-3.9470	0.	-2.3572
Fe I	383	5232.95	2.93	-0.21	-4.4913	0.9412	-1.6685	-3.9867	2.	-2.6097
Fe I	429	3903.90	2.98	-0.52	-4.9285	0.6409	-2.6753	-4.3583	1.	-3.3162
Fe I	497	3586.11	3.00	+0.50	-3.9454	1.6624	-2.6610	-4.3361	2.	-4.3235

TABLE XXI (Concluded)

Element	RMT	λ	χ(R,S)	Log gf	Log gfλ	Log C	Log (W/λ)*	Log (W/λ)	Wt.	Log N/N(H)
Fe I	523	4143.42	3.05	+0.61	-3.7726	1.7140	-2.8150	-4.4300	3.	-4.5290
Fe I	553	5263.31	3.25	-0.89	-5.1687	0.0268	-1.6926	-3.9971	1.	-1.7194
Fe I	606	3916.73	3.22	-0.33	-4.7371	0.6582	-2.6677	-4.3559	3.	-3.3259
Fe I	611	3586.11	3.22	+0.50	-3.9454	1.5041	-2.6610	-4.3361	2.	-4.1652
Fe I	687	4950.11	3.40	-1.70	-6.0054	-0.9208	-2.9544	-4.5200	3.	-2.0337
Fe I	687	4966.10	3.32	-0.74	-5.0440	0.0998	-2.7316	-4.4443	3.	-2.8313
Fe I	693	4238.82	3.40	+0.47	-3.9028	1.3298	-2.4825	-4.3100	3.	-3.8117
Fe I	695	4150.26	3.43	-0.71	-5.0919	0.1182	-3.4387	-4.6000	3.	-3.5570
Fe I	695	4153.91	3.40	+0.33	-4.0515	1.1804	-2.2578	-4.2200	3.	-3.4382
Fe I	695	4157.79	3.42	+0.17	-4.2111	1.0063	-2.8762	-4.4500	3.	-3.8825
Fe I	698	4065.40	3.43	-0.70	-5.0909	0.1192	-4.2113	-4.8000	3.	-4.3305
Fe I	726	4137.00	3.41	+0.12	-4.2633	0.9614	-2.4062	-4.2800	3.	-3.3675
Fe I	843	5242.49	3.62	-0.82	-5.1005	-0.1779	-1.8698	-4.0795	1.	-1.6918
Fe I	965	5001.87	3.86	-0.10	-4.4009	0.3454	-2.0293	-4.1658	3.	-2.3747
Fe I	965	5014.95	3.93	-0.23	-4.5297	0.1651	-2.3173	-4.3008	3.	-2.4824
Fe I	966	4978.61	3.97	-0.77	-5.0729	-0.4075	-3.4542	-4.6667	3.	-3.0467
Fe I	984	4973.11	3.94	-0.68	-4.9834	-0.2959	-3.2501	-4.6114	3.	-2.9542
Fe I	1065	4991.28	4.17	-0.51	-4.8118	-0.2924	-2.5644	-4.3901	3.	-2.2720
Fe I	1066	4969.93	4.20	-0.82	-5.1237	-0.6261	-3.2077	-4.5991	3.	-2.5816
Fe I	1089	5162.29	4.16	+0.79	-3.4972	1.0295	-1.6566	-3.9816	3.	-2.6861
Fe I	1090	5090.79	4.24	-0.41	-4.7032	-0.2349	-2.1455	-4.2259	3.	-1.9106
Fe I	1090	5125.13	4.20	-0.08	-4.3703	0.1272	-1.7592	-4.0266	3.	-1.8864
Fe I	1091	5159.07	4.26	+0.55	-3.7374	0.7163	-1.9759	-4.1368	1.	-2.6923
Fe I	1092	5133.69	4.16	+0.20	-4.0896	0.4371	-1.8973	-4.0941	3.	-2.3344
Fe I	1094	5074.76	4.20	+0.00	-4.2946	0.2029	-2.0373	-4.1701	3.	-2.2402
Fe I	1097	4962.56	4.16	-1.43	-5.7343	-1.2076	-3.8531	-4.7696	2.	-2.6455

TABLE XXII

ABUNDANCE RESULTS FOR Fe II

Element	RMT	λ	χ(R,S)	Log gf	Log gfλ	Log C	Log (W/λ)*	Log (W/λ)	Wt.	Log N/N(H)
Fe II	27	4128.73	2.57	-2.76	-7.1442	1.0591	-2.7968	-4.4093	1.	-3.8559
Fe II	27	4273.32	2.69	-3.51	-7.8792	0.2360	-2.7631	-4.3995	3.	-2.9991
Fe II	27	4303.17	2.69	-2.00	-6.3662	1.7490	-2.3124	-4.2351	3.	-4.0614
Fe II	27	4416.82	2.77	-2.34	-6.6949	1.3393	-2.6435	-4.3681	3.	-3.9828
Fe II	28	4178.85	2.57	-2.00	-6.3789	1.8243	-2.4971	-4.3093	3.	-4.3214
Fe II	28	4369.40	2.77	-2.87	-7.2296	0.8046	-2.6549	-4.3722	3.	-3.4595
Fe II	37	4515.34	2.83	-2.35	-6.6953	1.2538	-2.4222	-4.3052	2.	-3.6760
Fe II	37	4520.22	2.79	-2.43	-6.7748	1.2039	-2.5278	-4.3449	3.	-3.7317
Fe II	37	4629.34	2.79	-2.27	-6.6045	1.3743	-3.1144	-4.5380	3.	-4.4887
Fe II	38	4508.28	2.84	-2.29	-6.6360	1.3058	-2.7469	-4.4234	3.	-4.0527
Fe II	38	4541.52	2.84	-2.57	-6.9128	1.0289	-2.7965	-4.4401	3.	-3.8254
Fe II	38	4576.33	2.83	-2.22	-6.5595	1.3897	-2.7334	-4.4188	3.	-4.1231
Fe II	38	4583.83	2.79	-1.85	-6.1888	1.7900	-2.3041	-4.2584	2.	-4.0941
Fe II	38	4620.51	2.82	-2.63	-6.9653	0.9912	-3.0050	-4.5062	3.	-3.9962
Fe II	42	4923.92	2.88	-1.44	-5.7477	2.1057	-1.9299	-4.1300	2.	-4.0355
Fe II	42	5018.43	2.88	-1.28	-5.5794	2.2525	-1.5804	-3.9634	3.	-3.8329
Fe II	48	5362.86	3.19	-1.95	-6.2206	1.3473	-1.4870	-3.9387	3.	-2.8343
Fe II	48	5414.09	3.21	-2.75	-7.0165	0.5366	-1.8329	-4.0854	3.	-2.3695
Fe II	49	5197.57	3.22	-2.23	-6.5142	1.0649	-1.7424	-4.0333	3.	-2.8073
Fe II	49	5234.62	3.21	-2.03	-6.3111	1.2754	-1.7182	-4.0229	2.	-2.9936

TABLE XXIII

ABUNDANCE RESULTS FOR Co I

Element	RMT	λ	χ(R,S)	Log gf	Log gfλ	Log C	Log (W/λ)*	Log (W/λ)	Wt.	Log N/N(H)
Co I	16	4020.90	0.43	-2.16	-6.5557	1.0439	-4.6716	-4.9709	2.	-5.7154
Co I	18	3881.87	0.58	-1.59	-6.0010	1.4855	-2.5582	-4.3749	1.	-4.0437
Co I	18	3940.89	0.63	-2.26	-6.6644	0.7845	-2.7282	-4.4249	1.	-3.5126
Co I	28	4121.32	0.92	-0.64	-5.0250	2.2059	-4.3265	-4.8299	1.	-6.5324
Co I	31	3995.31	0.92	-0.45	-4.8484	2.3824	-3.3382	-4.5821	1.	-5.7206
Co I	39	5247.92	1.78	-1.61	-5.8900	0.5415	-1.8268	-4.0709	2.	-2.3683
Co I	170	5126.20	3.61	-0.51	-4.8002	0.2680	-1.9956	-4.1567	3.	-2.2636
Co I	172	5268.50	3.72	-0.26	-4.5383	0.4491	-1.6278	-3.9841	3.	-2.0769
Co I	196	5310.22	4.19	-0.66	-4.9349	-0.2918	-2.1040	-4.2137	1.	-1.8122

TABLE XXIV

ABUNDANCE RESULTS FOR Ni I

Element	RMT	λ	χ(R,S)	Log gf	Log gfλ	Log C	Log (W/λ)*	Log (W/λ)	Wt.	Log N/N(H)
Ni I	3	3437.28	0.00	-1.04	-5.5038	2.3929	-2.0546	-4.3987	2.	-4.4475
Ni I	5	3519.77	0.27	-1.46	-5.9135	1.7707	-1.5756	-4.2047	2.	-3.3463
Ni I	9	3420.74	0.27	-3.08	-7.5459	0.1383	-2.6148	-4.5702	1.	-2.7531
Ni I	17	3461.65	0.03	-0.48	-4.9407	2.9323	-1.8443	-4.3209	2.	-4.7767
Ni I	18	3492.96	0.11	-0.08	-4.5368	3.2733	-2.2099	-4.4521	2.	-5.4832
Ni I	18	3510.34	0.21	-0.74	-5.1947	2.5368	-1.7275	-4.2735	3.	-4.2643
Ni I	18	3524.54	0.03	-0.18	-4.6329	3.2402	-1.7526	-4.2840	3.	-4.9927
Ni I	18	3597.70	0.21	-0.81	-5.2540	2.4775	-2.1199	-4.4217	2.	-4.5973
Ni I	19	3433.56	0.03	-0.91	-5.3743	2.4988	-1.6779	-4.2520	2.	-4.1767
Ni I	19	3515.05	0.11	-0.43	-4.8841	2.9260	-1.9323	-4.3544	3.	-4.8583
Ni I	20	3423.71	0.21	-0.72	-5.1855	2.5459	-3.1487	-4.6776	2.	-5.6946
Ni I	36	3566.37	0.42	-0.37	-4.8178	2.7484	-1.8212	-4.3118	3.	-4.5696
Ni I	86	4470.48	3.38	-0.13	-4.4796	1.0986	-4.8027	-5.0737	1.	-5.9013
Ni I	98	4714.42	3.37	-0.40	-4.7266	0.8590	-4.3318	-4.8706	1.	-5.1908
Ni I	98	4756.52	3.47	-0.21	-4.5327	0.9797	-4.9381	-5.1525	2.	-5.9177

TABLE XXV

ABUNDANCE RESULTS FOR Ni II

Element	RMT	λ	χ(R,S)	Log gf	Log gfλ	Log C	Log (W/λ)*	Log (W/λ)	Wt.	Log N/N(H)
Ni II	4	3407.30	3.07	-0.39	-4.8576	3.1958	-2.3824	-4.4893	1.	-5.5782
Ni II	4	3769.45	3.09	-0.03	-4.4537	4.0267	-2.4035	-4.2183	1.	-6.4302
Ni II	9	4244.80	4.01	-2.03	-6.4021	1.3231	-4.8318	-5.0725	2.	-6.1549

TABLE XXVI

ABUNDANCE RESULTS FOR Sr II

Element	RMT	λ	χ(R,S)	Log gf	Log gfλ	Log C	Log (W/λ)*	Log (W/λ)	Wt.	Log N/N(H)
Sr II	1	4077.71	0.00	-0.47	-4.8596	6.4441	-1.5064	-3.9964	2.	-7.9505
Sr II	1	4215.52	0.00	-0.65	-5.0251	6.2785	-1.5848	-4.0390	3.	-7.8633
Sr II	3	4161.80	2.93	-0.23	-4.6107	4.4693	-2.4129	-4.3130	3.	-6.8821
Sr II	3	4305.45	3.03	-0.04	-4.4060	4.5996	-2.1323	-4.1959	3.	-6.7319
Sr II	4	3464.46	3.03	+0.68	-3.7804	4.9079	-1.4071	-4.1149	3.	-6.3151
Sr II	4	3474.89	3.03	-0.22	-4.6791	4.0093	-1.8533	-4.3264	2.	-5.8626

TABLE XXVII

ABUNDANCE RESULTS FOR Ba II

Element	RMT	λ	χ(R,S)	Log gf	Log gfλ	Log C	Log (W/λ)*	Log (W/λ)	Wt.	Log N/N(H)
Ba II	1	4554.03	0.00	+0.17	-4.1716	6.5827	-2.3842	-4.4131	3.	-8.9669
Ba II	1	4934.09	0.00	-0.15	-4.4568	6.2679	-2.1244	-4.3224	3.	-8.3923
Ba II	2	5853.67	0.00	-1.00	-5.2326	5.3843	-2.5294	-4.5357	3.	-7.9137
Ba II	3	4524.93	2.50	-0.36	-4.7044	4.1383	-3.0410	-4.5724	2.	-7.1793
Ba II	3	4899.93	2.71	-0.08	-4.3898	4.2594	-3.2883	-4.6627	2.	-7.5477

TABLE XXVIII

ABUNDANCE RESULTS FOR Nd II

Element	RMT	λ	χ(R,S)	Log gf	Log gfλ	Log C	Log (W/λ)*	Log (W/λ)	Wt.	Log N/N(H)
Nd II	8	4247.37	0.00	-0.88	-5.2519	4.5572	-2.7195	-4.4753	3.	-7.2767
Nd II	10	4061.08	0.47	+0.03	-4.3614	5.0878	-3.3117	-4.6345	2.	-8.3995
Nd II	10	4156.08	0.18	-0.49	-4.8713	4.7999	-3.7700	-4.7364	3.	-8.5700
Nd II	32	4030.47	0.18	-1.31	-5.7046	3.9666	-1.9192	-4.1731	2.	-5.8858
Nd II	62	4075.12	0.20	-1.07	-5.4599	4.1961	-4.0076	-4.7898	1.	-8.2037

TABLE XXIX

ABUNDANCE RESULTS FOR Sm II

Element	RMT	λ	χ(R,S)	Log gf	Log gfλ	Log C	Log (W/λ)*	Log (W/λ)	Wt.	Log N/N(H)
Sm II	3	4523.04	0.04	-1.72	-6.0646	3.8465	-3.0820	-4.6081	2.	-6.9285
Sm II	7	4458.52	0.10	-1.27	-5.6208	4.2441	-3.3403	-4.6696	3.	-7.5844
Sm II	7	4745.68	0.10	-1.51	-5.8337	4.0312	-3.8487	-4.7786	3.	-7.8799
Sm II	14	4511.83	0.18	-1.47	-5.8156	3.9876	-2.4930	-4.4367	3.	-6.4806
Sm II	22	4615.69	0.19	-1.57	-5.9058	3.8898	-3.4573	-4.6947	2.	-7.3471
Sm II	23	4499.47	0.25	-1.58	-5.9268	3.8226	-5.3861	-5.4925	2.	-9.2086
Sm II	26	4646.68	0.28	-1.70	-6.0329	3.6934	-2.5106	-4.4432	2.	-6.2040
Sm II	32	4566.21	0.33	-1.41	-5.7504	3.9374	-5.1641	-5.3211	2.	-9.1014
Sm II	36	4642.24	0.38	-1.12	-5.4533	4.1960	-4.0039	-4.8127	2.	-8.1999
Sm II	49	4615.44	0.54	-1.42	-5.7558	3.7705	-3.4568	-4.6946	2.	-7.2274

TABLE XXX

ABUNDANCE RESULTS FOR Eu II

Element	RMT	λ	χ(R,S)	Log gf	Log gfλ	Log C	Log (W/λ)*	Log (W/λ)	Wt.	Log N/N(H)
Eu II	1	4129.73	0.00	-0.31	-4.6941	5.8446	-1.4652	-3.9276	3.	-7.3098
Eu II	1	4205.05	0.00	-0.08	-4.4562	6.0824	-1.6431	-4.0085	3.	-7.7255
Eu II	4	4522.59	0.21	+0.05	-4.2926	6.0369	-1.8008	-4.1262	3.	-7.8377
Eu II	5	3907.10	0.21	+0.03	-4.3781	6.0236	-1.8068	-4.0810	3.	-7.8304
Eu II	5	3971.98	0.21	+0.80	-3.6010	6.8008	-1.4121	-3.8909	2.	-8.2128
Eu II	10	3928.87	1.24	-1.78	-6.1857	3.4343	-3.8333	-4.7426	1.	-7.2677
Eu II	10	4017.58	1.31	-1.30	-5.6960	3.8446	-2.5071	-4.4028	3.	-6.3517
Eu II	10	4151.52	1.27	-2.09	-6.4718	3.0991	-3.0334	-4.5597	2.	-6.1325

TABLE XXXI

ABUNDANCE RESULTS FOR U II

Element	RMT	λ	χ(R,S)	Log gf	Log gfλ	Log C	Log (W/λ)*	Log (W/λ)	Wt.	Log N/N(H)
U II	0	3859.58	0.04	-0.62	-5.0335	5.2095	-2.5914	-4.4346	2.	-7.8009
U II	0	3865.92	0.28	-0.85	-5.2627	4.7967	-2.4211	-4.3706	2.	-7.2179
U II	0	3881.46	0.57	-1.00	-5.4110	4.4272	-4.9968	-5.1946	1.	-9.4240
U II	0	4050.04	0.00	-1.11	-5.5025	4.7710	-4.4923	-4.9380	2.	-9.2633
U II	0	4090.14	0.22	-0.70	-5.0883	5.0171	-4.4870	-4.9361	1.	-9.5041
U II	0	4472.34	0.04	-1.18	-5.5295	4.6425	-4.7400	-5.0700	2.	-9.3825
U II	0	4569.91	0.04	-1.68	-6.0201	4.1518	-5.7863	-5.8400	2.	-9.9382
U II	0	4722.73	0.22	-1.55	-5.8758	4.1574	-4.5761	-5.0000	2.	-8.7335

If the spectral line under investigation showed no signs of blending, a weight of three was assigned. When the line under investigation showed signs of blending a weight of two was assigned. If the line under investigation was located in the wing of a Balmer line (where there is some uncertainty in the location of the continuum) or was a weak line (where the profile was difficult to draw) a weight of one was assigned. Finally, if the deviation in the measurements of the equivalent width departed significantly from the average a weight of zero was assigned to the line.

The errors involved in the determination of the abundances are very difficult to assess. The error involved in the ordinate of the curve of growth has already been discussed elsewhere in this study and attention must now be directed to the abscissa of the empirical curve of growth. A significant source of error for abundance determination lies in the values of log gf used for computing the empirical curve of growth. In many instances systematic errors are included in the published results in an unknown manner. Whenever possible, all wavelength or excitation potential dependence was reduced or eliminated to some degree. In addition to this, little is known about the line broadening mechanism for the wings of spectral lines. The amount of uncertainty in the physical constants is entirely open to debate. Some of the values used for this analysis could be in error by a factor of two or more. The random error reported in the measurements of the oscillator strengths gives a lower limit to the uncertainty ($\sim$0.3 dex) while the upper limit may be as great as 1.0 dex.

Further, limitations upon the fine-analysis procedure restrict the reliability of the results. The temperature distribution was

based upon a solar-type model which may not completely described the state of affairs at all points in the stellar atmosphere or account for the influence of the chromosphere. The manner in which turbulence is incorporated theoretically into the calculations may not exactly describe the actual physical situation. There is also the possibility of deviations from thermodynamic equilibrium to be considered, especially for the strong lines.

From a given model atmosphere, the empirical curve of growth consists of a plot of the measured saturated equivalent width, log (W/λ), as the ordinate and the quantity log C_λ as the abscissa. The theoretical curve of growth is a plot of the logarithm of the saturated equivalent width as a function of the unsaturated equivalent width, log $(W/\lambda)^*$, for a line representative of the range of wavelengths of interest.

For the selected model, the computation begins with the evaluation of the theoretical curve of growth to be used for the mean abundance calculations. The abscissa for the theoretical curve of growth is computed from Equation (3-26) while the ordinate is calculated from Equations (3-21) and (3-29). Then, for each individual line, log C_λ is determined from Equation (3-30). The observed value of log (W/λ) is read into the computer program and the shift in the abscissa necessary to place the point on the mean theoretical curve of growth is evaluated. Thus, for a particular wavelength region and for similar excitation potentials, a unique abundance is obtained for each line of an element. The program then calculates an average abundance for each wavelength region. This is accomplished by summing products of line abundances and weights and dividing by the

the sum of the line weights.

Figures 9 through 20 are representative of the theoretical and empirical curves of growth used in this investigation. The wavelength region of interest is indicated in the upper right hand portion of each figure. The abscissa for the empirical curve of growth is log C_λ. Also included on the abscissa for the empirical curve of growth is the corresponding abscissa coordinate for the theoretical curve of growth. The horizontal shift thus indicated on each figure produces the derived average abundance for the wavelength region under investigation. The range of excitation potentials of the lower level are also displayed in the lower right hand portion of each figure. The theoretical curves of growth are all plotted for a microturbulent velocity of 1.50 kilometers per second.

Mean abundances for an element were then determined combining results from all wavelength regions. The procedure employed was identical to that used for each wavelength region as described above. If the average abundances were consistent or if there was only one wavelength region, only one mean abundance is displayed. For those elements for which there were obvious inconsistencies (e.g., iron in the wavelength region centered on 5150Å), two mean abundances are tabulated. The ones enclosed in parentheses are mean abundances evaluated using all the observational data, including the results considered to be inconsistent. Abundances without parentheses were obtained by essentially assigning a zero weight to the average abundances from wavelength regions yielding inconsistent results. These values are considered to more accurately represent the abundances in the stellar atmosphere.

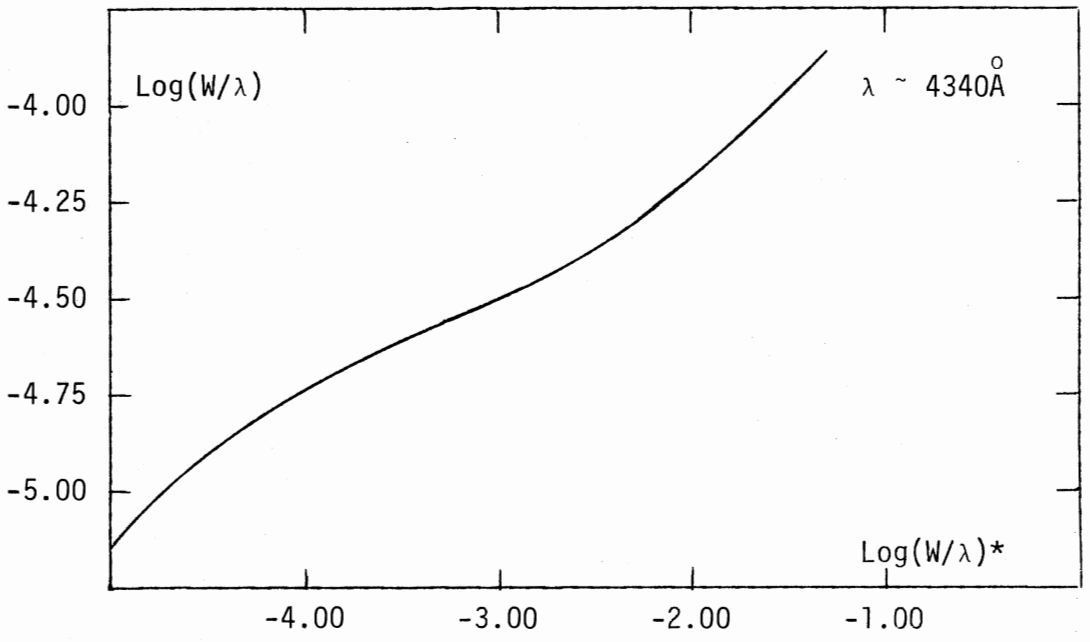

Figure 9. Theoretical Curve of Growth for Sc II

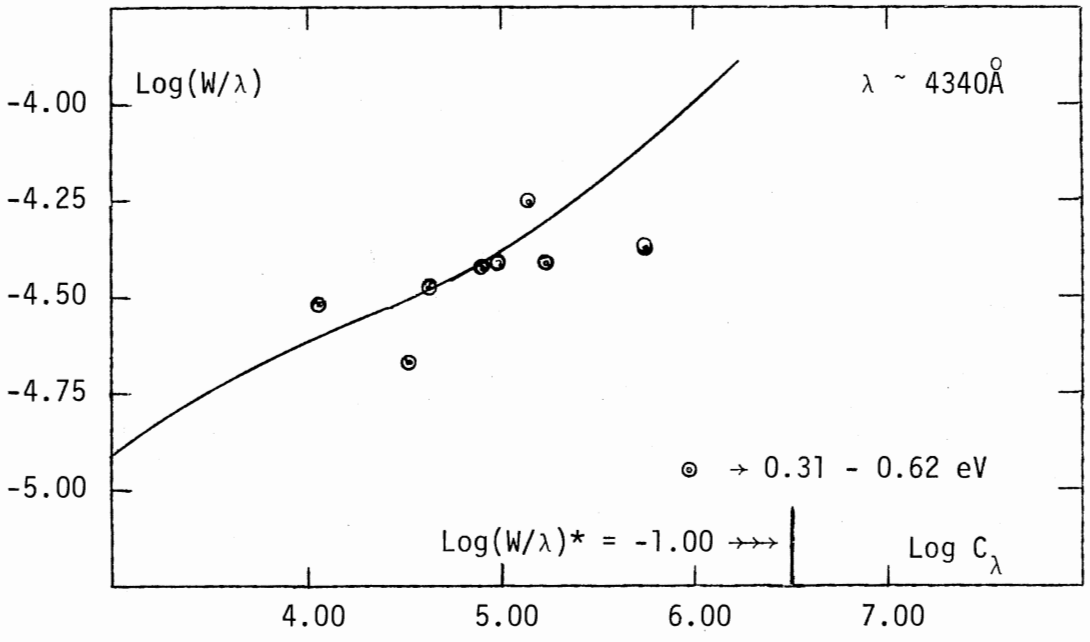

Figure 10. Empirical Curve of Growth for Sc II

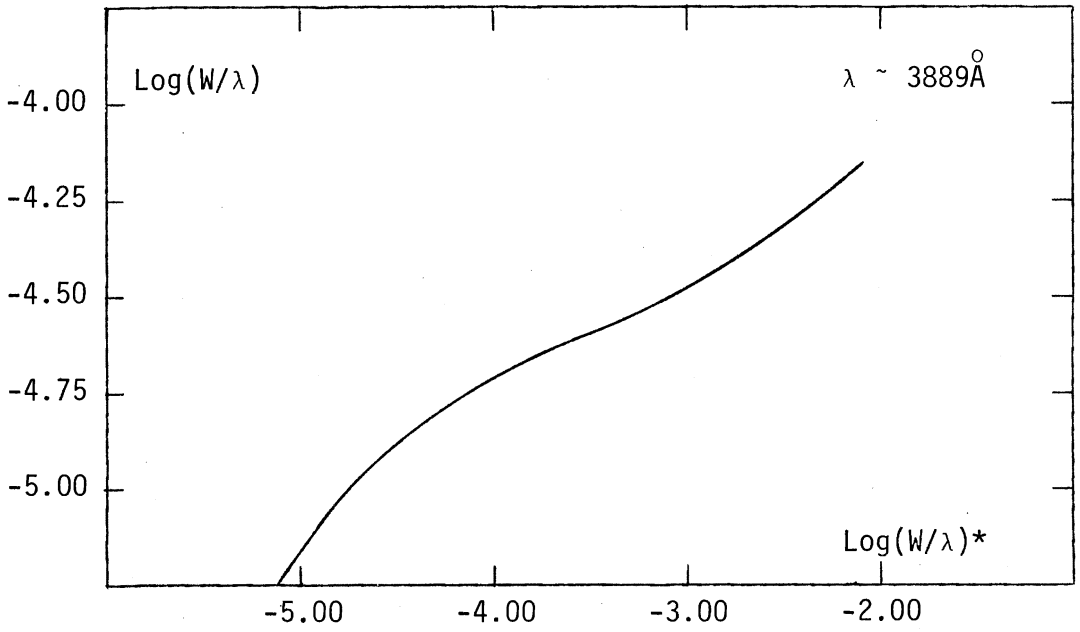

Figure 11. Theoretical Curve of Growth for Ti I

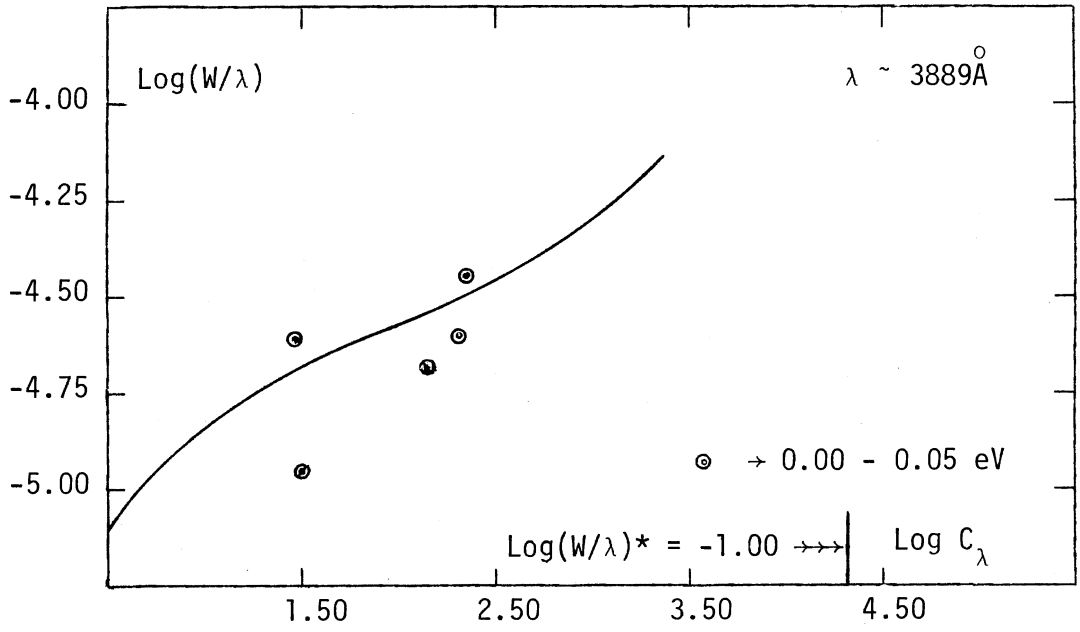

Figure 12. Empirical Curve of Growth for Ti I

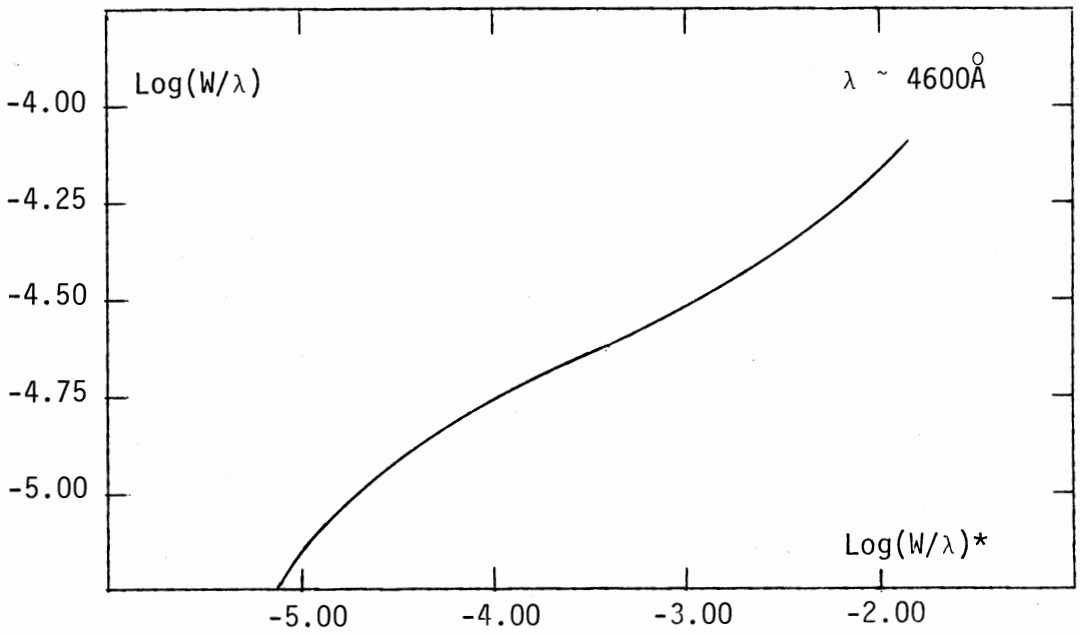

Figure 13. Theoretical Curve of Growth for Ti II

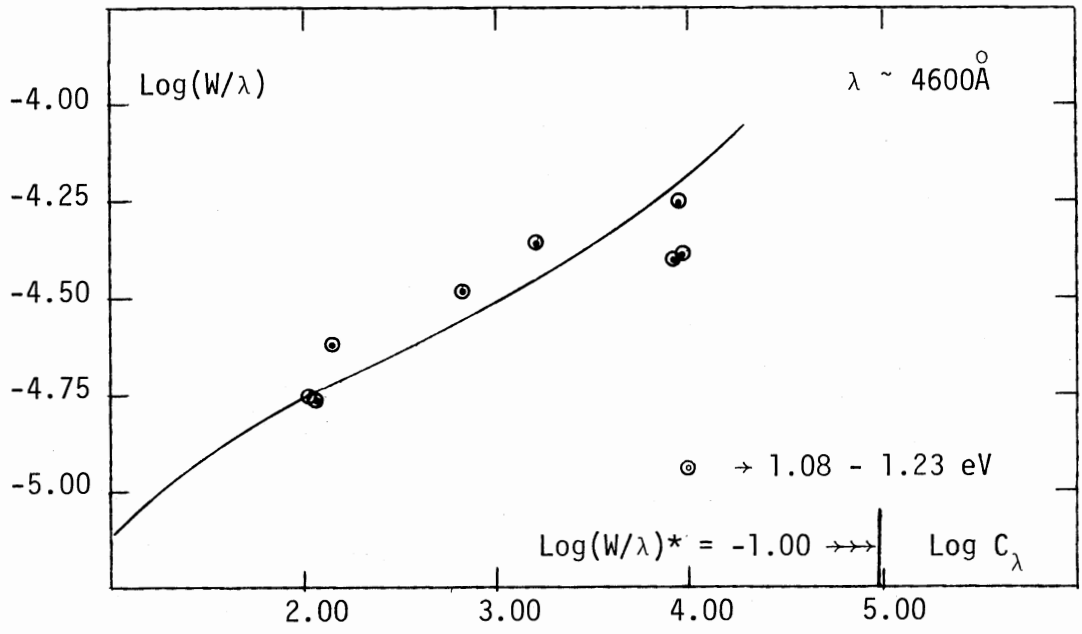

Figure 14. Empirical Curve of Growth for Ti II

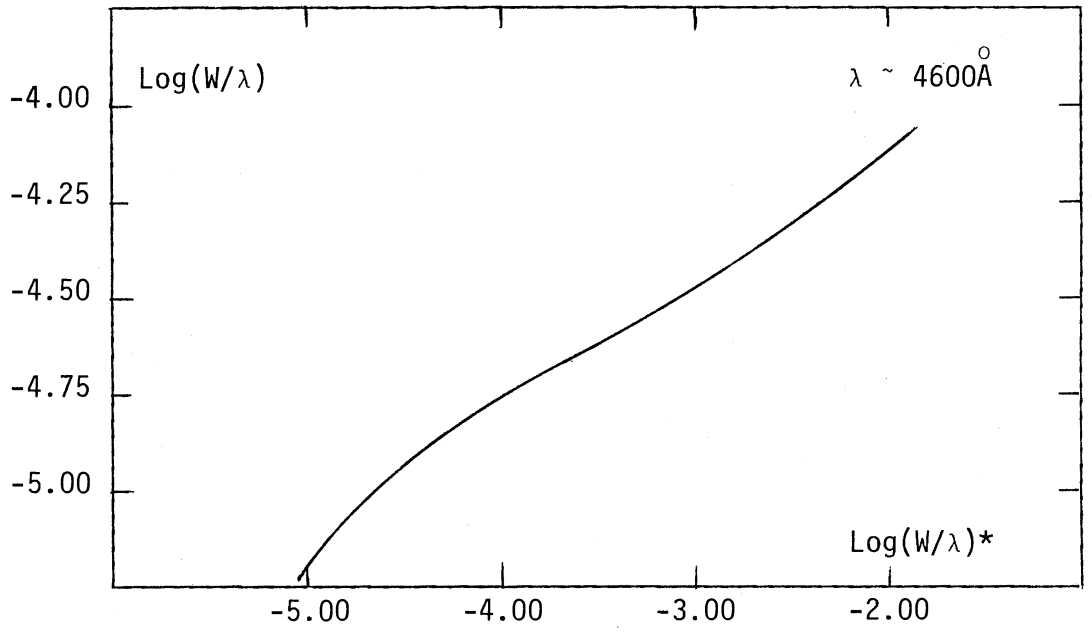

Figure 15. Theoretical Curve of Growth for Cr I

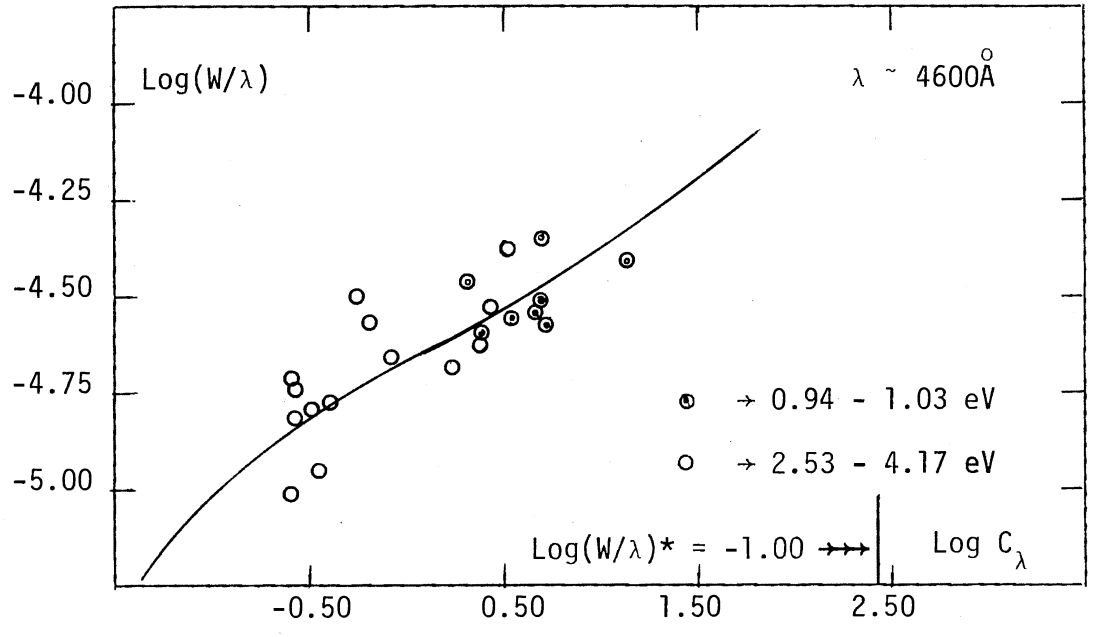

Figure 16. Empirical Curve of Growth for Cr I

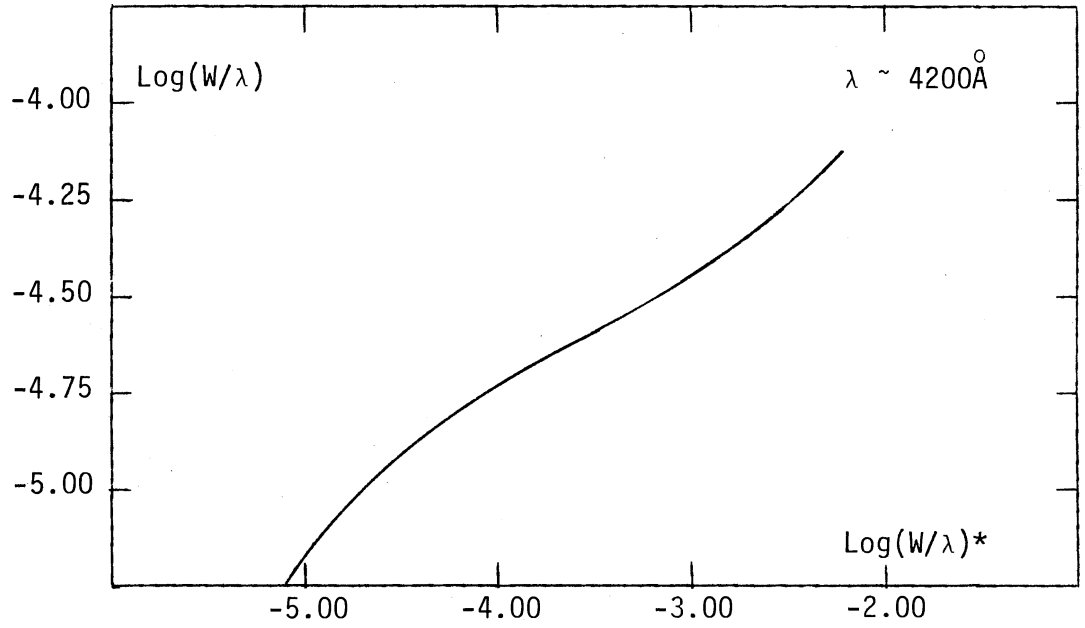

Figure 17. Theoretical Curve of Growth for Cr II

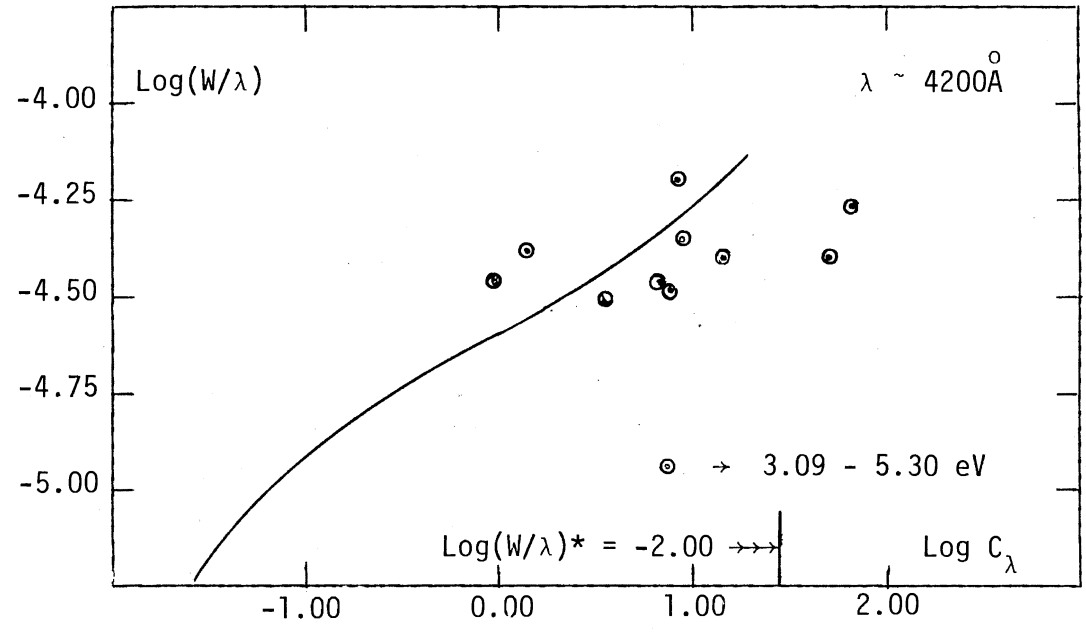

Figure 18. Empirical Curve of Growth for Cr II

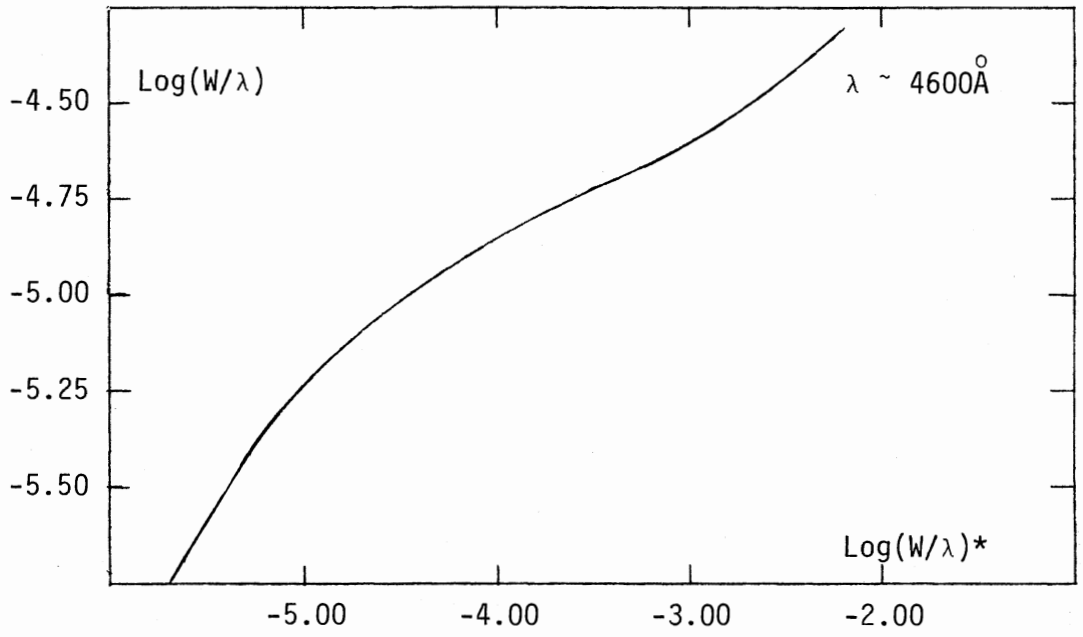

Figure 19. Theoretical Curve of Growth for Sm II

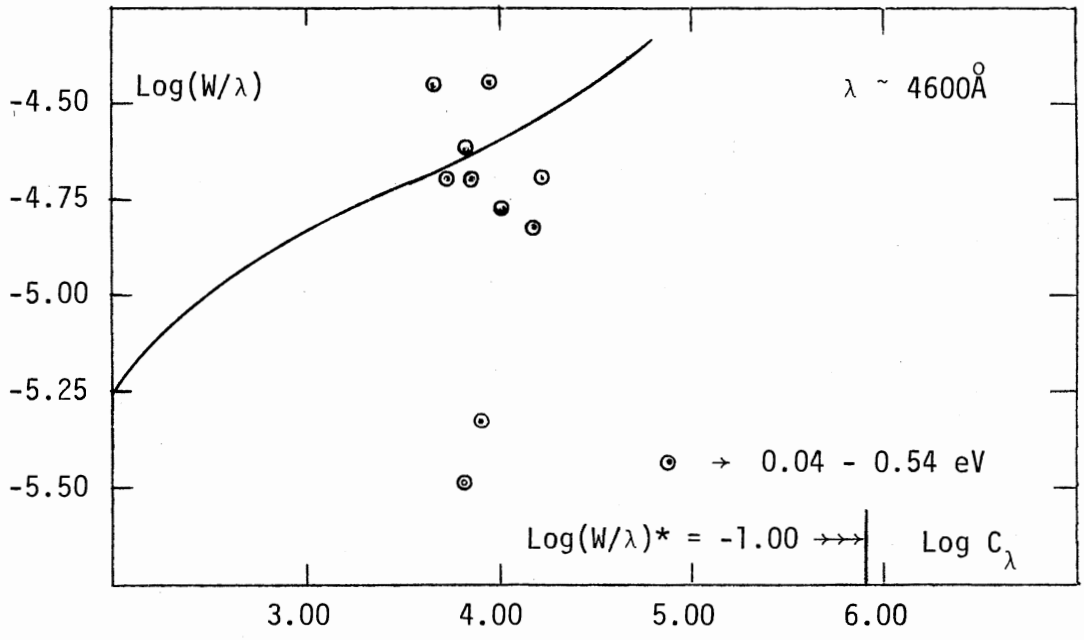

Figure 20. Empirical Curve of Growth for Sm II

For an objective assessment of the findings of this investigation, these factors must be kept in mind. The cause of these anomalies is uncertain at this time. However, the most probable cause may lie in the values of log gf or in the uncertainties of the measured equivalent widths. The values without these anomalies are in reasonable agreement with results of other investigators as is indicated in the next chapter.

Results for Individual Elements

Mean abundances for each element and stage of ionization are discussed below. The abundances are weighted means calculated in the program using data from columns ten and eleven in Tables IV through XXXI.

Sodium

The results for neutral sodium are displayed in Table IV. The f-values used for the analysis come from a tabulation by Weise, Smith and Miles (1969). For the wavelength region covered a derived mean abundance of

$$\log \frac{N_{NaI}}{N_H} = -5.20\ (-3.39),$$

was obtained. The accuracy in the absolute f-values of the sodium D-lines is three per cent and for the higher excitation potential ones, twenty-five per cent. This tends to lend support to the reliability of the abundance results even though the number of observations is low.

Magnesium

The results for neutral magnesium are given in Table V while those of singly ionized magnesium are shown in Table VI. The f-values are also taken from Wiese, Smith, and Miles (1969). Again the accuracies of the reported values range from 10% to 50%, so in addition to the small number of observational data available, the uncertainty in the abscissa is large. The derived mean abundances of neutral and

singly ionized magnesium were found to be

$$\log \frac{N_{MgI}}{N_H} = -3.57\ (-3.65),$$

and

$$\log \frac{N_{MgII}}{N_H} = -3.46.$$

Even though both stages of ionization yielded similar values the results are questionable as to their accuracy due to the low number of data available.

Silicon

The observational data used for the analysis of neutral silicon are given in Table VII, while those of the singly ionized ions are given in Table VIII. The number of available data are disappointingly low and the reliability of the f-values no better than 50%. The mean abundances of neutral silicon and singly ionized silicon were found to be

$$\log \frac{N_{SiI}}{N_H} = -2.29\ (-2.43),$$

and

$$\log \frac{N_{SiII}}{N_H} = -3.38\ (-3.55).$$

Calcium

The results for neutral calcium are given in Table IX while those of singly ionized calcium are given in Table X. The f-values used in the analysis are again from Weise, Smith, and Miles (1969).

For a large majority of lines an accuracy of no greater than 10% and as much as 50% can be expected. The derived mean abundances of neutral and singly ionized calcium were found to be

$$\log \frac{N_{CaI}}{N_H} = -3.75\ (-3.07),$$

and

$$\log \frac{N_{CaII}}{N_H} = -3.25\ (-3.48).$$

Scandium

The results of neutral scandium are given in Table XI while those of singly ionized scandium are given in Table XII and Figures 9 and 10. The analyses of both the neutral and singly ionized ions of scandium were performed using the corrected (Takens, 1970) f-values of Corliss and Bozman (1962); therefore, the observational data should be relatively free from any excitation potential dependence. If for no other reason the lack of observations introduces some doubts about the reliability of the results. However, the scatter is low indicating the absence of any systematic errors. The mean abundances derived from the curve of growth and by the weighting method for both the neutral and the singly ionized ions of scandium are

$$\log \frac{N_{ScI}}{N_H} = -5.74\ (-3.69),$$

and

$$\log \frac{N_{ScII}}{N_H} = -6.53\ (-5.59).$$

Titanium

The results for neutral titanium are given in Table XIII and Figures 11 and 12 while those of singly ionized titanium are given in Table XIV and Figures 13 and 14. The f-values used for the analysis of neutral titanium were taken from the tabulation of Wolnik and Berthel (1973) and Bell, Kalman, and Tubbs (1975). The f-values that were used in the analysis of singly ionized titanium were taken from tabulations by Wolnik and Berthel (1973) and Roberts, Anderson, and Sorensen (1973). No systematic dependence upon excitation potential is known for these f-values.

Theoretical curves of growth were calculated using the turbulence model suggested by the analysis of the iron lines. This yielded a curve of growth falling below the observational points on the empirical curve of growth. The microturbulent velocity was then increased until a best fit was achieved for both Ti I and Ti II. It is significant that this phenomenon is common to both stages of ionization, not just an effect due to an abnormal population difference for the two stages of ionization. That is, the ionization equilibrium is correct. Stream motions could be the physical cause or perhaps some other factor unaccounted for by the theory used to compute the curve of growth.

The curves of growth yielded mean abundances of

$$\log \frac{N_{TiI}}{N_H} = -3.95 \ (-3.83),$$

and

$$\log \frac{N_{TiII}}{N_H} = -4.77.$$

The difference between the results for the two stages of ionization are probably due to the differences between the absolute scales of the f-values used for the analyses. The accuracy of the result is quite high since a large number of observational data was available covering a large range of excitation potentials. The weights assigned to a majority of lines were large which indicates that the measured equivalent widths used in the analyses were quite reliable.

Vanadium

The results for neutral vanadium are given in Table XV while those of singly ionized vanadium are given in Table XVI. The f-values used for the neutral ions are those of Corliss and Bozman (1962). Systematic errors were removed using appropriate correction factors (Takens, 1970) for the excitation potential of the upper levels of the transitions. The scatter and quality of data is such that the abundance results show some error. The f-values used for the singly ionized ions are those of Roberts, Andersen, and Sorensen (1973). There is no known excitation potential dependence for these f-values.

The mean abundances derived for neutral and singly ionized vanadium were

$$\log \frac{N_{VI}}{N_H} = -5.47\ (-4.90),$$

and

$$\log \frac{N_{VII}}{N_H} = -5.06\ (-5.19).$$

Chromium

The analysis of this element was carried out upon both the neutral atom and the first stage of ionization. The observational data for neutral chromium are given in Table XVII and Figures 15 and 16 while those of singly ionized chromium are given in Table XVIII and Figures 17 and 18. The f-values for neutral chromium were taken primarily from the tabulated results of Wolnik, Berthel, Larsen, Carnevale, and Wares (1968). Other f-values were taken from the published results of Wolnik, Berthel, Carnevale, and Wares (1969) and Cooke, Stark, and Evans (1973). The f-values used for the singly ionized chromium lines were taken from the results of Warner (1968). Some of the Warner f-values are empirically derived from stellar sources and so should produce less scatter in the data.

The curves of growth yielded mean abundances of

$$\log \frac{N_{CrI}}{N_H} = -3.17,$$

and

$$\log \frac{N_{CrII}}{N_H} = -3.66\ (-3.40).$$

Manganese

The observational data used for the analysis of neutral manganese are given in Table XIX while those of singly ionized manganese are given in Table XX. The f-values used for neutral manganese are those of Corliss and Bozman (1962). Systematic errors were removed using the appropriate correction factor (Takens, 1970) for the excitation

potential of the upper level of the transition. The f-values used for singly ionized manganese are those compiled by Warner (1968).

The derived mean abundances for neutral and singly ionized manganese were found to be

$$\log \frac{N_{MnI}}{N_H} = -5.41 \ (-4.57),$$

and

$$\log \frac{N_{MnII}}{N_H} = -5.70.$$

Iron

The observation data used for neutral iron are given in Table XXI and Figures 6 and 7 while those of singly ionized iron are given in Table XXII and Figure 8. The f-values used for the analysis of neutral iron were primarily taken from the results of Wolnik, Berthel, and Wares (1970) and Wolnik, Berthel, and Wares (1971). Other f-values were obtained from the published results of Huber and Tobey (1968), Garz and Kock (1969), Bridges and Weise (1970), and finally, Huber and Parkinson (1972). The f-values used in the analysis of singly ionized iron were taken from the results compiled by Bridges and Wiese (1970) and Wolnik, Berthel, and Wares (1971).

The curves of growth yielded mean abundances of

$$\log \frac{N_{FeI}}{N_H} = -3.72 \ (-2.50),$$

and

$$\log \frac{N_{FeII}}{N_H} = -3.51 \ (-3.23).$$

Even though the abundances derived from both stages of ionization are very nearly the same, it should be pointed out that anomalies do exist here, especially for those Fe I lines whose wavelengths are greater than 4950Å. For those lines whose wavelengths were less than 4950Å, a value for the mean abundance was calculated to be -3.72 dex while that for lines greater than 4950Å was determined to be -2.50 dex. By the curve of growth analysis (Figures 6 and 7) a reasonable fit is obtained for a microturbulent velocity of 1.50 kilometers per second for both wavelength regions.

The reasons for the anomalies are somewhat uncertain at this time. They could possibly lie in the values of log gf used for computing the empirical curve of growth. Or, there may be systematic errors introduced in some other unknown fashion. The temperature distribution used (a solar-type model) may not completely describe the conditions that exist in this portion of the stellar atmosphere. And, finally, there is the strong possibility that we are looking at deviations from thermodynamic equilibrium in this wavelength region.

Cobalt

The observational data used for the analysis of neutral cobalt are given in Table XXIII. The f-values used in the analysis were those compiled by Corliss and Bozman (1962). These f-values were known to contain a systematic excitation potential dependence. An attempt was made to remove this dependence by using a correction factor obtained from the publication by Takens (1970). The possibility of large systematic errors in the data resulted in low weights for

the lines used in the analysis. The abundance derived for Co I in Beta Coronae Borealis was found to be

$$\log \frac{N_{CoI}}{N_H} = -4.17\ (-2.36).$$

Nickel

The observational data used for neutral nickel are given in Table XXIV while those for singly ionized nickel are given in Table XXV. The f-values used in the analysis of neutral nickel were taken from the results compiled by Garz, Heise, and Richter (1970) and Lennard, Whaling, Sills, and Zajc (1973). The f-values used in the analysis of singly ionized nickel were taken from the published results of Warner (1968). Since the number of lines for Ni II is quite low, the mean abundance derived is somewhat questionable.

The mean abundances derived for neutral and singly ionized nickel were found to be

$$\log \frac{N_{NiI}}{N_H} = -5.60\ (-3.97),$$

and

$$\log \frac{N_{NiII}}{N_H} = -5.96.$$

Strontium

The observational data used for the analysis of singly ionized strontium are given in Table XXVI. The f-values used for the analysis were those compiled by Corliss and Bozman (1962). Since the f-values are known to contain systematic excitation potential dependence,

an attempt was made to improve them by using the appropriate correction factor (Takens, 1970) for the excitation potential of the upper level of the transition.

The mean abundance derived for singly ionized strontium was

$$\log \frac{N_{SrII}}{N_H} = -6.49.$$

Since there is a small number of data within each wavelength region under investigation, the mean abundance derived may not be an accurate one.

Barium

The observation data for singly ionized barium are given in Table XXVII. The f-values used were taken from the results compiled by Miles and Weise (1969). The low number of lines prevents a very accurate abundance determination.

A mean abundance for singly ionized barium was found to be

$$\log \frac{N_{BaII}}{N_H} = -8.00\ (-7.73).$$

Neodymium

The observational data used for the analysis of this rare earth element are given in Table XXVIII. The f-values used were those published by Corliss and Bozman (1962). The available data are limited and the f-values used are not too reliable.

The mean abundance of singly ionized neodynium was found to be

$$\log \frac{N_{NdII}}{N_H} = -7.70\ (-6.60).$$

Samarium

The observational data for this rare earth element are given in Table XXIX and Figures 19 and 20. The f-values used were those published by Corliss and Bozman (1962). The available data are again somewhat limited and the f-values used are also not reliable which accounts for the large scatter.

The mean abundance of singly ionized samarium in Beta Coronae Borealis was found to be

$$\log \frac{N_{SmII}}{N_H} = -6.78 \ (-6.91).$$

Europium

The observational data for this rare earth element are given in Table XXX. The f-values used in the analysis were again taken from Corliss and Bozman (1962).

The mean abundance derived for singly ionized europium was found to be

$$\log \frac{N_{EuII}}{N_H} = -6.80 \ .$$

The accuracy of this abundance is somewhat questionable due to the low number of data points.

Uranium

Other investigators (Brandi and Jaschek, 1970; Hardorp and Shore, 1971; Hartoog and Cowley, 1972; Adelmen, 1973b; Adelman and Shore, 1973; Jordan, 1974) have reported the presence of singly ionized uranium in Beta Coronae Borealis. An attempt was made in this study to determine its mean abundance.

The observational data used for the analysis are given in Table XXXI. The f-values used in the analysis as well as the excitation potential of the lower level were taken from the results published by Voight (1975).

The mean abundance derived for singly ionized uranium was found to be

$$\log \frac{N_{UII}}{N_H} = -9.18 \ (-7.94).$$

In 1974, the author performed an extensive analysis of the spectrum of β CrB in search of the rare earth elements. All of the lanthanide series in both stages of ionization were found with the exception of PmII whose identification was somewhat doubtful. In addition to the lanthanides, some of the elements belonging to the actinide series were also tenatively identified. Adelman, Shore, and Tiernan (1973) reported the presence of some of the doubly ionized rare earth ions in Beta Coronae Borealis. These were also confirmed by the author. Those ions identified were La III, Ce III, Pr III, Nd III, Sm III, Tb III, and Er III. Due to lack of data, abundance analyses of these ions were not included in this study.

CHAPTER VI

SUMMARY AND CONCLUSIONS

The Model Atmosphere

The spectral analysis of the star Beta Coronae Borealis was performed using a pressure-opacity flux model with a scaled solar-type temperature distribution. A representative model atmosphere of a similar A-star, Gamma Equulei, was used in the analysis. This model atmosphere employed an effective temperature of 7700°K and logarithm of the surface gravity of 3.50.

The Turbulence Model

The presence of small scale mass motions in the atmosphere of β CrB was investigated from the analysis of both the neutral and singly ionized lines of iron. All theoretical calculations assumed local thermodynamic equilibrium and utilized the Planckian gradient technique.

Both theoretical and empirical curves of growth were computed for the model atmosphere selected for Beta Coronae Borealis. In order to achieve a fit between the empirical and calculated curve, it was necessary to include a small microturbulent velocity of 1.50 kilometers per second. This value is somewhat smaller than the value of 4.00 kilometers per second reported by Hack (1958), but

in good agreement with the value obtained by Hardorp and Shore (1971) and Opitz (1974).

Overall, the line profiles were sharp instead of broad, which suggests that the large scale mass motions, macroturbulence, are very small if they even exist at all in the atmosphere of Beta Coronae Borealis. In this study the macroturbulent velocity was considered to be negligible. From the correlation existing between the half-width of a line and its equivalent width, an assessment of the amount of macroturbulent motion in a stellar atmosphere can be calculated for those stars for which it is not negligible.

The Abundances

The abundances of eighteen elements found to exist in Beta Coronae Borealis were determined. Selection was based upon the availability and the quality of observational data. The abundance of each individual line was computed using a theoretical curve of growth with a micro-turbulence value based upon the analyses of Fe I and Fe II lines.

The analysis of all elements, some in two stages of ionization, confirm the conclusion derived from the Fe I and Fe II lines that the microturbulence in the atmosphere is very close to 1.50 kilometers per second. For a few elements there is a considerable difference in the mean abundances determined from the lines of the neutral element and that determined from the lines of the singly ionized element.

There is no readily apparent explanation for the inconsistency in the abundance determinations found in this study for different wavelength regions for an element in a particular stage of ionization. It does not seem likely that either the abundance differences

themselves or possible wavelength dependences of the abundances are due to systematic errors in the oscillator strengths. There have been enough stellar investigations to indicate that the absolute f-values used in this investigation do give quite consistent results for other stars. There are several other possibilities to which serious consideration should be given. The presence of the magnetic field may alter the distribution of absorbing particles from equilibrium values as mentioned earlier. The variations in brightness measured by Wolff and Morrison (1971) along with the magnetic field suggest that deviations from LTE may be more important than suspected.

Finally, the abundance results from this study are compared to those obtained in a coarse analysis of Beta Coronae Borealis by Miss Hack (1958) and to the results obtained by Adelman (1973b). The abundances listed in Table XXXII are determined relative to the hydrogen abundance in the stellar atmosphere. In this table are also the abundances derived by Evans (1966) for a similar star, Gamma Equulei, as well as those of the solar abundances reported by Withbroe (1971). The first column lists the element and ionization state for which an abundance was derived. Column two gives the results of this study. Column three lists the abundances derived by Adelman (1973b). Column four gives the abundances derived by the coarse analysis of Miss Hack (1958). Column five lists the abundances derived for a similar Ap star Gamma Equulei (Evans, 1966). Column six gives the solar abundances reported by Withbroe (1971).

The abundances determined in this study are considerably larger than those published by Miss Hack (1958) who performed a coarse

TABLE XXXII

COMPARISON OF STELLAR ABUNDANCES

	Beta Coronae Borealis				
Element	Jordan	Adelman	Hack	Gamma Equulei	Sun
Na I	-5.20			-4.59	-5.76
Mg I	-3.57		-4.40*	-4.08	-4.46*
Mg II	-3.46	-4.47		-4.08	
Si I	-2.29			-3.99	-4.45*
Si II	-3.38	-4.59		-3.62	
Ca I	-3.75	-4.18	-5.70	-4.76	-5.67*
Ca II	-3.25			-4.36	
Sc I	-5.74				-8.93*
Sc II	-6.53	-7.22	-8.78	-9.43	
Ti I	-3.95	-5.39	-6.43*		-7.26
Ti II	-4.77	-5.67			
V I	-5.47				-7.90
V II	-5.06	-7.50	-7.90		
Cr I	-3.17	-3.94	-5.16*	-5.36	-6.30*
Cr II	-3.66	-4.24		-6.97	
Mn I	-5.41	-5.47	-5.50	-5.89	-6.80
Mn II	-5.70	-5.37		-6.22	
Fe I	-3.72	-3.10	-4.51*	-4.52	-4.60*
Fe II	-3.51	-3.08		-4.85	
Co I	-4.17	-5.69	-6.34		-7.50
Ni I	-5.60	-4.77	-5.83*		-5.72
Ni II	-6.23	-4.62			
Sr II	-6.49	-6.98	-7.80	-7.44	-9.18
Ba II	-8.00	-8.58	-9.25	-8.70	-10.20
Nd II	-7.70	-7.72	-8.46	-8.77	-10.18
Sm II	-6.78	-6.76	-8.82	-9.55	-10.34
Eu II	-6.80	-5.48	-8.36	-8.39	-11.51
U II	-9.18	-8.83			-11.40

*Average of two ionization stages.

analysis employing a solar curve of growth. For the most part, they are slightly larger than those reported by Adelman (1973b) who performed a fine analysis employing a model atmosphere. Many of the differences in the derived abundances between this study and those of other investigators may be due to differences in effective temperatures, surface gravities, oscillator strengths, and lines used. Different values for the microturbulent velocity could induce some differences in the abundances obtained in the various investigations. The abundances derived in this study should be similar to those obtained by Evans (1966) for Gamma Equulei since they are similar stars.

Conclusions

The discrepancies found in the abundances derived for different wavelength regions may be indicators of the influence of light variations or the magnetic field on either the mode of line formation or the photospheric structure. However, this statement should be qualified by remembering the assumption that underlie the entire analysis and the ever present difficulty of the accuracy of the data. This investigation confirms the previous conclusions that there is a significant difference between Beta Coronae Borealis and the Sun in the abundance of a number of elements, notably Si, Ca, Sc, Ti, V, Cr, Mn, Fe, Co, Sr, Nd, Sm, Eu, and U.

The presence of singly ionized uranium in the spectrum of Beta Coronae Borealis suggests that the stellar material has been r-processed (Adelman, 1973a). The over-abundance of the heavy elements in Beta Coronae Borealis may lead to a possible conclusion as to its evolutionary stage and its path on the Hertzsprung-Russell diagram. It has been

proposed by Fowler, et al (1965) that diffusion may play an important role in the production of the heavy elements in Ap stars. One other process should be mentioned and that is the role of the magnetic field. It may lead to an accretion of the stellar material on the surface of the star. This might in turn possibly account for the over-abundance of some of the elements present in this star.

These over-abundances imply that Beta Coronae Borealis may be at an advanced stage of evolution, i.e., it has passed through the giant stage and has returned to the vicinity of the unevolved main sequence, or else that such a process has gone on in a close binary companion and mass has been transferred to the surface of the star. One other possibility may be that Beta Coronae Borealis is a second generation star which might account for its "non-normal" composition.

SELECTED BIBLIOGRAPHY

Abt, H. A., and Golson, J. C. 1962, Ap. J., 136, 363.

Adelman, S. J. 1973a, Ap. J., 183, 95.

_____. 1973b, Ap. J. Suppl., 26, 1.

_____. 1974, private communication.

Adelman, S. J., and Shore, S. N. 1973, Ap. J., 183, 121.

Adelman, S. J., Shore, S. N., and Tiernan, M. F. 1973, Ap. J., 186, 605.

Allen, C. W. 1963, Astrophysical Quantities, (London: The Athlone Press).

Aller, L. H. 1942, Ap. J., 95, 73.

_____. 1949, Ap. J., 109, 244.

_____. 1960, Stellar Atmospheres, ed. J. L. Greenstein (Chicago: University of Chicago Press), p. 156.

_____. 1963, Astrophysics (2nd ed.; New York: The Ronald Press Company).

_____. 1966, I.A.U. Symposium No. 26, Abundance Determinations in Stellar Spectra, ed. H. Hubenet (New York: Academic Press).

Aller, L. H., Elste, G., and Jugaku, J. 1957, Ap. J. Suppl., 3, 1.

Baranger, M. 1962, Atomic and Molecular Processes, ed. D. R. Bates (New York: Academic Press), p. 493.

Bell, G. D., Kalman, L. B., and Tubbs, E. F. 1975, Ap. J., 200, 520.

Bidelman, W. P. 1972, private communication.

Böhm, K. 1960, Stellar Atmospheres, ed. J. L. Greenstein (Chicago: University of Chicago Press), p. 88.

Brandi, E., and Jaschek, M. 1970, Pub. A. S. P., 82, 847.

Breene, R. G. 1961, The Shift and Shape of Spectral Lines (New York: Pergamon Press).

_____. 1964, Handbuch der Physik (Berlin: Pringer-Verdag), Vol. 27, p. 1.

Bridges, J. M., and Wiese, W. L. 1970, Ap. J. (Letters), 161, L71.

Bulman, J. A. 1971, Ph.D. Thesis, Oklahoma State University, unpublished.

Byard, P. L. 1968, J. Quant. Spectrosc. Radiat. Transfer., 8, 1543.

Cocke, C. L., Stark, A., and Evans, J. C. 1973, Ap. J., 184, 653.

Conway, J. G., and Fred, M. 1953, J. Opt. Soc. Am., 43, 216.

Conway, J. G., and McLaughlin, R. D. 1956, J. Opt. Soc. Am., 46, 91.

Conway, J. G., Hulet, E. K., and Lougheed, R. 1965, J. Opt. Soc. Am., 52, 222.

Corliss, C. H., and Bozman, W. R. 1962, Experimental Transition Probabilities for Spectral Lines of Seventy Elements (NBS Monogr. No. 53 [Washington, D.C.: Dept. of Commerce]).

Corliss, C. H. and Tech, J. L. 1968, NBS Monogr. No. 108 (Washington, D.C.: Dept. of Commerce).

Corliss, C. H., and Warner, B. 1963, Ap. J. Suppl., 8, 395.

Cowley, C. R. 1970, The Theory of Stellar Spectra (New York: Gordon and Breach).

David, K. 1961, Z. f. Ap., 53, 37.

Flste, G. 1955, Z. F. Ap., 37, 184.

Evans, J. C. 1966, Ph.D. Thesis, University of Michigan, unpublished.

_____. 1970, private communication.

_____. 1971, private communication.

_____. 1972, private communication.

_____. 1974, private communication.

Evans, J. C., and Schroeder, L. W. 1969, Bull. Am. Astro. Soc., 1, No. 1, 341.

Evans, J. C., Weems, M. L. B., and Schroeder, L. W. 1970, Bull. Am. Astron. Soc., Vol. 3, No. 1, pt. 1, p. 10.

Fowler, W. A., Burbidge, E. M., Burbidge, G. R., and Hoyle, F. 1965, Ap. J., 142, 423.

Fred, M., and Tomkins, F. S. 1957, J. Opt. Soc. Am., 47, 1076.

Fuhr, J. R., and Wiese, W. L. 1971, NBS Spec. Publ. 320; Suppl. I (Washington, D.C.: Dept. of Commerce).

_____. 1973, NBS Spec. Publ. 320, Suppl. II (Washington, D.C.: Dept. of Commerce).

Garz, T., and Kock, M. 1969, Astro. and Astrophys., 2, 274.

Garz, T., Heise, H., and Richter, J. 1970, Astro. and Astrophys., 9, 296.

Giacche Hetti, A. 1967, J. Opt. Soc. Am., 57, 728.

Gingerich, O. 1964, First Harvard-Smithsonian Conference on Stellar Atmospheres (Smithsonian Special Report No. 767), p. 17.

_____. 1969, Theory and Observation of Normal Stellar Atmospheres (Cambridge: The Mo. I. T. Press).

Glennon, B. M., and Wiese, W. L. 1962, NBS Monogr. No. 50 (Washington, D.C.: Dept. of Commerce).

Gruber, J. C. 1972, Ed.D. Thesis, Oklahoma State University, unpublished.

Gussman, E. A. 1963, Naturwissenschaften, 50, 495.

Gutmacher, R. G., Hulet, E. K., and Lougheed, R. 1965, J. Opt. Soc. Am., 55, 1029.

Gutmacher, R. G., Evans, J. E., and Hulet, E. K. 1967, J. Opt. Soc. Am., 57, 1389.

Haagland, J. 1957, Jener Report No. 51, Kjeller, Norway Joint Establishment for Nuclear Energy Research.

Hack, M. 1958, Mem. S.A.I., 29, 263.

Hardorp, J., and Shore, S. N. 1971, Pub. A.S.P., 83, 605.

Harrison, G. R. 1969, The Massachusetts Institutes of Technology Wavelength Tables (Cambridge, Massachusetts and London, England: The M.I.T. Press).

Hartoog, M. R., and Cowley, C. R. 1972, Bull. A.A.S., 4, 311.

Heuvel, E. P. J. van den 1963, B.A.N., 17, 148.

Hiltner, W. A. 1945, Ap. J., 102, 438.

Huang, S. S., and Struve, O. 1952, Ap. J., 116, 410.

_____. 1960, Stellar Atmospheres, ed. J. L. Greenstein (Chicago: University of Chicago Press), p. 321.

Huber, M. C. E., and Parkinson, W. H. 1972, Ap. J., 172, 229.

Huber, M. C. E., and Tobey, F. L., Jr., 1968, Ap. J., 152, 609.

Jordan, T. M. 1974, M. S. Thesis, Oklahoma State University, unpublished.

Jugaku, J. 1957, Ph.D. Thesis, University of Michigan, unpublished.

Kaufman, V., and Sugar, J. 1971, J. Opt. Soc. Am., 61, 1693.

Kourganoff, V. 1952, Basic Methods in Trasfer Problems, (Oxford: Oxford University Press).

Krueger, T. K., Aller, L. H., Ross, J., and Czyzak, S. J. 1968, Ap. J., 152, 765.

Lennard, W. N., Whaling W., Sills, R. M., and Zajc, W. A. 1973, Nucl. Inst. and Meth., 110, 385.

Matsuhima, S. 1964, Proc. Harvard-Smithsonian Conf. Stellar Atmospheres, 1st (Cambridge: The M.I.T. Press), p. 5.

Mattig, W., and Schroter, E. H. 1961, Z. f. Ap., 52, 195.

Mazing, M. A. 1961, Trans. Lebedev Inst., Moscow.

Meggers, W. F. 1957, Spectrochimica, 10, 195.

Meggers, W. F., and Scribner, B. F. 1937, J. Res. NBS, 19, 31.

_____. 1950, J. Res. NBS, 45, 470.

Meggers, W. F. and Stanley, R. W. 1958, J. Res. NBS, 61, 95.

Meggers, W. F., Corliss, C. H., and Scribner, B. F. 1961, NBS Monograph No. 32, Parts I and II, (Washington, D.C.: Dept. of Commerce).

Meggers, W. F., Scribner, B. F., and Bozman, W. R. 1951, J. Res. NBS, 46, 85.

Miles, B. M., and Wiese, W. L. 1969, NBS Tech. Note No. 474 (Washington, D.C.: Dept. of Commerce), 1.

_____. 1970, NBS Spec. Publ. 320 (Washington, D.C.: Dept. of Commerce).

Minnaert, M. S., and Slob, C. 1931, Proc. Amsterdam Acad., 3A, Part 1, 542.

Motz, L. 1970, Astrophysics and Stellar Structure (Waltham, Massachusetts: Ginn and Company).

Moore, C. E. 1959, A Multiplet Table of Astrophysical Interest (revised edition), Contr. Princeton U. Obs., No. 20.

_____. 1971, NSRDS-NBS No. 35, (Washington, D.C.: Dept. of Commerce), Vols. I, II, and III, p. 1.

Mugglestone, D. 1958, Mon. Not. R. Astr. Soc., 118, 432.

_____. 1965, Second Harvard-Smithsonian Conference on Stellar Structures (Smithsonian Special Report No. 174).

Neubauer, F. J. 1944, Ap. J., 99,134.

Odabasi, H. 1967, J. Opt. Soc. Am., 57, 1459.

Optiz, R. M. 1974, M.S. Thesis, Oklahoma State University, unpublished.

Preston, G. W. 1969, Ap. J., 158, 1081.

_____. 1971, Ap. J., 164, 309.

Regemorter, H. van. 1965, Annual Review of Astronomy and Astrophysics (Palo Alto: Annual Reviews, Inc.), Vol. 3, p. 71.

Roberts, J. R., Andersen, T., and Sorensen, G. 1973, Ap. J., 181, 567.

_____. ibid., 587.

Sargent, W. L. W., and Searle, L. 1962, Ap. J., 136, 408.

Schmalberger, D. C. 1963, Ap. J., 138, 693.

Smith, P. L. 1973, Nucl. Inst. and Methods, 110,395.

Spector, N. 1973, J. Opt. Soc. Am., 63, 358.

Strömgren, B. 1940, Pub. Copenhagen Obs., Vol. 1, 127.

Sugar, J. 1964, J. Opt. Soc. Am., 55, 33.

_____. 1969, J. Res. NBS, 73A, 333.

_____. 1970, J. Opt. Soc. Am., 60, 454.

Takens, R. J. 1970, Astro. and Astrophy., 5, 244.

Thackeray, A. 1936, Ap. J., 84, 433.

Tomkins, F. S., and Fred, M. 1949, J. Opt. Soc. Am., 39, 357.

Traving, G. 1960, Über die Theorie der Druckverbreiterung von Spektrallinien (Braun: Karlsruhe).

Unsöld, A. 1955, Physik der Sternatmosphären (2nd ed.; Berlin, Göttingen, Heidelberg: Springer-Verlag).

Voight, P. 1975, Phys. Rev., 11A, No. 6, 1845.

Warner, B. 1967, Mem. R.A.S., 70, 165.

_____ . 1968, Mon. Not. R. Astr. Soc., 138, 229.

Weidmann, V. 1955, Z. f. Ap., 36, 101.

Weise, W. L., Smith, M. W., and Glennon, B. M. 1966, NSRDS-NBS No. 4, (Washington, D.C.: Dept. of Commerce), Vol. I, p. 1.

Weise, W. L., Smith, M. W., and Miles, B. M. 1969, NSRDS-NBS No. 22, (Washington, D.C.: Dept. of Commerce), Vol. II, p. 1.

Withbroe, G. L. 1971, NBS Spec. Publ. 353, (Washington, D.C.: Dept. of Commerce), 127.

Wolff, S. C., and Morrison, N. D. 1971, Pub. A. S. P., 83, 609.

Wolnik, S. J., and Berthel, R. O. 1973, Ap. J., 179, 665.

Wolnik, S. F., Berthel, R. O., Carnevale, E. H., and Wares, G. W. 1969, Ap. J., 157, 983.

Wolnik, S. F., Berthel, R. O., and Wares, G. W. 1970, Ap. J., 162, 1037.

_____. 1971, Ap. J. (Letters), 166, L31.

Wolnik, S. J., Berthel, R. O., Larson, G. S., Carnevale, E. H., and Wares, G. W. 1968, Phys. Fluids, 11, 1002.

Wright, K. O. 1948, Publ. Dom. Ap. Obs., Victoria, 8, No. 1.

APPENDIX A

THE MODEL ATMOSPHERE: THEORY AND COMPUTATIONAL METHOD

This appendix covers the details of the theory used for a fine analysis of a stellar atmosphere. The model atmosphere program is based upon a computer program developed by Elste and Evans (1966, 1969,1972). All the programs used for the analysis may be obtained from Dr. J. C. Evans, George Mason University.

Excitation and Ionization of Atoms in Stellar Atmospheres

In a gaseous atmosphere in which a condition of LTE exists at each layer, the atoms, ions, and electrons all interact to bring about a distribution among the various levels to which the atoms may be excited. Considering only the neutral and singly ionized particles, the Saha equation, the Boltzman equation, and the perfect gas law specify the contribution to the total gas pressure and the electron gas pressure of the various species occuring in the stellar atmosphere. Through the Saha equation, Aller (1963) expresses the number of ionized atoms in the r^{th} excited state for a given temperature and electron pressure as

$$\frac{n_1}{n_o} = 10^{\log(u_1/u_o) + (9.0801 - 2.5 \log \theta - \log P_e) - \chi_o \theta} ,$$

$$\equiv \frac{\Phi_i}{P_e} \quad , \tag{A-1}$$

where

$u_1(\theta)$ = the partition function for singly ionized atoms,

$u_o(\theta)$ = the partition function for neutral atoms,

n_1 = the number of singly ionized atoms of species i per unit volume,

n_o = the number of neutral atoms of species i per unit volume,

θ = $5040/T(^oK)$,

P_e = $N_e kT$ = the electron pressure in the atmosphere,

χ_r = the ionization potential between the r^{th} and $(r + 1)^{st}$ ionization stages in electron volts,

Φ_i/P_e = the Saha equation for the ratio of singly ionized particles to neutral particles of species i.

One can define the degree of ionization to be the ratio of the number of ionized atoms to the total number of atoms as

$$\chi_i \equiv \frac{n_1}{n_o + n_1} = \frac{n_1/n_o}{1 + n_1/n_o} = \frac{\Phi_i/P_e}{1 + \Phi_i/P_e} \quad , \tag{A-2}$$

If we neglect helium ionization, molecular dissociation, and negative ions, and assume one ionization stage, the number of free electrons due to the ionization of a particle species is equal to the number of ions of that species. The ratio of all atoms, ions, and electrons to electrons is

$$\frac{N}{N_e} = n_{He} + \frac{\sum_i (n_o + n_1 + n_e)i}{\sum_i (n_e)i} \quad , \tag{A-3}$$

where n_{He} is the number of helium atoms. If there is but one stage of ionization, that is, $n_e = n_1$, then Equation (A-3) may be written as

$$\frac{N}{N_e} = n_{He} + \frac{\sum_i (1 + \chi_i)(n_o + n_1)i}{\sum_i \chi_i (n_o + n_1)i} \quad . \tag{A-4}$$

Dividing both the numerator and denominator of Equation (A-4) by the number of hydrogen atoms, N_H, and using the perfect gas law to convert to a ratio of pressures, Equation (A-4) becomes

$$\frac{N}{N_e} = \frac{P_g}{P_e} = \frac{\sum_i (1 + \chi_i)\, \varepsilon_i}{\sum_i \chi_i\, \varepsilon_i} \quad , \tag{A-5}$$

where

$$\varepsilon_i = \frac{N_i}{N_H} = \frac{(n_o + n_1)i}{n_H} \quad ,$$

represents the number abundance of species i. $\chi_{He} \equiv 0$ since we assumed no helium ionization, and the summation is over all elements. For computational purposes Weidmann (1955) has shown that the ratio P_g/P_e^2 is important since this ratio is less sensitive to P_e than θ. Hence, Equation (A-5) can be written as

$$\frac{P_g}{P_e^2} = \frac{\sum_i (1 + \chi_i)\, \varepsilon_i}{\sum_i \chi_i\, \varepsilon_i\, P_e} \quad . \tag{A-6}$$

The Continuous Absorption Coefficient

To calculate a model atmosphere it is sufficient, once the effective temperature and surface gravity are defined, to know the opacity as functions of the physical parameters. The calculation of the continuous absorption coefficient for the continuum proceeds under the following assumptions: (1) all molecular absorption is negligible with the exception of H_2^+; (2) all negative ion absorption is neglected except for H^-; and (3) the absorption by metals can be treated in the same manner as hydrogen. The principle source of absorption in the continuum is due to the bound-free (bf) and free-free (ff) absorption due to H^-, H, H_2^+. In addition to these, the metals may become appreciable absorbers and there may be Thompson scattering by electrons and Rayleigh scattering by hydrogen. Gingerich (1969) gives the following expression for the Rayleigh scattering coefficient per hydrogen atom as

$$\sigma_R = \frac{5.799 \times 10^{-13}}{\lambda^4} + \frac{1.422 \times 10^{-6}}{\lambda^6} + \frac{2.784}{\lambda^8} \quad .$$

Unsöld (1955) gives the following expression for the Thompson scattering coefficient by free electrons per electron as

$$\sigma_T = \frac{8\pi e^4}{3m^2c^4} = 0.66515 \times 10^{-24} \quad .$$

While the relative importance of the positive hydrogen molecule as a function of the temperature is relatively small (Matsushima, 1964), its contribution is included in the total absorption coefficient. Evans (1966) has tabulated the continuous absorption coefficient

data for hydrogen for various wavelength intervals ranging from λλ2000-21,000. The total absorption coefficient, K_λ, per hydrogen particle per unit electron pressure at any depth in the atmosphere as expressed by Evans (1966) can be written as

$$\frac{K_\lambda}{P_e} = \left[\frac{K_\lambda(\text{Hydrogen})}{P_e} + \frac{K_\lambda(\text{metals})}{P_e}\right] (1 + 10^{-\chi_\lambda \theta}) + \frac{\sigma}{P_e} \quad , \qquad \text{(A-7)}$$

where the term in parenthesis represents the correction term for stimulated emission which must be incorporated into all absorption processes. The total absorption coefficient per hydrogen particle per unit electron pressure, K_λ/P_e, is an implicit function of depth.

Hydrostatic Equilibrium

The equation for hydrostatic equilibrium can be written in terms of the continuous absorption coefficient at 5000Å, the effective surface gravity, and a conversion to a logarithmic optical depth scale. The form of this equation is

$$dP_g(x) = \frac{g\, m_o}{K_o} \sum_i \varepsilon_i \mu_i \left(\frac{\tau_o}{\log e}\right) dx \quad , \qquad \text{(A-8)}$$

where

g = the effective surface gravity,

τ_o = the optical depth at 5000Å,

ε_i = the number abundance of species i to hydrogen,

μ_i = the atomic weight of species i,

m_o = the mass in grams of a unit of atomic weight,

K_o = the continuous absorption coefficient per hydrogen particle at 5000Å.

This expression is most easily integrated, from the top of the stellar atmosphere ($P_g \equiv 0$) to the depth x, to obtain the gas pressure by first multiplying by $P_g^{1/2}$ (Evans, 1966). Equation (A-8) then becomes

$$\int_o^{P_g} P_g^{1/2}\, dP_g(x) = \frac{g\, m_o \sum_i \varepsilon_i\, \mu_i}{\log e} \int_o^x \left(\frac{P_g(x)}{P_e^2}\right) \frac{\tau_o}{(K_o/P_e)}\, dx, \quad \text{(A-9)}$$

The integrand on the right hand side of Equation (A-9) has been rearranged so as to employ the use of the known function P_g/P_e^2. Integration of the left hand side yields

$$\frac{2}{3} \cdot P_g^{3/2} = \frac{g\, m_o \sum_i \varepsilon_i\, \mu_i}{\log e} \int_{-\infty}^x \left(\frac{P_g}{P_e^2}\right) \frac{\tau_o}{K_o/P_e}\, dx\ , \quad \text{(A-10)}$$

or in the more convenient form

$$\log P_g = \frac{2}{3} \log \left\{\frac{3}{2} \frac{g\, m_o \sum_i \varepsilon_i\, \mu_i}{\log e}\right\} + \frac{2}{3} \log \left\{ \int_{-\infty}^x \left(\frac{P_g(x)}{P_e^2}\right)^{1/2} \cdot \frac{\tau_o}{K_o/P_e}\, dx\right\} \cdot \quad \text{(A-11)}$$

Writing the electron pressure as

$$P_e = [P_g(P_e^2/P_g)]^{1/2}\ , \quad \text{(A-12)}$$

and taking the logarithm of this expression gives the electron pressure in terms of the gas pressure and the function P_g/P_e^2. Hence, Equation (A-12) becomes

$$\log P_e = \frac{1}{2}[\log P_g + \log (P_g/P_e^2)] \quad . \qquad \text{(A-13)}$$

Surface Flux

Aller (1963) gives the solution to the equation of radiative transfer for the surface flux. The equation of transfer of radiation through a stellar atmosphere for the monochromatic radiant flux has been solved by Kourganoff (1952) to yield an integral equation for the radiative flux

$$F_\lambda(0) = 2 \int_o^\infty S_\lambda(\tau_\lambda') \, E_2(\tau_\lambda') \, d\tau_\lambda' \quad . \qquad \text{(A-14)}$$

The quantity S_λ appearing in the integrand is the source function which under the assumption of LTE is none other than the Planck function, $B_\lambda(T)$. $E_2(\tau_\lambda')$ represents the exponential-integral function,

$$E_2(x) = \int_1^\infty \frac{e^{-xy}}{y^2} \, dy \quad ,$$

while the optical depth at the wavelength λ is defined as

$$\tau_\lambda' = \int_{-\infty}^{x} \frac{K_\lambda}{K_o} \, \frac{\tau_o}{\log e} \, dx \quad . \qquad \text{(A-15)}$$

The actual physical flux is $\pi F_\lambda(0)$.

Assuming that $B_\lambda(\tau_\lambda')$ remains practically constant over the range $0 \leq \tau_\lambda \leq \varepsilon$, Equation (A-14) becomes,

$$F_\lambda(0) = 2B_\lambda(\varepsilon) \int_{\tau_\lambda=o}^{\tau_\lambda=\varepsilon} E_2(\tau_\lambda) d\tau_\lambda' + \int_{\tau_\lambda=\varepsilon}^{\tau_\lambda=\infty} 2B_\lambda(\tau_\lambda) \, E_2(\tau_\lambda) d\tau_\lambda \quad . \qquad \text{(A-16)}$$

From the definition of the exponential-integral function, the first integral on the right hand side of Equation (A-16) is

$$\int_{\tau_\lambda=0}^{\tau_\lambda=\varepsilon} E_2(\tau_\lambda)d\tau_\lambda = -E_3(\tau_\lambda) + \frac{1}{2} \quad , \tag{A-17}$$

while the second integral, when evaluated by integration by parts, is found to be

$$\int_{\tau_\lambda=\varepsilon}^{\tau_\lambda=\infty} 2B_\lambda(\tau_\lambda)\, E_2(\tau_\lambda)d\tau_\lambda = \int_{\log\,\tau_o(\varepsilon)}^{\infty} 2E_3(\tau_\lambda)\, \frac{dB_\lambda(\tau_\lambda)}{d(\log\,\tau_\lambda)}$$

$$\cdot\, (\frac{\log\, e}{\tau_\lambda})\, d\tau_\lambda \quad . \tag{A-18}$$

When Equation (A-17) and Equation (A-18) are combined, they yield the expression for the flux,

$$F_\lambda(0) = B_\lambda(\varepsilon) + \int_{\log\,\tau_o(\varepsilon)}^{\infty} 2E_3(\tau_\lambda)\, \frac{dB_\lambda(\tau_\lambda)}{d(\log\,\tau_\lambda)}\, (\frac{\log\, e}{\tau_\lambda})d\tau_\lambda \quad , \tag{A-19}$$

where

$$d\tau_\lambda = (\frac{\tau_\lambda}{\log\, e})\, d(\log\,\tau_\lambda),$$

$$\tau_\lambda(x) = \int_{-\infty}^{x} \frac{K_\lambda}{K_o}\, (\frac{\tau_o}{\log\, e})dx,$$

$$B_\lambda = \frac{2hc^2}{\lambda^5}\, [\frac{1}{e^{hc/\lambda kT} - 1}],$$

$$E_3(x) = \int_1^\infty \frac{e^{-xy}}{y^3}\, dy.$$

Equation (A-19) has been derived under the assumption that $B_\lambda(\tau_\lambda)$ increases less than exponentially over the range $\varepsilon \leq \tau_\lambda \leq \infty$. For small enough intervals in $x = \log\,\tau_o$, the gradient of the source function can be assumed to be independent of τ_λ (Evans, 1966) so the integration can be replaced by summations of the type

$$F_\lambda(0) = B_\lambda(\varepsilon) + (\log\, e) \sum_x^\infty \frac{dB_\lambda}{d(\log\,\tau_\lambda)}\, \Delta(x) \quad , \tag{A-20}$$

where

$$\Delta(x) = \int_{\tau_\lambda(x_1)}^{\tau_\lambda(x_2)} 2E_3(\tau_\lambda)\,\frac{d\tau_\lambda}{\tau_\lambda}\,,$$

$$= \int_{\tau_\lambda(x_1)}^{\tau_\lambda(x_2)} 2\left[\int_1^\infty e^{-\tau_\lambda y}\,\frac{dy}{y^3}\right]\frac{d\tau_\lambda}{\tau_\lambda}\,,$$

$$= \frac{1}{2}\left[E_1(\tau_\lambda)(2 - \tau_\lambda^2) - e^{-\tau_\lambda}(1 - \tau_\lambda)\right]_{\tau_\lambda(x_1)}^{\tau_\lambda(x_2)}\,.$$

As the optical depth increases, $\Delta(x)$ decreased rapidly (Evans, 1966) so that the summation in Equation (A-20) need only cover the contributions from the deepest layers, $-4.0 \leq x \leq +1.2$. The gradient of the Planck function is evaluated from the derivative of Sterlings interpolation formula,

$$\left.\frac{dB_\lambda}{d(\log \tau_\lambda)}\right|_{\tau_\lambda(x)} = \frac{1}{2}\left[\frac{B_\lambda[\tau_\lambda(x + \Delta x)] - B_\lambda[\tau_\lambda(x - \Delta x)]}{\Delta(\log \tau_\lambda)}\right]\cdot \qquad \text{(A-21)}$$

The Computational Procedure

For a given chemical composition, effective surface gravity, and temperature distribution a model atmosphere is calculated using an iterative procedure based upon an initial estimate of the electron pressure. The first two input parameters as well as the electron pressure were obtained from a coarse analysis performed upon Gamma Equueli by Evans (1966). The temperature distribution is also based upon a scale model of Gamma Equueli. This model was developed by Elste and later modified by Evans (1969, 1972). The model of Gamma Equueli was chosen because it is very much like Beta Coronae Borealis.

The iterative scheme begins with a computation of the ionization equilibrium, P_g/P_e^2, for the initial estimate of the electron pressure, using Equation (A-6). The effective temperature and electron pressure are then used to calculate the absorption coefficient at 5000Å, i.e., the quantity K_o/P_e from Equation (A-7). Once these quantities have been determined an initial estimate of the total gas pressure P_g can be determined through Equation (A-11). From the total gas pressure and the function P_g/P_e^2, another estimate of the electron pressure is made. A second iteration on the gas pressure is then accomplished through recycling of the entire process. The computations will continue until convergence of the electron pressure is obtained. Commonly this requires but a few iterations because of the behavior of the significant functions, P_g/P_e^2 and K_o/P_e, which fluctuate more rapidly for variations in temperature rather than in pressure (Bulman, 1971).

The computation of the opacity uses an identical iterative scheme except that before the calculation of the optical depth at various wavelengths from Equation (A-15) the absorption coefficient must be determined. The absorption coefficient for wavelength λ is computed from Equation (A-7), placed in Equation (A-15) and integrated to find $\tau_\lambda(x)$. Through Equation (A-20), the flux model is calculated at wavelength intervals of approximately 300Å for the interval of $\lambda\lambda$1000-10,000 and one each for 15,000Å, 21,000Å, and 32,000Å. The results, the variation of the parameters specifying the model atmosphere with depth, then form the basis for the input data which will enable the calculation of the chemical abundances to be made.

APPENDIX B

THE COMPUTER PROGRAMS USED IN THE ANALYSIS

The Metal Line Program

The expression for the absorption coefficient per absorbing particle for simultaneous damping and Doppler broadening as a convolution of the two effects acting independently is (Aller, 1963; Cowley, 1970)

$$K_{atomic}(x,\Delta\lambda) = \frac{\sqrt{\pi}e^2}{mc^2} \frac{\lambda^2}{\Delta\lambda_D} f_{r,s} H(a,v), \qquad \text{(B-1)}$$

where

$\Delta\lambda_D$ = the Doppler width (Equation (3-23)),

$f_{r,s}$ = the oscillator strength, for the transition, from level s, for the r^{th} stage of ionization,

$$a(x) = \frac{\Gamma_T(x)}{4\pi} \frac{\lambda}{\sqrt{\frac{83.83}{\mu_i \theta} - \varepsilon_{mt}^2}},$$

$$\Gamma_T(x) = \Gamma_{rad} + \Gamma_{Stark} + \Gamma_{van\ der\ Waals},$$

$$v(x) = \Delta\lambda/\Delta\lambda_D ,$$

$H(a,v)$ = the Voigt function,

$$\equiv \frac{a}{\pi} \int_{-\infty}^{\infty} \frac{e^{-y^2}}{(v-y)^2 + a^2} dy \ .$$

The Voigt function is approximated by a series expansion for large values of the distance from the line center, $\Delta\lambda$. In order to transform to the absorption coefficient per hydrogen particle, used in Equation (3-25), Equation (B-1) must be multiplied by the Boltzmann equation, $(\frac{n_{r,s}}{n_r})$; the degree of ionization involving the Saha equation $(\frac{n_r}{\Sigma n_r})$; and the relative abundance of hydrogen ions to the sum of hydrogen atoms and ions, $(\frac{N_i}{N_H})$. Thus

$$K^{\ell} = \frac{n_{r,s}}{N_H} K_{atomic} = (\frac{n_{r,s}}{n_r})(\frac{n_r}{\Sigma n_r})(\frac{N_i}{N_H})K_{atomic}, \qquad (B\text{-}2)$$

where the summation is carried out over all stages of ionization and excitation for the atoms of a given element and is just equal to N_i. The factor $\frac{n_{r,s}}{\Sigma n_r}$ is quite sensitive to the depth of the stellar atmosphere and it varies from one level to the next (Aller, 1960). For a given model atmosphere one can calculate this depth dependence by utilizing the Saha and Boltzmann equations.

For most stellar atmospheres, there are only three stages of ionization of importance, that is, r-1, r, r+1. If s represents the lower level of the transition being considered and u_r the partition function for the r^{th} stage of ionization, then the first two terms of Equation (B-2) may be written as

$$(\frac{n_{r,s}}{n_r})(\frac{n_r}{\Sigma n_r}) = \frac{n_{r,s}}{n_r} (\frac{n_r}{n_{r-1} + n_r + n_{r+1}}) \ ,$$

$$= \frac{n_{r,s}}{n_r/u_r} \left(\frac{1}{u_r}\right) \left[\frac{1}{\frac{n_{r-1}}{n_r} + 1 + \frac{n_{r+1}}{n_r}}\right] . \qquad \text{(B-3)}$$

Defining

$$U_r \equiv u_r\left(\frac{n_{r-1}}{n_r} + 1 + \frac{n_{r+1}}{n_r}\right), \qquad \text{(B-4)}$$

allows one to express Equation (B-3) as

$$\left(\frac{n_{r,s}}{n_r}\right)\left(\frac{n_r}{\Sigma n_r}\right) = \left(\frac{u_r n_{r,s}}{n_r}\right)\left(\frac{1}{U_r}\right) . \qquad \text{(B-5)}$$

The Saha ionization equation ,

$$\log\left(\frac{n_{r+1}}{n_r}P_e\right) = \frac{5040}{T}\chi_r + \frac{5}{2}\log T - 0.48 + \log\left(\frac{2u_{r+1}}{u_r}\right) ,$$

where

χ_r = the ionization potential in electron volts,

n_{r+1} = the number of ionized atoms,

n_r = the number of neutral atoms,

P_e = the electron pressure,

u_{r+1} = the partition function of the ionized atoms,

u_r = the partition function of the neutral atoms ,

can be written as

$$\log\left(u_r\frac{n_{r+1}}{n_r}\right) = \log u_{r+1} - \chi_r\theta + \left(9.0801-\frac{5}{2}\log\theta-\log P_e\right), \qquad \text{(B-6)}$$

and

$$\log\left(u_r\frac{n_{r-1}}{n_r}\right) = \log u_{r-1} + \chi_{r-1}\theta - \left(9.0801-\frac{5}{2}\log\theta-\log P_e\right). \qquad \text{(B-7)}$$

Substitution of Equations (B-6) and (B-7) into Equation (B-4) gives

$$U_r = 10^{[\log u_{r-1} + \chi_{r-1}\theta - (9.0801 - \frac{5}{2}\log\theta - \log P_e)]} + 10^{[\log u_r]} + 10^{[\log u_{r+1} - \chi_r\theta + (9.0801 - \frac{5}{2}\log\theta - \log P_e)]} \quad \text{(B-8)}$$

The term in parenthesis in Equation (B-5) depends upon the stage of ionization and, using the combined Boltzmann and Saha equations, can be written as (Evans, 1966)

$$\log\left(u_r\left(\frac{n_{r',s}}{n_r}\right)\right) = \log g_{r',s} + \Delta\chi\theta + h(9.0801 - \frac{5}{2}\log\theta - \log P_e), \quad \text{(B-9)}$$

where

$g_{r',s}$ = the statistical weight of the lower level,

$$h = \begin{cases} -1 \text{ if } r' = r-1, \\ 0 \text{ if } r' = r, \\ +1 \text{ if } r' = r+1 \end{cases}$$

and

$$\Delta\chi = \begin{cases} \chi_{r-1} - \chi_{r-1,s}, & \text{for } (r-1,s), \\ -\chi_{r,s}, & \text{for } (r,s), \\ -\chi_{r+1,s} - \chi_r, & \text{for } (r+1,s). \end{cases}$$

Making use of Equations (B-1), (B-2), (B-5), (B-8), and (B-9) the line absorption coefficient per hydrogen particle becomes

$$K^{\ell}(x,\Delta\lambda) = \frac{\sqrt{\pi}e^2}{mc^2}\frac{\lambda^2}{\Delta\lambda_D}\frac{(gf)_{r,s}}{U_r}\varepsilon_i[10^{\{\Delta\chi\theta + h(9.0801 - \frac{5}{2}\log\theta - \log P_e\}}] \cdot H(a,v) . \quad \text{(B-10)}$$

Using Equation (B-10), the optical depth in the line is computed as a function of x and $\Delta\lambda$. It is common practice to facilitate discussion (Aller, 1963) by writing the integrand of Equation (3-3) as a product of four functions,

$$\frac{K^{\ell}}{K_o}\left(\frac{\tau_o}{\log e}\right)\left(1 - 10^{-\chi_{\lambda m}\theta}\right) = \varepsilon_i \; Z_i(x,\lambda) \; H(a,v), \tag{B-11}$$

where

$$Z_i(x,\lambda) = M(x) \; N_i(x) \; L_{r,s}(x,\lambda)\left(1 - 10^{-\chi_{\lambda m}\theta}\right) .$$

The advantage of this is that it allows for a more rapid and complete computational scheme when applied to an electronic computer. The first of the terms in $Z_i(x,\lambda)$ is defined as

$$M(x) = \frac{\sqrt{\pi}e^2}{mc^2} \; \frac{P_e}{K_o} \; \left(\frac{1}{P_e}\right) \frac{\tau_o}{\log e} \quad , \tag{B-12}$$

and is constant for all elements and wavelength regions, λ_m.

$N_i(x)$ is defined as

$$N_i(x) = \left(\frac{1}{U_i}\right) \frac{10^{h\left(9.0801 - \frac{5}{2}\log\theta - \log P_e\right)}}{\sqrt{\frac{83.83}{\mu_i\theta} - \varepsilon_{mt}^2}} \quad , \tag{B-13}$$

and is also not dependent upon wavelength. Finally, $L_{r,s}(x,\lambda)$ contains the dependence of the line optical depth upon the explicit transition under consideration and is defined as

$$L_{r,s}(x,\lambda) = 10^{\log (gf\lambda)_{r,s} + \Delta\chi\theta} \quad . \tag{B-14}$$

For lines forming doublets, the computational scheme relies on the assumption that the broadening of the separate components are independent of each other (Evans, 1966). Then Equation (B-11) may be written as

$$\left(\frac{K^{\ell_1}}{K_o} + \frac{K^{\ell_2}}{K_o}\right)\left(\frac{\tau_o}{\log e}\right)\left[1 - 10^{-\chi_{\lambda} m^{\theta}}\right] = \varepsilon_i\left[Z_1(x,\lambda_1)\, H(a_1,v_1) + Z_2(x,\lambda_2)\, H(a_2,v_2)\right]. \quad \text{(B-15)}$$

However, the two functions, $Z_1(x,\lambda_1)$ and $Z_2(x,\lambda_2)$ are not linearly independent if the wavelengths are assigned an identical value and the damping constant is the same for both. The two functions are then connected through

$$Z_2(x,\lambda_2) = \frac{(gf)_{r_2 s_2}}{(gf)_{r_1 s_1}}\, Z_1(x,\lambda_1) ,$$

and Equation (B-15) then becomes

$$\left(\frac{K^{\ell_1}}{K_o} + \frac{K^{\ell_2}}{K_o}\right)\left(1 - 10^{-\chi_{\lambda} m^{\theta}}\right) = \varepsilon_i\left[Z_1(x,\lambda)\right]\left[H(a,v_1) + \frac{(gf)_{r_2 s_2}}{(gf)_{r_1 s_1}}\, H(a,v_2)\right], \quad \text{(B-16)}$$

where

$$v_2 = \frac{\Delta\lambda - d}{\Delta\lambda_D} ,$$

d = the separation of the centers of the individual components of the doublet,

$= \lambda_2 - \lambda_1$.

The Damping Parameters

The total damping constant in Equation (3-24) is given by the sum of the contributions from natural or radiation broadening, the Stark effect, and van der Waals broadening. Aller (1963) has discussed the importance of radiation damping. For most stellar

applications, he indicates that the contribution to the total damping constant due to this mechanism is of least importance and can be represented by the classical formula,

$$\Gamma_{rad} = \frac{8\pi^2 e^2}{3mc} \left(\frac{1}{\lambda^2}\right) = \frac{0.22234 \times 10^{16}}{\lambda^2} (sec^{-1}), \qquad (B\text{-}17)$$

where λ is expressed in Angström units.

The damping constant for the quadratic Stark effect is determined from the Lindholm relation applied to both ions and electrons and is given by (Aller, 1963) as

$$\Gamma_{Stark} = \Gamma_{electrons} + \Gamma_{ions}$$

$$= 38.8\, C_4^{2/3} [v_e^{1/3} N_e + v_{ions}^{1/3} N_{ions}], \qquad (B\text{-}18)$$

where v_e and v_{ions} represent the velocities of the perturbing particles. The constant is given by

$$C_4 = 6.21 \times 10^{-10} (\Delta\tilde{\nu}/F^2) , \qquad (B\text{-}19)$$

where

$\Delta\tilde{\nu}$ = the shift of the energy levels expressed in wavenumbers, and

F = the electric field strength in kvolts/cm.

Evans (1966) has calculated the numerical values of this constant for a few lines of C, Na, Si, and Mg. Since the experimental and theoretical data are inadequate for almost all of the observed lines in Beta Coronae Borealis, the range of the values of the constant was extended to include all of the observed lines for all the elements used in this investigation.

Finally, the damping constant for van der Waals interactions given by the Lindholm theory is given by the expression (Aller, 1963)

$$\Gamma_{\text{van der Waals}} = 17.0\, C_6^{2/5}\, v_{\text{atoms}}^{3/5}\, N_{\text{atoms}}, \qquad \text{(B-20)}$$

where the constant, C_6, is the van der Waals interaction constant. The numerical value of C_6 can be approximated (Aller, 1963), assuming a hydrogen-like particle, as

$$C_6 = 1.61 \times 10^{-33}\left[\left(\frac{13.5\, Z}{\chi_r - \chi_{r,s'}}\right)^2 - \left(\frac{13.5\, Z}{\chi_r - \chi_{r,s}}\right)^2\right], \qquad \text{(B-21)}$$

where

Z = the effective nuclear charge,

χ_r = the ionization potential of the atom,

$\chi_{r,s}$ = the excitation potential of the lower level,

$\chi_{r,s'}$ = the excitation potential of the upper level.

The Theoretical Curve of Growth

In the expression for $\log C_\lambda$ from Equation (3-28), the absorption coefficient at the line center is taken from a publication by Aller, Elste, and Jugaku (1957); so that

$$\frac{K_c^{\ell}}{K_o}\left(\frac{\tau_o}{\log e}\right)\left[1 - 10^{-\chi_{\lambda m}\theta}\right] = \varepsilon_i \frac{\sqrt{\pi}}{c}\left(\frac{\Delta\lambda_D}{\lambda}\right) Z,$$

and the quantity $\log C_\lambda$ becomes

$$\log C_\lambda = \log\left\{\frac{\sqrt{\pi}}{c}\int_{-\infty}^{\infty}\left(\frac{\Delta\lambda_D}{\lambda}\right) Z\, G_{\lambda m}\, dx\right\}. \qquad \text{(B-22)}$$

The flux weight function is given by the expression (Aller, 1960)

$$G_{\lambda m}(\tau_\lambda) = \frac{2}{F_T^c(0)} \int_x^\infty \frac{dB_{\lambda m}}{dx} E_2(\tau_{\lambda m})\, dx \,. \qquad \text{(B-23)}$$

The integration is carried out over a finite range, $-4.0 \leq x \leq +1.2$, since the behavior of the exponential integral is to decrease rapidly with increasing optical depth. The saturated equivalent width is calculated from the line depth, Equation (3-29). Since the line depth for large values of $\Delta\lambda$ is negligible for weak or medium strong lines, integration of Equation (3-29) may be truncated after only a few calculations.

The Metal Line Program

The computer program used for the analysis of the metal lines in stellar atmospheres was originally developed by Evans (1966). The program is designed to compute a single line profile and curve of growth for a given model atmosphere; however, it will calculate this for a variety of parameters.

The program initially begins by calculating all the quantities which are dependent only upon the model atmosphere, macroturbulence model, and microturbulence model. With the electron pressure, the temperature, the gas pressure, and the continuous absorption coefficient given as functions of the optical depth at 5000Å, the optical depth in the continuum for other necessary wavelengths is then computed. The integration is performed over the range in depth of $-4.0 \leq x \leq +1.2$ in steps of 0.2. The stimulated emission factor and the weighting function can also be evaluated at this time for the range of wavelengths overlapping the observed spectral region. The gradient of the source

function is then obtained through Stirling's interpolation formula and is expressed as

$$\left(\frac{dB}{dx}\right)_x = \frac{B_\lambda(x + \Delta x) - B_\lambda(x - \Delta x)}{2\Delta x} . \qquad \text{(B-24)}$$

The line absorption coefficient is then calculated as a function of x and $\Delta\lambda$ from Equation (B-10) in order that the optical depth in the line may be evaluated from Equation (3-3). In order to retain the necessary accuracy, the third exponential integral is approximated by a Taylor series expansion as

$$E_3(\tau^c) - E_3(\tau^c + \tau^\ell) = \tau^\ell E_2(\tau^c) \qquad \text{if } \tau^\ell << \tau^c ,$$

and by

$$E_3(\tau^c) - E_3(\tau^c + \tau^\ell) = E_3(\tau^c) \qquad \text{if } \tau^\ell >> \tau^c .$$

If τ^c is on the order of τ^ℓ, then only the difference in the two functions,

$$E_3(\tau^c) - E_3(\tau^c + \tau^\ell),$$

is calculated. Then for a particular element of interest U_r may be calculated from Equation (B-8) for the energy levels of interest. For this step appropriate tables of the partition functions for the elements of interest have been tabulated by Evans (1966). This completes the calculation of all the quantities which are independent of the individual transition under investigation.

Computations are then made for all terms which depend only upon the depth in the stellar atmosphere and the individual line under consideration. This calculation involves the Doppler width $\Delta\lambda_D$ from Equation (3-23), the damping constant $\Gamma_T(x)$ and the damping

parameter a(x) from Equation (B-1), the abscissa for the empirical curve of growth, log C_λ, from Equation (B-22) and, finally, log $Z(x,\lambda)$ from Equations (B-11), (B-12), (B-13), and (B-14).

At this point a cycling procedure is initialized for the computation of the theoretical curve of growth. An initial abundance estimate is used to compute the optical depth in the line from Equations (3-3) and (B-11) as a function of $\Delta\lambda$. The values of $\Delta\lambda$ are arbitrarily selected up to a maximum of 20 equal increments across the line. A variety of possible scaled values can also be chosen by the investigator. The integration of the line optical depth is achieved in the same fashion as for the continuum. Both employ a Gauss-Encke formula with a starting integration formula of Elste (Evans, 1966). The ordinate for the theoretical curve of growth, log (W/λ), is then computed using the line depth expression, Equation (3-21), in conjunction with Equation (3-29). This procedure is then repeated for twice and half the initial abundance estimate. If the observed value of the equivalent width for the line fails to lie within this range, additional multiples of the initial abundance estimate are utilized to compute additional points so that the observed value falls on the curve of growth.

The output of the metal line program has a number of options available. Upon command, the line profiles for the estimated abundance may be graphed and the mean value of the integrand of the line depth, sometimes referred to as the contribution function for the line, may be determined. The recycling of the entire program is achieved by first reading in all the lines and ordering them in their respective wavelength regions. After the lines in one wavelength

region have been exhausted, the computer proceeds to the next wavelength region. This process is repeated up to a maximum of ten wavelength regions.

The Abundance Program

For a given model atmosphere, the empirical curve of growth consists of a plot of the saturated equivalent width versus log C_λ where

$$\log C_\lambda = \log g_{r,s} f_{r,s} \lambda + \log L_\lambda^* (\chi_{r,s}).$$

With the help of Equation (3-27), the abundance of an element can be determined from the horizontal displacement of the axis with no vertical translation. If Δ_x represents the linear transformation necessary to bring the empirical curve of growth into coincidence with the theoretical curve of growth, then

$$\Delta_x = \log (W/\lambda)^* - \log C_\lambda = \log \varepsilon. \qquad \text{(B-25)}$$

This procedure has been systemized with the development of a computer program (Evans, 1970, 1971). The program is capable of determining the abundance for from one to fifty lines of a single element based upon a theoretical curve of growth for a line representative of the range of wavelenths of interest.

For the selected model, the computation begins with the evaluation of the theoretical curve of growth to be used for the mean abundance calculations. For this step, the optical depth is computed and the weighting functions are evaluated for the wavelength region of interest. For the desired element, U_r and log $Z(x,\lambda)$ are computed for the energy levels of interest. The details of the calculation are identical with

those outlined previously for the metal line program. The abscissa for the theoretical curve of growth is computed from Equation (3-26) while the ordinate is evaluated from Equations (3-21) and (3-29). With the help of Equation (3-31), log $L_\lambda(\chi_{r,s})$ is computed for each level $\chi_{r,s}$ of interest and for the wavelength region covering the observed spectral lines. Then for each individual line, or log $\{g_{r,s} f_{r,s} \lambda\}$, log C_λ is determined from Equation (3-30). The observed value of log (W/λ) is read into the computer program and the shift in the abscissa necessary to place the point on the mean theoretical curve of growth is evaluated. The abundance for the line thus determined, the program recycles until all observed lines have been read into the computer program and each individual abundance calculated. At this point, the weighted mean abundance is calculated in the standard fashion and the program terminated. The printed output consists of the model atmosphere, the turbulence model, the flux curve of growth, the abscissa for the theoretical curve of growth, and the resutls of the abundance analysis.

VITA

Thomas Morris Jordan

Candidate for the Degree of

Doctor of Philosophy

Thesis: A FINE-DETAILED ANALYSIS OF THE CHEMICAL ABUNDANCES FOR THE PECULIAR A-STAR BETA CORONAE BOREALIS

Major Field: Physics

Biographical:

Personal Data: Born in Crawfordsville, Indiana, the son of Morris B. and Edith C. Jordan.

Education: Graduated from Crawfordsville High School, Crawfordsville, Indiana in June, 1965; awarded the Bachelor of Arts degree from Indiana State University in August, 1969 with an emphasis in physics; received the Master of Science degree from Oklahoma State University in July, 1974 with a major in physics; completed requirements for the Doctor of Philosophy degree in July, 1977.

Professional Experience: Graduate Teaching Assistant, Oklahoma State University, Department of Physics, 1969-70; Graduate Teaching Assistant, Oklahoma State University, 1972; guest investigator, Kitt Peak National Observatory, 1972; Graduate Teaching Assistant, Oklahoma State University, 1972-77.